University of Massachusetts Amherst
ScholarWorks@UMass Amherst

Doctoral Dissertations 1896 - February 2014

1-1-1985

The classically conditioned nictitating membrane response : analysis of learning-related single neurons of the brain stem.

John E. Desmond
University of Massachusetts Amherst

Follow this and additional works at: https://scholarworks.umass.edu/dissertations_1

Recommended Citation

Desmond, John E., "The classically conditioned nictitating membrane response : analysis of learning-related single neurons of the brain stem." (1985). *Doctoral Dissertations 1896 - February 2014*. 1864.
https://scholarworks.umass.edu/dissertations_1/1864

This Open Access Dissertation is brought to you for free and open access by ScholarWorks@UMass Amherst. It has been accepted for inclusion in Doctoral Dissertations 1896 - February 2014 by an authorized administrator of ScholarWorks@UMass Amherst. For more information, please contact scholarworks@library.umass.edu.

UMASS/AMHERST
312066 0298 6593 1

FIVE COLLEGE
DEPOSITORY

UNIVERSITY OF MASSACHUSETTS
LIBRARY

ARCHIVES

LD
3234
M267
1985
D464

THE CLASSICALLY CONDITIONED NICTITATING MEMBRANE RESPONSE: ANALYSIS OF LEARNING-RELATED SINGLE NEURONS OF THE BRAIN STEM

A Dissertation Presented

By

John E. Desmond

Submitted to the Graduate School of the
University of Massachusetts in partial fulfillment
of the requirements for the degree of

DOCTOR OF PHILOSOPHY

September 1985

Psychology

John E. Desmond

©

All Rights Reserved

Apple IIe is a trademark of Apple Computer Inc.

National Science Foundation
BNS 82-15816

Air Force Office of Scientific Research
83-0215

National Institutes of Mental Health
1 F31 MH08951

THE CLASSICALLY CONDITIONED NICTITATING MEMBRANE RESPONSE: ANALYSIS OF LEARNING-RELATED SINGLE NEURONS OF THE BRAIN STEM

A Dissertation Presented

By

John E. Desmond

Approved as to style and content by:

John W Moore

John W. Moore, Chairperson of Committee

Andrew G Barto

Andrew G. Barto, Member

Paul Herron

Paul Herron, Member

Gordon A Wyse

Gordon A. Wyse, Member

Seymour M. Berger, Department Head
Psychology

ACKNOWLEDGEMENT

I would like to thank the members of my committee, Drs. John W. Moore, Andy G. Barto, Paul Herron, and Gordon A. Wyse for their helpful comments and words of encouragement. A special thanks to Dr. John Moore for providing stimulation and enlightenment during this project and over the past several years.

I am also grateful to Dr. Neil E. Berthier for sharing his technical expertise, and for many useful comments and suggestions concerning this project. I would also like to thank Marcy Rosenfield and Anne Lewin for technical and histological assistance, and Drs. Paul Solomon and Bryce Babcock for providing software and technical assistance for data acquisition.

I would like to thank my wife, Ellen, not only for proof-reading and commenting on the manuscript, but also for the constant support, understanding, and encouragement that make work and life much easier to take. A special thanks to my parents, Mr. and Mrs. John Desmond, for the years of financial support, for always having confidence in me, and for waiting so patiently for that steak and Lowenbrau.

ABSTRACT

THE CLASSICALLY CONDITIONED NICTITATING MEMBRANE RESPONSE: ANALYSIS OF LEARNING-RELATED SINGLE NEURONS OF THE BRAIN STEM

September 1985

John E. Desmond, B.A., University of South Florida
M.S., Ph.D., University of Massachusetts
Directed by: Professor John W. Moore

New Zealand albino rabbits were trained to partially discriminate between a reinforced conditioned stimulus (CS+) and a nonreinforced CS- (tones of 1200 or 600 Hz, 75 db SPL). The rabbits were then surgically prepared for single-unit extracellular recording. A stimulating electrode was implanted into the right accessory abducens nucleus (AAN), the principal nucleus mediating the nictitating membrane (NM) reflex. Following recovery, neuronal activity was recorded from the brain stem of the awake restrained animal during CS+ and CS- presentations. Incomplete discrimination resulted in conditioned response (CR) and non-CR trial types for each CS. Units were tested for antidromic response to AAN stimulation.

Statistical tools were developed to investigate CR-related unit activity. (1) A binomial method was used to compare rates of firing for CR and non-CR trials. (2) CR onset histograms were used to reveal CR onset-dependent neuronal responses. (3) Multiple correlations were computed to assess trial by trial spike/CR relationships. CR onset latency and CR magnitude were behavioral variables. Spike variables were the number of spikes that occurred during the CS Period, the mean time of spike occurrence, and the standard deviation of the time of spike occurrence. (4) Cross-correlations of unit activity with the CR, or with the CR first derivative, were used in determining whether spike activity temporally preceded or followed the CR.

Units displaying both CR-related excitation and CR-related inhibition were found. Excitatory units with activity leading the behavior were located in proximity to the motor trigeminal nucleus, including the supratrigeminal region, or dorsomedial to the brachium conjunctivum. Lead times were sufficiently long for causal involvement, typically ranging from 30-100 ms. Inhibitory units leading the CR were predominately located in dorsal and dorsomedial aspects of nucleus reticularis pontis oralis (RPO). One case of antidromic activation was observed in an excitatory cell in dorsolateral RPO. However, this cell probably fired concurrently with the CR. Possible circuits mediating the conditioned NM response and potential interactions among brain stem and cerebellar structures are discussed.

TABLE OF CONTENTS

ACKNOWLEDGEMENT iv

ABSTRACT v

LIST OF TABLES ix

LIST OF FIGURES x

CHAPTER

I. INTRODUCTION 1

Background 1
Control of the UR 2
Prosencephalic Influences on the CR . . . 4
Brain Regions Essential for the CR . . . 6
Goals of the Present Study 14

II. METHOD 24

Data Acquisition 24
Subjects 24
Conditioning Procedures 24
Surgery 26
Electrophysiological Recording 29
Procedural Exceptions 34
Data Analysis 35
Off-line Digitizing 35
Conventions for Naming Cells 36
Peristimulus Time Histograms 36
Binomial PSTH Comparisons 45
CR Onset Histograms 47
Multiple Correlation and Regression . . . 48
Cross-correlations 60

III. RESULTS 66

Cell Classifications 66
Excitatory Cells 72
Inhibitory Cells 120
Temporal Cells 131

IV. DISCUSSION 157

Analysis of CR-related Unit Activity 157
Locations of CR-related Recordings 164
CR-related Activity and Concomitant Responses 167

The Relationship of Brain Stem and Cerebellar Circuits 171

. . . .

BIBLIOGRAPHY 178

LIST OF TABLES

1. Regression of CR Area on Spike Variables 68
2. Regression of Maximum CR Amplitude on Spike Variables 69
3. Regression of CR Onset Latency on Spike Variables 70
4. Variance Partitioning for Excitatory Cells 77
5. Variance Partitioning for Inhibitory Cells 121
6. Variance Partitioning for Temporal Cells 134

LIST OF FIGURES

1. CR and non-CR PSTHs for Cell 43 19
2. CR and non-CR PSTHs for Cell 07 39
3. CR PSTH, non-CR PSTH, and binomial histogram comparison for Cell 02A 42
4. CR PSTH, non-CR PSTH, and binomial histogram comparison for Cell 35A 44
5. CR PSTH and CR onset histogram for Cell 46C 50
6. Cross-correlations and scatterplot for Cell 02A 54
7. CR PSTH, non-CR PSTH, and scatterplot for Cell 17A 56
8. PSTHs and binomial histogram comparison for Cell 61B 59
9. CR and non-CR PSTHs and cross-correlations for Cell 52B 65
10. Reconstruction of recording electrode positions 74
11. Reconstruction of stimulating electrode positions 76
12. CR and non-CR PSTHs and unit activity for Cell 53 81
13. Scatterplots and unit activity for Cell 53 83
14. Binomial histogram comparison, CR onset histogram, and cross-correlations for Cell 53 86
15. CR PSTH, non-CR PSTH, and binomial histogram comparison for Cell 61 88
16. CR onset histogram and cross-correlations for Cell 61 90
17. CR onset histogram and scatterplot for Cell 46E 92
18. CR and non-CR PSTHs and unit activity for Cell 61C 95
19. Binomial histogram comparison and cross-correlations for Cell 61C 97
20. CR PSTH, non-CR PSTH, and binomial histogram comparison for Cell 35 99
21. Scatterplot and cross-correlations for Cell 35 101
22. PSTHs, binomial histogram comparison, and unit activity for Cell 32A 103
23. CR and non-CR PSTHs and unit activity for Cell 26 105
24. CR and non-CR PSTHs and unit activity for Cell 64 108
25. Binomial histogram comparison, CR onset histogram, and cross-correlations for Cell 64 110
26. CR PSTH and scatterplot for Cell 42 112

27. CR and non-CR PSTHs and unit activity for Cell 42C 115
28. Cross-correlations and scatterplot for Cell 42C 117
29. Binomial histogram comparison, CR onset histogram, and antidromically elicited responses for Cell 42C 119
30. CR and non-CR PSTHs and unit activity for Cell 17 123
31. Scatterplots for Cell 17 126
32. Binomial histogram comparison, CR onset histogram, and cross-correlations for Cell 17 128
33. CR onset histogram and cross-correlations for Cell 35A 130
34. CR PSTH, CR onset histogram, and scatterplot for Cell 52 133
35. CR PSTH, non-CR PSTH, and binomial histogram comparison for Cell 43F. 137
36. CR onset histogram and scatterplot for Cell 43F 139
37. CR PSTH, non-CR PSTH, and binomial histogram comparison for Cell 50 142
38. Scatterplot and CR onset histogram for Cell 50 144
39. CR PSTH, CR onset histogram, and scatterplot for Cell 54A 146
40. CR PSTH, non-CR PSTH, and binomial histogram comparison for Cell 60A2 149
41. CR PSTH, non-CR PSTH, and binomial histogram comparison for Cell 09 151
42. CR onset histogram and cross-correlations for Cell 09 153
43. CR PSTH, CR onset histogram, and unit activity for Cell 18 156

CHAPTER I

INTRODUCTION

Background

The classically conditioned rabbit nictitating membrane (NM) response preparation is a widely adopted model system for studying learning at both behavioral and physiological levels (Gormezano, Kehoe, and Marshall, 1983; Moore, 1979; Thompson, Berger, Cegavske, Patterson, Roemer, Teyler, and Young, 1976). Basically, a conditioned stimulus (CS), a behaviorally neutral cue which can be auditory, visual, or tactile in nature, is paired with an unconditioned stimulus (US), a brief periocular electrostimulation, or in some laboratories, a puff of air to the cornea. The pairing is such that the CS precedes the US. Before any association between the CS and US is established, the rabbit responds only to the US in the form of an unconditioned response (UR), in which the NM extends from its resting position in the nasal canthus across the cornea toward the temporal canthus, and then retracts to its resting position. However, after sufficient training, a conditioned response (CR), which is identical to the UR, is observed after the onset of the CS and prior to the onset of the US.

Control of the UR

Present knowledge of the nictitating membrane (NM) reflex is derived from studies on both the rabbit and the cat. The sweep of the NM appears to be a passive consequence of eyeball retraction (Berthier and Moore, 1980a; Harrison and Cegavske, 1981; Motais, 1885, cited in Bach-y-Rita, 1971). Eyeball retraction is accomplished via the retractor bulbi muscles, which surround the optic nerve at the point where the nerve exits the globe. Retraction of the globe forces orbital fatty tissue and the Hardarian gland against the medial surface of the NM, resulting in the extension of the membrane across the corneal surface. Although contraction of the retractor bulbi muscle is probably the most important mechanism in effecting globe retraction and NM extension, there is strong evidence that the extraocular muscles also participate in this function. (Baldissera and Broggi, 1968; Berthier, 1984; Berthier and Moore, 1980a; Disterhoft, Quinn, Weiss, and Shipley, 1985; Evinger, 1984; Lorente de No, 1932; however, see Harvey, Marek, Johanssen, McMaster, Land, and Gormezano, 1983).

Retractor bulbi motoneurons for rabbits and cats were found in ipsilateral abducens, oculomotor, and accessory abducens nuclei (AAN) using horseradish peroxidase (HRP) procedures (Berthier and Moore, 1980a; Disterhoft and Shipley, 1980; Disterhoft et al., 1985; Grant, Gueritaud, Horcholle-Bossavit, and Tyc-Dumont, 1979; Gray, McMaster, Harvey, and Gormezano, 1981; Guegan, Gueritaud, and Horcholle-Bossavit, 1978; Spencer, Baker, and McCrea, 1980). Innervation of the retractor bulbi muscle originates primarily from the VIth nerve, and axons of the abducens and AAN motoneurons supply this nerve. Stimulation of the VIth nerve, but not the IIIrd or IVth nerves or the superior cervical ganglion, causes globe retraction and extension of the NM (Cegavske, Thompson, Patterson, and Gormezano, 1976). Harvey et al. (1983), using pontine lesions of the VIIth nerve, concluded that the facial nucleus contributes to NM extension, particularly when electrostimulation is used to elicit the reflex. However, Berthier (1984) found no effect of peripheral transection of the VIIth nerve on the NM response unless the VIth nerve was cut and extraocular muscles were disinserted; he concluded that the VIIth nerve can generate only small (1 mm) NM extensions, but not globe retraction.

Thus, it appears that the AAN and abducens nucleus are primarily responsible for eyeball retraction and NM extension. Concerning the respective roles of these nuclei in generating the UR, electrophysiological studies in cat and rabbit suggest that the AAN is principally involved in defensive eyeball retraction, whereas the abducens (and oculomotor) nucleus participates in patterned eye movement (Baker, McCrea, and Spencer, 1980; Berthier and Moore, 1983; Berthier, Desmond, and Moore, in press; Disterhoft et al., 1985).

The sensory component of the NM reflex is probably mediated via opthalmic and maxillary branches of the Vth nerve. Berthier and Moore (1983) concluded that activation of rabbit AAN neurons following eye stimulation involves two synapses; Baker et al. (1980) reached the same conclusion for the cat. Transverse knife cuts of the brain stem caudal to the facial and accessory abducens nuclei did not eliminate abducens nerve response to ipsilateral eye shock (Berthier and Moore, 1983). These data, in conjunction with the results from HRP administration to the AAN (Desmond, Rosenfield, and Moore, 1983a; Harvey, Land, and McMaster, 1984), and the cornea (Torigoe, Wenokor, and Cegavske, 1981; Harvey et al., 1984), suggest that secondary fibers of sensory trigeminal neurons in ventral pars oralis of the spinal trigeminal nucleus project to AAN to form the reflex arc.

Prosencephalic Influences on the CR

Brain regions rostral to the mesencephalon do not appear to be necessary for the manifestation of CRs. For example, nearly complete neodecortication does not impair a rabbit's ability to acquire or retain CRs (Moore, Yeo, Oakley, and Russell, 1980; Oakley and Russell, 1974; Oakley and Russel, 1975; Oakley and Russell, 1977; Yeo, Hardiman, Moore, and Steele-Russell, 1983), although CR onset latency is increased (Oakley and Russell, 1972; Oakley and Russell, 1977).

Unit recordings from the hippocampus (Berger, 1984; Berger, Alger, and Thompson, 1976; Berger and Thompson, 1978; Thompson, Berger, Berry, Hoeler, Kettner, and Weisz, 1980) and septal nuclei (Berger and Thompson, 1977) reveal learning-dependent changes in neuronal firing patterns. However, lesions of septal nuclei do not disrupt conditioning (Lockhart and Moore, 1975; Maser, Dienst, and O'Neal, 1974). Lesions of hippocampus affect certain derivative phenomena such as blocking (Solomon, 1977), latent inhibition (Solomon and Moore, 1975), discrimination reversal (Orr and Berger, 1981; Berger and Orr, 1983), and sensory preconditioning (Port and Patterson, 1984). Hippocampal lesions may also impair conditioning in a long-trace paradigm with an air puff US (Solomon, Vander Schaaf, Nobre, Weisz, and Thompson, 1983; Weisz, Solomon and Thompson, 1980), but do not disrupt CRs in a delay paradigm (Moore and Solomon, 1980; Moore and Solomon, 1984; Solomon, 1977). However, disruption of hippocampal function by small medial septal lesions (Berry and Thompson, 1979) or central scopolomine administration (Solomon, Solomon, Vander Schaaf, and Perry, 1983) can retard the acquisition of CRs.

Bilateral lesions of the lateral hypothalamus similarly do not affect rabbit eyeblink CRs, although extinction is affected (Francis, Hernandez, and Powell, 1981; Blazis, thesis). However, the nigrostriatal system may be involved in the acquisition of eyeblink conditioning. Large bilateral lesions destroying 2/3 of the anterior portion of the head of the caudate nucleus severely disrupted the acquisition of eyeblink conditioning (Powell, Mankowski, and Buchanan, 1978). Unilateral lesions, however, were not disruptive. Bilateral substantia nigra lesions similarly disrupted acquisition (Kao and Powell, 1983). There are presently no data concerning electrophysiological correlates of the NM CR in either the caudate nucleus or substantia nigra.

Brain Regions Essential for the CR

In 1981, the first evidence that the NM CR could be permanently eliminated without affecting the UR was reported by Desmond, Berthier, and Moore (1981a,b). Unilateral lesions of the dorsolateral pons (DLP) severely impaired both acquisition and retention of ipsilateral CRs to tone and light CSs. Conditioning of the eye contralateral to the lesion was not impaired. The fact that the UR was not impaired, that disruption was not confined to one sensory modality, and that contralateral CRs were not affected suggested that CR disruption was not a result of motor, sensory, or attentional impairment

(Desmond, Berthier, and Moore, 1981a,b; Desmond and Moore, 1982; Moore, Desmond, and Berthier, 1982). The structures in the DLP affected by the lesions, and thus, implicated in the conditioned NM response were the parabrachial nuclei, locus subcoeruleus, the brachium conjunctivum, and the supratrigeminal region (SR). The SR is a region dorsal and rostrodorsal to the motor trigeminal nucleus (Mizuno, 1970), and corresponds to the dorsal portion of cell zone h of Meessen and Olszewsky (1949). Subsequent lesions in more rostral regions of the pons produced similar conditioning deficits (Lavond, McCormick, Clark, Holmes, and Thompson, 1981).

Multiple-unit activity recorded from the DLP during classical conditioning revealed a conditioned increase in firing which developed and extinguished concurrently with the acquisition and extinction of the behavioral CR (Desmond, Berthier, and Moore, 1981a,b; Desmond and Moore, 1983; Moore, Berthier, and Desmond, 1981; Moore, Desmond, and Berthier, 1982). Similar increases in unit activity were not observed during pseudoconditioning, suggesting that the neural activity was related to the CR rather than the CS and US alone. The CR-related activity was predominately recorded from SR, and electrical stimulation to this region (using stimulation parameters that would preclude direct stimulation of AAN motoneurons) often produced a robust ipsilateral NM response, suggesting a projection from SR to AAN motoneurons.

The results of administering HRP to the AAN further implicated the SR in conditioning (Desmond et al., 1983a,b). A number of small-diameter supratrigeminal neurons were labeled, along with a network of fibers and apparent terminations within and surrounding the motor trigeminal nucleus. HRP administered to the supratrigeminal and nearby regions revealed fibers and terminal fields in the lateral parvocellular reticular formation encompassing the ipsilateral AAN.

These labeling patterns suggest that SR neurons project to the parvocellular reticular formation, but alone do not prove that supratrigeminal neurons synapse upon accessory abducens neurons. The fact that SR stimulation elicits ipsilateral NM responses (Desmond and Moore, 1983) is, however, consistent with this interpretation.

That brain regions other than the SR are critically involved in conditioning was suggested by R. F. Thompson and his collaborators, who found that unilateral destruction of cerebellar dentate and interposed nuclei in rabbit disrupt ipsilateral, but not contralateral, CRs, without affecting URs (Clark, McCormick, Lavond, and Thompson, 1984; McCormick, Lavond, Clark, Kettner, Rising, and Thompson, 1981; McCormick, Clark, Lavond, and Thompson, 1982). Similar lesions also prevented acquisition of CRs (Lincoln, McCormick, and Thompson, 1982). Yeo, Hardiman, and Glickstein (1982; 1985a) determined that the anterior interposed nucleus is the critical region responsible for the disruptive effect, and that lesions of the posterior interpositus, fastigial nucleus, or dentate nucleus, did not produce CR impairment. Multiple-unit (McCormick, Clark, Lavond, and Thompson, 1982) and single-unit (Foy, Steinmetz, and Thompson, 1984) recordings from the dentate/interpositus region have revealed CR-related increases in firing.

Consistent with an interpositus role in conditioning, lesions of the brachium conjunctivum also disrupted ipsilateral CRs (McCormick, Guyer, and Thompson, 1982). Interpositus (as well as dentate) neurons send efferents through the brachium conjunctivum, and these projections decussate at caudal midbrain levels to form the crossed ascending and descending limbs (Cohen, Chambers, and Sprague, 1958). Some of the axons from nucleus interpositus project to thalamic nuclei, while others terminate in contralateral red nucleus (Nakamura and Mizuno, 1971). Thus, if the red nucleus receives conditioning information from interpositus, then a unilateral lesion of the red nucleus should disrupt contralateral CRs.

Consistent with this prediction, unilateral radio-frequency lesions of the magnocellular red nucleus disrupted retention (Desmond et al., 1983b; Rosenfield and

Moore, 1983) and acquisition (Rosenfield and Moore, in press) of conditioned responding in the contralateral, but not ipsilateral, eye without affecting URs. Larger electrolytic lesions of the red nucleus produced CR disruption with some impairment of the UR (Haley, Lavond, and Thompson, 1983). In another study, infusion of the GABA antagonist picrotoxin into the red nucleus also disrupted CRs (Madden, Haley, Barchas, and Thompson, 1983). Given that GABA is an inhibitory transmitter and that the interpositus projection to red nucleus is excitatory (Ito, 1984), the picrotoxin impairment suggests, among other possibilities, that inhibitory interneurons within the red nucleus are involved in the conditioning circuit, or that inhibitory modulation of red nucleus neurons is necessary for generating CRs.

The red nucleus was further implicated in conditioning when HRP administered to the AAN labeled cells in the contralateral magnocellular red nucleus (Desmond et al., 1983a). These data are consistent with earlier silver impregnation studies that demonstrated crossed rubro-bulbar projections from red nucleus to lateral reticular formation in rabbit (Mizuno, Mochizuki, Akimoto, Matsushima, and Nakamura, 1973). However, anterograde tracing of HRP administered to the red nucleus (Rosenfield, Dovydaitis, and Moore, 1985) did not reveal terminals in the AAN. Thus, it is not clear how a cerebellar-red nucleus circuit would ultimately drive the AAN motoneurons. However, Moore (personal communication) reports terminal labeling in pars oralis of the sensory trigeminal complex after administering HRP to contralateral red nucleus. As noted earlier, cells in ventral pars oralis probably project to AAN as part of the reflex arc. Davis and Dostrovsky (1984) report that trigeminal pars oralis cells in cats are predominately inhibited by ipsi- or contralateral red nucleus stimulation. Therefore, AAN may be driven via red nucleus projections to trigeminal neurons (Moore, personal communication). If one assumes that (1) this hypothesis is correct, (2) the excitation of trigeminal pars oralis neurons is required to excite AAN neurons, and (3) the results of Davis and Dostrovsky (1984) are generalizable to rabbit, then one would expect that a conditioned decrease in red nucleus (or interneuron) activity would be needed to generate CRs. A test of this hypothesis would require single-unit recordings in red nucleus while conditioning the contralateral eye; to date, no such recordings have been reported.

McCormick and Thompson (1983a,b) have suggested that the neuronal changes that encode learning originate in dentate/interposed nuclei, and that cerebellar cortex is not necessary for CRs. However, this interpretation of cortex involvement was challenged by Yeo, Hardiman and Glickstein (1984; 1985b) after they discovered that discrete unilateral lesions of hemispheric lobule VI (HVI) produce irretrievable loss of ipsilateral CRs without UR impairment (Glickstein, Hardiman, and Yeo, 1984; Yeo, Hardiman, and Glickstein, 1984a,b; 1985b). In addition, HRP administration to HVI revealed terminal labeling in anterior interpositus (Yeo, Hardiman, and Glickstein, 1985c). Thus, HVI may relay critical learning information to the brain stem via anterior interpositus. Consistent with this interpretation, microinfusion of the GABA antagonists bicuculine and picrotoxin into the dentate/interpositus region disrupted ipsilateral conditioning, but glycine and strychnine were ineffective (Mamounas, Madden, Barchas, and Thompson, 1983). The impairment may have been due to the blocking of inhibitory Purkinje cell output from HVI to interpositus.

HRP administration to HVI also revealed retrograde labeling in the contralateral rostromedial dorsal accessory olivary nucleus and the adjacent medial portion of the principal olivary nucleus. In addition, bilateral labeling was observed mainly in pars oralis of the spinal trigeminal nucleus, caudal pontine nuclei including nucleus reticularis tegmenti pontis, and lateral reticular nucleus (Yeo et al., 1985c).

The labeling in the olivary nuclei was consistent with degeneration patterns observed in the olive after CR-disrupting HVI lesions (Yeo et al., 1985b). Bilateral lesions of rostromedial dorsal accessory olive produced a gradual loss of CRs and prevented acquisition in one study (Steinmetz, McCormick, Baier, and Thompson, 1984). In another report, stimulation of the inferior olive was used as a US for classical conditioning (Mauk and Thompson, 1984). Although CRs did develop, the current was of sufficient magnitude to excite adjacent structures, and thus, the specificity of the stimulation is questionable.

In cat, the rostromedial dorsal accessory olive receives input from the spinal trigeminal nucleus (Berkley and Hand, 1978), and responds to ipsilateral stimulation to the face (Gellman, Houk, and Gibson, 1983). It is possible that HVI lesions, by causing degeneration of these olivary neurons, deprive the anterior interpositus of collateral fibers containing US-related information. Hence, HVI lesions may produce CR impairment because of the effect such lesions have on nucleus interpositus.

The relationship of the DLP/SR to the cerebellar circuit is an issue which will be treated in the Discussion, but suffice it to say that there are probably no direct SR connections with red nucleus, HVI, or nucleus interpositus. For the present, it is useful to consider the SR/DLP as a circuit separate from and parallel to the cerebellar circuit.

Goals of The Present Study

Multiple-unit recordings in the DLP suggested that the SR is a locus of excitatory CR-related neural activity, and that the increase in activity leads the CR by 40-50 ms (Desmond and Moore, 1983). One problem with this interpretation is that multiple-unit activity may be recorded from the axons of neurons in other regions of the brain. A second problem is that individual firing patterns of units are lost in multiple-unit recordings. One cannot determine, for example, if the rate of firing of a neuron tends to increase as the CR amplitude increases, as observed in the hippocampus (Berger and Thompson, 1978), or if the rate transiently increases at the onset of the CR. In addition, if inhibitory as well as excitatory CR-related units are present, the sum of the activity would mask the inhibitory contribution, leaving an erroneous impression of the spike/behavior relationships.

Thus, one goal of the present study is to record from single units in the DLP during conditioning and compare the location of CR-related recordings with those from the multiple-unit study. High-impedance recording electrodes are likely to record from cell bodies rather than axons (Schlag, 1978). If the multiple-unit recordings from the SR were obtained mostly from axons of passage, then the anatomical distribution of CR-related single-unit recording sites might differ from those of the multiple-unit study. The temporal relationships of the spikes and the CR will be assessed to determine whether unit activity leads or follows the behavior.

The amount of time by which an increase or decrease in a cell's firing precedes the CR is important in determining whether the cell could be causally involved in the generation of the CR. By considering the reflex arc, the minimum amount of lead-time consistent with causal involvement can be estimated. Berthier and Moore (1983) found that periocular stimulation elicits a response in AAN with a 4 ms latency. Once AAN motoneurons are activated, it takes 5.5 ms for conduction to retractor bulbi muscles, synaptic transmission, and recruitment of retractor bulbi muscle fibers to occur (Quinn, Kennedy, Weiss, and Disterhoft, 1984), and an additional 4 ms for the NM to initiate its sweep after eyeball retraction (Cegavske et al., 1976).

Summing these latencies yields a total of 13.5 ms between periocular stimulation and onset of the NM response, or 9.5 ms from AAN activation to NM response. One would predict, therefore, that a cell would have to lead the CR by more than 9.5 ms in order for that cell to be causally involved in generating the CR. However, 9.5 ms may be an underestimation because very strong stimuli were used to elicit the NM response, and hence, the rate of recruitment of AAN motoneurons was probably more rapid than would be expected during normal generation of the CR. On the basis of response latencies observed for weaker eliciting stimuli, Moore and Desmond (1982) have suggested that neuronal activity should lead the CR in excess of 25 ms before being considered for causal involvement.

The SR was implicated in the conditioned NM response not only on the basis of CR-related multiple-unit activity but also by the labeling of neurons in SR subsequent to HRP administration to AAN. A second goal of the present study is to test the hypothesis that the cells in SR that project to AAN are the same cells responsible for the CR-related unit activity. Thus, units displaying conditioned activity will be tested for antidromic responses to AAN stimulation. Positive evidence of antidromic activation would not, however, prove that a neuron synapses on AAN; such proof would require intracellular recording and subseqent labeling with HRP.

A third goal of the present report is to develop a methodology whereby CR-related unit activity can be distinguished from activity that is not related to the CR. The typical procedure for analyzing spike/CR relationships is to tape record during the presentation of conditioning trials the unit activity and CRs from a well-trained rabbit. The spike activity is then converted into a peristimulus time histogram (PSTH), which depicts cumulative spike counts in discrete time periods before, during, and after the CS onset. The CRs over all the conditioning trials are depicted as one averaged CR, and visual inspection is used to detect CR-associated changes in spike activity.

Although the PSTH is a very convenient means of summarizing both unit and CR activity, visual inspection is not always adequate for detecting CR-related trends. Small but significant spike/CR correlations do not become apparent by inspection until many trials are collected. In addition, CR-related excitation or inhibition is judged on the basis of perceived trends between the cumulative spike counts and the averaged CR. However, such perceived trends can be misleading, because the discharge pattern of the unit may have a time course similar to that of the CR, but the firing may be completely independent of the CR.

For example, the top panel of Figure 1 illustrates the PSTH and averaged CR over 16 trials for Cell 43. The abcissa for this graph represents time, and the ordinate represents both spike counts and CR amplitude. Time is divided into 10 ms bins, so the height of each vertical bar along the abcissa represents the spike counts within a particular 10 ms bin. Note that time is also divided into 3 major periods. The first period, represented along the abcissa from the origin to the first vertical bar, is referred to as the Pre-CS Period. Baseline activity of the

Figure 1

CR and non-CR PSTHs for Cell 43. Top: CR PSTH. Bottom: Non-CR PSTH. Abbreviations for this figure and subsequent figures: V.CAL. = Vertical calibration (for Y axis); CNTS = Spike counts. Time per bin and the number of trials for each PSTH are denoted in the figure. See text for further explanation.

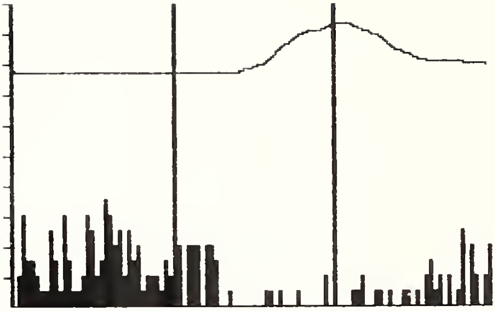

CELL: 43 TRIALS=16 CS=350 MS
BIN=10 MS V.CAL.=2 CNTS, 8 VOLTS

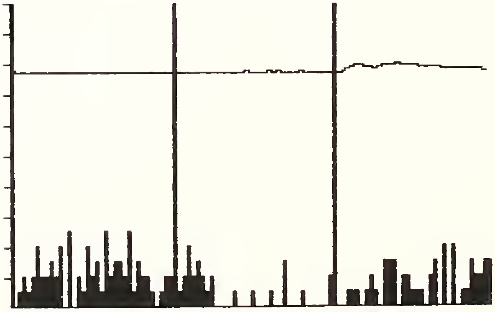

CELL: 43 TRIALS=10 CS=350 MS
BIN=10 MS V.CAL.=2 CNTS, 8 VOLTS

cell is collected during this period. The second period is referred to as the CS Period: the first vertical bar represents the CS onset, the second vertical bar its offset. The period extending from the second vertical bar to the end of the graph is referred to as the US Period, although a US is not always presented. The US occurs at the second vertical bar and coterminates with the CS during this 10 ms bin. The averaged CR is represented immediately above the histogram bars. An upward deflection of the tracing represents extension of the nictitating membrane. On CR trials, this extension occurs within the CS Period, as illustrated in the top panel of Figure 1.

Note also in the top panel of Figure 1 that the unit activity tends to decrease and remain inhibited during the performance of the CR, the inhibition beginning just prior to the CR onset. In the absence of any other information, one might conclude that the cell is displaying CR-related inhibition. However, the bottom panel of Figure 1 illustrates a PSTH for the same cell accumulated over 10 trials in which the CR did not occur. Note that the inhibition observed in the CS Period for the CR trials occurs at the same time and to the same degree for the non-CR trials. Thus, the inhibition is apparently not CR-related, and is more likely a delayed tone response that happens to occur with a latency similar to that of the CR. The non-CR trials were crucial in making this distinction.

Reliably obtaining both CR and non-CR trials during a recording session was a major methodological focus for this study. Initially, a single CS was used for this purpose. Paired CS-US trials were presented while a unit was recorded. When sufficient CR trials were obtained, the US was eliminated, and extinction trials were presented. The CRs eventually extinguished and the unit activity for non-CR trials was accumulated.

This method has two major disadvantages, however. The first is that the rate of extinction is highly variable and unpredictable across animals. In many instances, the cell was lost before extinction was complete. A second disadvantage is that CR and non-CR trials are obtained serially. If there are any time-dependent changes in the activity of the cell, due to injury or other factors, then a comparison of CR and non-CR activity can be misleading.

Thus, it was necessary to develop a procedure in which CR and non-CR trials could be obtained reliably and non-serially. A discrimination procedure, in which a reinforced CS+ and nonreinforced CS- are presented in a pseudorandom sequence, was adopted for this purpose. Initially, white noise and a 1200 Hz tone were used as the discriminative stimuli. However, these CSs were too easily discriminated, so that the rabbits made CRs exclusively to the CS+. It is preferable to obtain CR and non-CR trials for each stimulus so that differential auditory responses to CS+ and CS- are not mistaken for CR vs. non-CR activity. Consider, for example, a white noise CS+ which elicits a CR-independent excitatory neuronal response and a 1200 Hz CS- which does not alter baseline neuronal activity. If the rabbit makes CRs exclusively to the CS+, then the noise-related increase in activity might appear to be a CR-related phenomenon when compared to the non-CR activity of the CS-, depending on the time course of the noise-related response.

Because of its tendency to elicit auditory responses from many neurons, white noise was abandoned as a discriminative CS and replaced by a 600 Hz tone. Tones of 1200 Hz and 600 Hz have been used successfully in differential conditioning (see Moore, 1972), but the discrimination develops less rapidly than that of noise and 1200 Hz tone. The majority of rabbits in this study, therefore, received 600 Hz and 1200 Hz tones as discriminative stimuli.

Although discrimination training was generally successful in yielding CR and non-CR trials, an occasional rabbit discriminated too well or too little. Trial-by-trial correlation techniques developed for this study were especially helpful in these cases for assessing whether neuronal activity was related to the CR. Spike and CR information on individual trials, rather than across-trial averages, are utilized with these methods. For example, the number of spikes occurring in the CS Period and the magnitude of the CR are collected as pairs of data points over the training session. If on a trial-to-trial basis the CR magnitude tends to reliably covary with the number of spikes--that is, if these variables are significantly correlated--then the neuronal firing is CR-related. For Cell 43 in Figure 1, CR magnitude was not correlated with the number of spikes, consistent with the visual inspection of CR and non-CR PSTHs.

The power of the correlational technique is maximized when the full range of the variables is sampled, so it is advantageous to have both CR and non-CR occurrences. However, even in the absence of non-CR trials, there is often sufficient variability among the CRs to detect spike-CR relationships, if they exist. Note that obtaining a significant correlation does not address lead or lag time of the spike activity relative to the CR. Other methods were used for assessing temporal relationships. The trial-by-trial correlation techniques and other statistical tools developed for this study are fully described in the next chapter.

CHAPTER II

METHOD

Data Acquisition

Subjects

The experimental subjects in this study were 31 male and female New Zealand albino rabbits obtained from a licensed supplier. Animal weights ranged from 2.5-4.0 kg, but best results were obtained from animals weighing 3-4 kg. This was due to the larger skull size and greater skull thickness of the heavier animals. The rabbits were individually housed and given ad libidum access to food and water.

Conditioning Procedures

Rabbits were given approximately 3 days of pre-surgical discrimination training. The conditioning cage used during electrophysiological recording was capable of training only one rabbit at a time. However, it was desirable to keep a pool of trained animals ready for surgery. Thus, pre-surgical training was conducted in a different apparatus, where as many as 4 rabbits could be conditioned simultaneously. This apparatus was constructed from ventilated, fire-proofed, and sound attenuated filing cabinets. Programming equipment was kept in an adjacent room, and fans in the conditioning room provided background noise.

Rabbits were restrained in a Plexiglas apparatus (Gormezano, 1966). The CS+ and CS- were either 1200 or 600 Hz sinusoidal tones (counterbalanced) of 350 ms duration and 75 db SPL intensity, presented in a pseudorandom sequence. CSs were presented by speakers mounted in front of the animal. The US, a 10 ms, 1 mA (ac) electrostimulation to the periorbital region, coterminated with the CS+ in a forward delay conditioning procedure. The US was delivered via 9-mm stainless steel wound clips to which alligator leads from the stimulus source were attached. These clips were crimped within 3 mm of the marginal region of the right eye: one located in an inferior position and the other in a posterior position.

CRs and URs were recorded using a head-mounted mini-torque potentiometer which was connected by thread and a small hook to a loop of suture on the right NM. Movement of the membrane created a dc signal which was amplified and recorded on an ink-writing oscillograph. CRs were defined as a 0.5 mm extension of the NM, measured by an upward pen deflection of at least 1 mm, occurring after CS onset but before US onset. The intertrial interval was 15 sec., and training consisted of 100 trials (50 for each CS) per day. The animals were trained to partially discriminate between CS+ and CS- so that CR and non-CR occurrences to both stimuli would occur during subsequent recording. CRs to CS+ and CS- initially developed with nearly equal likelihoods of occurrence. Training was usually terminated when CRs to CS+ exceeded 60% and CRs to CS- were at least 25% below responses to CS+.

The conditioning procedures were modified slightly for electrophysiological recording. Conditioning was conducted in an electrically shielded chamber that was not sound-attenuated. Low levels of light were provided for the convenience of the experimenter. Background noise was provided by a white noise generator (65 dB SPL). To minimize electrical artifacts, the US was a single dc pulse of .05-0.5 ms in duration and up to 10 mA in intensity, delivered via a Grass S88 stimulator and a Grass SIU8 stimulus isolation unit. The intertrial interval was lengthened to 20 sec. The head of the animal was immobilized (described below), and the mini-torque potentiometer was mounted to the immobilization device rather than on the head of the rabbit. CRs were monitored on a storage oscilloscope. Although the changes in the conditioning apparatus dramatically altered the contextual cues, the training obtained in the previous conditioning apparatus transferred rapidly in the new environment.

Surgery

Following discrimination pre-training, the rabbits were surgically prepared for subsequent recording. The animals were anesthetized with sodium pentobarbital (20-25 mg/kg, i.v.) 30-45 minutes after receiving a chlorpromazine pretreatment (4 mg/kg, i.m.). The head was shaved, Xylocaine was applied to the scalp, and the rabbits were positioned in Kopf Model 900 stereotaxic instrument equipped with a rabbit head holder. A midline incision was made in the scalp and the skull was exposed. The skull was aligned such that Bregma was 1.5 mm above Lambda. A dental drill was used to make 5 holes in the skull. The recording hole was placed 13-15 mm posterior to Bregma and about 3 mm lateral to midline on the right side. The diameter was 1-2 mm, and care was exercised to prevent puncture of the dura. A second hole was positioned 14-15 mm posterior to Bregma and 2-3 mm lateral to midline on the left side for the AAN stimulating electrode. The 3 remaining holes, drilled in a "keyhole" shape, were used for anchoring screws. One was placed laterally on the right and about 10 mm posterior to Bregma, the second in a corresponding position on the left side, the third rostral to Bregma and just lateral to the midline on the right side.

Stainless steel machine screws with flattened heads were placed inverted into the wide part of the keyhole and then moved forward into the narrow part of the keyhole. A nut was fastened on top so that the skull was wedged between the nut and the flat head of the screw. The rostral anchoring screw served as the indifferent electrode for recording. It was important to use no fewer than 3 anchoring screws so that a rabbit could not dislodge the pedestal by fidgeting.

A coaxial stimulating electrode (Rhodes SNE-100) was then implanted into the right AAN via a contralateral approach. The electrode was placed in an electrode carrier, and its leads were connected to a stimulus source (Grass S4 stimulator, stimulus isolation unit, and constant current unit). The electrode was angled 11 degrees in the coronal plane for an approach beginning 2 mm left of midline. The electrode tip was placed on Bregma and the dorsal-ventral height was measured. The posterior coordinate for the implant was calculated using a modification of the Gray et al. (1981) equation. The electrode was then lowered approximately 22 mm relative to the height of Bregma. Trains of stimulus pulses (20-30 Hz, 30 microamps, .025 ms duration) were manually delivered as the electrode was lowered. Eyeball retraction and NM responses to the stimulation guided final placement. Twitching of the right ear and face was frequently observed, presumably due to facial nerve activation. The electrode was fastened in place with dental cement.

Recording pedestals, approximately 35 mm long, were hollowed out of 1/2 inch diameter stainless steel bolts. The bottom 5 mm of each pedestal was machined into a shaft with an external diameter of 9 mm and an internal diameter of 6 mm. A nut was fastened just above the shaft, providing a flat surface at the base of the pedestal with 15-20 mm of the bolt extending above the nut. The portion of the bolt above the nut was subsequently used to immobilize the head during recording. The pedestal was stereotaxically manipulated over the recording hole and cemented in place. The pedestal was filled with mineral oil and covered. Neosporin powder was applied to the exposed skin, and the rostral and caudal ends of the incision were sutured. The rabbit was removed from the stereotaxic device and allowed a 1-2 day recovery period.

Electrophysiological Recording

Stable single-unit recording in the awake rabbit required immobilization of the head. The apparatus for accomplishing this (designed and manufactured by Dr. Neil Berthier) consisted of a heavy steel plate upon which the rabbit, in a Plexiglas restrainer, sat. Attached perpendicularly to the plate were 2 aluminum bars (which will be referred to as vertical bars) positioned on either side of the Plexiglas restrainer. A detachable horizontal bar stretched across the top of the vertical bars. The rabbit's pedestal fit through a hole in the center of the horizontal bar, and a nut fixed the pedestal in place. The potentiometer for measuring NM movement was attached to the vertical bar closest to the rabbit's right eye. The electrode carrier, with coarse adjustment controls along 3 axes, was attached to the horizontal bar. A Trent-Wells hydraulic micromanipulator provided fine control of dorsal/ventral electrode movement.

After recovery from surgery, each rabbits was placed in the novel conditioning apparatus and allowed to reestablish conditioned responses. No attempt was made to record from units during this session. Most rabbits appeared to rapidly habituate to head restraint, and could tolerate it for at least 2 hours. Occasionally, a rabbit had to be placed in a cloth restraining sleeve to prevent it from kicking. The animals were given discrimination training, and differential responding to CS+ and CS- usually reappeared within 100-200 trials.

The inside of the pedestals was cleaned daily by aspiration to prevent excess accumulation of blood or scar tissue on the surface of the dura. This procedure was performed under the guidance of a dissecting microscope and fiber-optic illumination while the animal was in the restraining device. Optimal unit recordings were obtained within 2-3 days of surgery, before the dura could accumulate excessive clotting and scar tissue. Occasionally, melted bone wax had to be applied to the drill hole to stop excess bone bleeding. Mineral oil was always replaced in the pedestal to prevent the dura from drying.

When a rabbit was ready for recording, an Epoxylite-insulated tungsten recording electrode (Frederick Haer & Co., 10-15 megohm impedance) was coarsely positioned over the dura under microscopic guidance. Using the Trent-Wells microdrive, the electrode was advanced through the dura and into the brain stem. Neural activity was amplified by a WPI battery powered differential ac preamplifier, filtered at 0.3-10 kHz.

CS+ and CS- trials were presented while unit activity and CRs were monitored on a Tektronix storage oscilloscope. A Keyboard-Interfaced Microprocessor (KIM) controlled stimulus timing, tape recorder onset and offset, oscilloscope triggering, and synchronization pulses. Software for the KIM was obtained from a published report (Solomon, Weisz, Clark, Hall, and Babcock, 1983). However, the program was modified to code the trial type (CS+ or CS-) in the synchronization pulse timing. An interface for the KIM (Solomon et al., 1983) activated the solid state relays controlling the CSs, US, and tape recorder.

Units were typically sampled throughout the 15 mm dorso/ventral excursion of the Trent-Wells micromanipulator. The length of time in which a unit could be recorded depended largely on the temperament of the rabbit. Some rabbits sat quietly for 3 hours or more with no signs of distress, but for most rabbits, the frequency of fidgeting tended to increase after 1-2 hours, and recording had to be discontinued. For most recordings, units could be held during minor movements of the rabbit.

Whenever a unit with a sufficient signal-to-noise quality and stability appeared to display CR-related firing patterns, that unit was taped for future analysis. Unit activity was fed into an FM input to a Crown-Vetter tape recorder (15 ips). A second FM plug-in was used to tape record the NM response. A third channel of the tape recorder (audio) received synchronization pulses marking the beginning of the trial.

With sufficient training, some rabbits learned to completely discriminate CS+ and CS-. Because it was desirable to have both CR and non-CR trials for at least one CS, two auxiliary procedures were used to generate the two trial types. The first was to remove the US in an attempt to extinguish the previously reinforced CS. Consistent with the reports of Moore (1972), rabbits which received discrimination training were less resistant to extinction than rabbits given only excitatory conditioning. After sufficient non-CR trials were collected, the US was reinstated, often resulting in the rabbit giving CRs to both CS+ and CS-. The second procedure was to introduce CSs of different frequencies (i.e., generalization). For example, a rabbit differentiating a 1200 Hz CS+ from a 600 Hz CS- might be presented with an 800 Hz tone located between the excitatory and inhibitory generalization gradients.

To test for antidromic activation, the AAN electrode was stimulated using single pulses of .01-.10 ms duration and up to 150 µA. Current and pulse duration were adjusted to determine threshold of activation. Multiple traces were displayed on a storage oscilloscope to determine variance of response latency, and were photographed with a Polaroid camera. High frequency twin pulses were used to test the frequency-following capabilities of the evoked spikes. Fuller and Schlag (1976) have outlined typical characteristics of antidromically activated units: (1) a stable and sharp threshold of activation, (2) latency of response varying less than 0.2 ms at intensities just above threshold, (3) ability to follow stimulation at frequencies of 100 Hz or more, and (4) collision of the antidromically elicited spike with a spontaneously occurring spike.

At the completion of the session, recording positions were marked by passing cathodal current through the recording electrode (25 µA for 15 seconds) at selected depths. A second track was made on subsequent recording sessions, but more than two tracks were rarely made. The rabbits were sacrificed 1-3 days after the recording track lesions were made, and were perfused transcardially under deep sodium pentobarbital anesthesia. Isotonic saline followed by 10% formaldehyde was gravity fed into the left ventricle. Brains were stored in 10% formaldehyde for 3 days followed by a 30% sucrose-formaldehyde solution for 7 days. The brains were sectioned at 40 µm in the coronal plane, mounted on slides, and stained with cresyl violet (0.5%) or neutral red (1%). Electrode positions were identified by the dark-staining gliosis along the recording track.

Procedural Exceptions

As noted in the Introduction, two early conditioning procedures for obtaining CR and non-CR trials were abandoned in preference for the present discrimination protocol described above. The data obtained from these procedures are included in this report. Rabbits 02-17 were presented with a single 1200 Hz tone CS. CR trials were obtained using paired CS-US presentations, while non-CR trials were obtained by eliminating the US and presenting extinction trials. Rabbits 18-35 were trained to discriminate between a white noise and a 1200 Hz tone; these rabbits are otherwise identical to those trained to discriminate 600 and 1200 Hz tones.

Data Analysis

Off-line Digitizing

Tape recorded unit activity and NM responses were digitized using an Apple IIe microcomputer. Spikes were passed through a window discriminator, which converted spikes of preselected amplitude into TTL pulses recognizable to the Apple. The NM responses were passed through an 8-bit A/D converter. For each taped trial, the synchronization pulses marking trial onset started a timer which enabled spike counts and the A/D output to be collected in 10 ms time bins. Three 350 ms time periods were collected, for a total of 105 bins per trial. The first time period was a Pre-CS Period, for establishing baseline activity, the second period was a CS Period, the third a US Period. Data were temporarily stored in a buffer memory in the Apple IIe. Each 10 ms bin required one byte for spike counts and one byte for the digitized NM response, for a total of 210 bytes per trial. An additional 18 bytes per trial were used to designate trial type and store other system information, for a grand total of 228 bytes per trial. Blocks of trials (usually 10 trials/block) were transferred from RAM to floppy disk, then sorted into CS+ and CS- trial types. Further analyses, described below, were also performed on an Apple IIe microcomputer.

Conventions for Naming Cells

The following conventions were used to organize and describe cell data. The first two digits in the cell name refer to the animal number. If more than one cell was obtained from an animal, then the first cell digitized has the number of the animal, while subsequent cells have a letter after the animal number. So, for example, 43, 43A, 43B designate 3 different cells from rabbit number 43.

If, in a table or illustration, a cell is referenced by a 2 or 3 character code only (such as 43A), then the CS+ and CS- data were pooled. However, if the cell name is followed by a period and a number, then the data are derived from a specific CS. The number following the period is the frequency of the CS divided by 100. If an "N" follows the period, then the CS was white noise. For example, 61B.6- refers to the 600 Hz CS for Cell 61B. The minus after the 6 indicates that it is nonreinforced. A plus would indicate reinforced trials only. An absence of a plus or minus indicates a mixture of reinforced and nonreinforced trials.

Peristimulus Time Histograms

The PSTH was discussed in the Introduction, and the drawbacks of using the PSTH to infer spike/CR relationships in the absence of Non-CR occurrences were noted (see Figure 1). The PSTH is nevertheless a useful and widely adopted means of summarizing unit activity and the CR, especially when interpreted in conjunction with other statistical techniques discussed below. Thus, the first step in data analysis after digitizing the taped spike and CR information was the construction of PSTHs.

CS+ and CS- trials were separately analyzed. Raw data for each block of trials were read by the Apple, and each trial was examined via an automated inspection routine to determine whether it was a CR or non-CR trial type. Every block of 10 trials was printed so that classification accuracy could be verified. Depending upon the responses of the rabbit to each CS, a maximum of 4 PSTHs were created for each cell, consisting of CR and non-CR trials for both CS+ and CS-.

One method of testing the statistical significance of neural activity in the CS Period and US Period is to obtain the mean and standard deviation of the spike counts in the Pre-CS Period (each bin is one observation) and perform a t-test using the following formula:

t = (Spikes in bin - Pre-CS Mean) / Standard deviation

The degrees of freedom are the number of Pre-CS bins minus 1 (34 for all PSTHs in this report). Figure 2 illustrates the use of this method. A dot above a bin indicates that the bin is statistically different from the Pre-CS mean at the .05 level (two-tailed tests). Whether a significant bin is greater or less than the mean can be inferred by

Figure 2

CR and non-CR PSTHs for Cell 07. Top: CR PSTH. Dotted line indicates CR onset at 5% maximum deflection. Bottom: Non-CR PSTH. For this figure and subsequent figures, spike counts that are significant relative to the mean baseline spike count are indicated by dots above the histogram bars (t-test, 34 degrees of freedom, 2-tailed, $p < .05$).

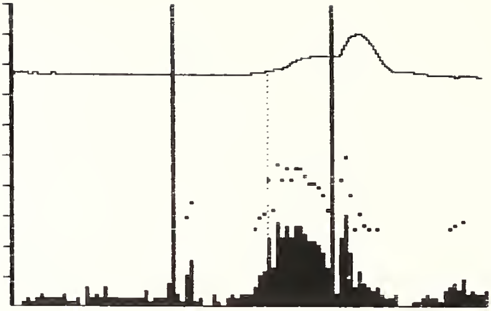

SUB: 07 CR TRIALS=19 CS=350 MS
BIN=10 MS V.CAL.=8 CNTS, 10.66 VOLTS

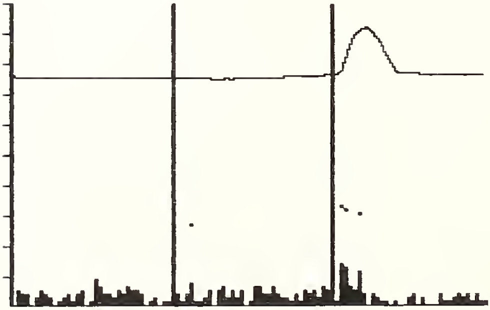

SUB: 07 NO CR TRIALS=11 CS=350 MS
BIN=10 MS V.CAL.=8 CNTS, 10.66 VOLTS

inspection. In Figure 2, note that the CR onset (defined as either 1% or 5% of the maximum CR deflection; 1% was used only for large CRs with very stable baselines) is represented by the dotted vertical line extending from the CR trace to the histogram bars. The number of significant bins to the left of the CR onset line, excluding those bins shortly after the tone response, may be used as a measure of the lead time (or lag time) of spike activity over the behavior.

This method of testing statistical significance has disadvantages, which are illustrated in Figures 3 and 4 (top and middle panels). In Figure 3, note that the pre-CS activity for Cell 02A is very low for both CR and non-CR trial types. Consequently, nearly every CS Period and US Period bin is significantly different from the pre-CS mean (not illustrated in the figure). An increase in activity is evident for both trial types, perhaps due to an excitatory tone response, yet a greater neuronal response occurs on CR trials than on non-CR trials. Thus, one consideration in testing significant bins is that CS Period activity may contain both tone and CR-related firing.

In Figure 4, which represents data from Cell 35A, a comparison of CR and non-CR PSTHs suggests a CR-related decrease in firing occurs, yet none of the CS Period bins are significantly different from the Pre-CS Period mean for either trial type. Relying exclusively on the

Figure 3

CR PSTH, non-CR PSTH, and binomial histogram comparison for Cell 02A. Top: CR PSTH. Middle: Non-CR PSTH. Bottom: Binomial PSTH comparison. For this and subsequent binomial histogram comparisons, the bin size used for comparison is indicated below the graph (30 ms in this figure). Bars extending above the X axis depict CR unit activity that is excitatory relative to non-CR activity. Bars extending downward depict inhibitory CR unit activity relative to non-CR activity. Levels of significance are indicated on the Y axis.

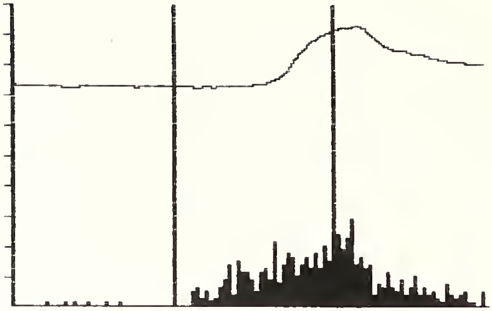

CELL: 02A   TRIALS=33   CS=350 MS
BIN=10 MS   V.CAL.=8 CNTS, 8 VOLTS

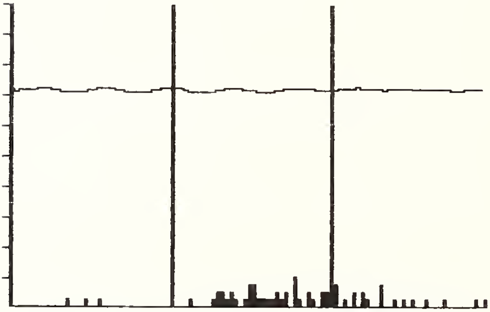

CELL: 02A   TRIALS=12   CS=350 MS
BIN=10 MS   V.CAL.=4 CNTS, 8 VOLTS

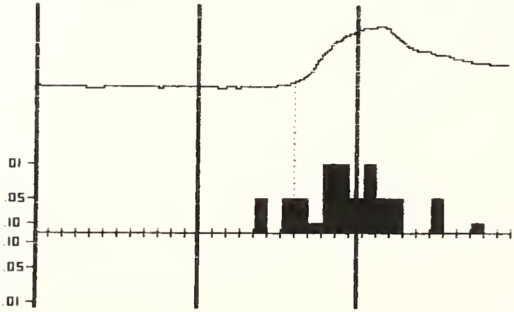

CELL: 02A   BIN: 30 MS   CS: 350 MS
BINOMIAL HISTOGRAM COMPARISON
CR ONSET AT 5% MAX AMP

Figure 4

CR PSTH, non-CR PSTH, and binomial histogram comparison for Cell 35A. Top: CR PSTH. Middle: Non-CR PSTH. Bottom: Binomial PSTH comparison. Note that 4 post-US bins are omitted because of stimulus artifact.

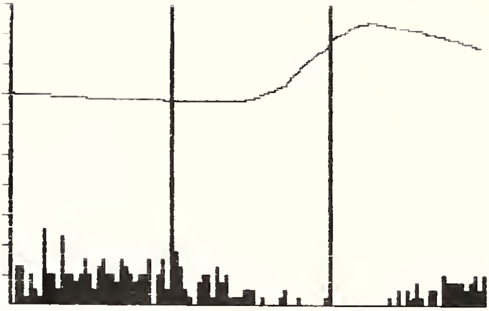

CELL: 35A TRIALS=31 CS=350 MS
BIN=10 MS V.CAL.=4 CNTS, 8 VOLTS

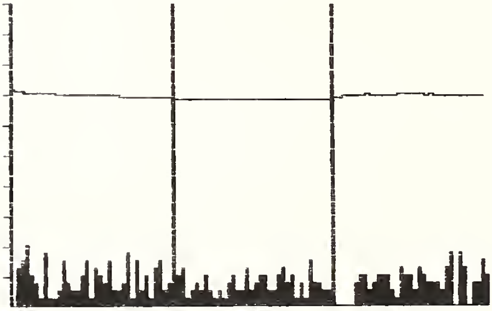

CELL: 35A TRIALS=30 CS=350 MS
BIN=10 MS V.CAL.=4 CNTS, 8 VOLTS

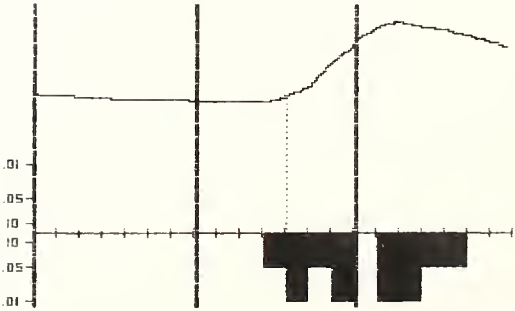

CELL: 35A BIN: 50 MS CS: 350 MS
BINOMIAL HISTOGRAM COMPARISON
CR ONSET AT 1% MAX AMP

significant bin method, one might dismiss the apparent inhibition as nonsignificant. However, the lack of significance is probably the result of a floor effect, because more sensitive correlational techniques introduced below confirm that the apparent CR-related inhibition is genuine.

Binomial PSTH Comparisons

If CR and non-CR trial types are collected for the same cell, then a comparison of neuronal response rates during corresponding time periods can be performed using a method suggested by Dorrscheidt (1981). Assuming under the null hypothesis that response rates are identical for CR and non-CR trials, then the distribution of the total number of CR and non-CR spikes should be proportional to the number of CR and non-CR trials.

To illustrate the use of the method, refer to the bottom panel of Figure 4. Note that 50 ms time periods are being compared, i.e., starting at the beginning of the Pre-CS Period, spike counts for five consecutive 10 ms bins are summed into larger 50 ms bins. In the bottom panel of Figure 4, the hash marks along the horizontal axis represent 50 ms bins. Let: $T1$ = number of CR trials (31 in this case), $T2$ = number of non-CR trials (30), $T = T1 + T2$, $p = T1 / T$, $q = T2 / T$. For each 50 ms period, let: $n1$ = number of spikes in CR histogram during that period, n2 = number of spikes in non-CR histogram during that period, and N = n1 + n2. The expected value of the number of spikes in the CR histogram during that time period is Np. Looking at the last 50 ms before the US, if there are n1 = 2 spikes for the CR histogram and n2 = 16 spikes in the non-CR histogram, then N = 18. T1 and T2 are nearly equal, so for this example the approximation p = q = .5 is adequate. Thus, the expected number of spikes in the CR histogram would be Np = 9, and the actual number, n1 = 2, is below expectation. To test whether it is significantly below expectation, compute :

$$\text{prob} = \sum_{i=n2}^{N} \binom{N}{i} p^{N-i} q^{i}$$

For this example, prob = .000656, which is significant below the .01 level. Thus, in Figure 4, the binomial histogram comparison has a downward bar extending to the .01 mark on the abcissa during this 50 ms time period. The downward direction indicates that the CR bin is inhibitory relative to the non-CR bin. An upward direction, as illustrated in the bottom panel of Figure 3, depicts CR excitation relative to the non-CR trials. As N gets large, a normal approximation to the binomial with mean of Np and standard deviation equal to the square root of Npq can be used to compute a Z score.

In comparing CR and non-CR activity in this manner, extraneous variables, such as neuronal excitation or inhibition originating from the tone itself, are presumably held constant, and the observed differences are theoretically due to the CR alone. Any time-dependent changes in firing patterns are assumed to be reflected equally among CR and non-CR trial types.

One disadvantage to this method is that it is insensitive to trends in firing pattern, because every bin is evaluated independently of previous bins. Another disadvantage is that, while larger bin sizes require less of a rate differential to yield significance than smaller bins do, inferences concerning temporal relationships of spike activity and the CR are less precise when larger bins are analyzed. Thus, this method is not the most sensitive method for determining latency differences.

CR Onset Histograms

PSTHs illustrate unit and behavioral responses relative to stimulus onsets. This type of histogram is especially useful for examining stimulus-locked unit responses. It is not satisfactory, however, for demonstrating behavior-dependent responses, particularly when the behavior varies in its time of occurrence. A better illustration of behavior-dependent responses is provided by CR onset histograms. This type of histogram depicts neuronal activity relative to the onset of the CR, defined as the time when the amplitude reaches 5% of the maximum amplitude.

The bottom panel of Figure 5 illustrates a CR onset histogram for Cell 46C. The zero point along the abcissa represents the CR onset time for each CR trial. The CS onset time on the graph can be approximately located by using the mean and standard deviation of the CR latency from CS onset, which was 166.15 ms and 36.95 ms, repsectively, and locating this time to the left of the zero point. The approximate US onset time is equal to 350 - 166.15 = 183.85 ms, and is located to the right of the zero point.

Note in the upper panel of Figure 5 how the increased unit activity appears to be spread out before and after the CR onset. In contrast, the CR onset histogram clearly shows the bulk of the unit activity occurring prior to CR onset.

Multiple Correlation and Regression

PSTHs and CR onset histograms are both somewhat limited because they depict the averaged responses of the CR and the unit activity over all trials. The differential conditioning paradigm used in this study was designed to maximize CR variability over trials, but this variability is lost in the averaging process. Correlation and regression techniques were used to examine the

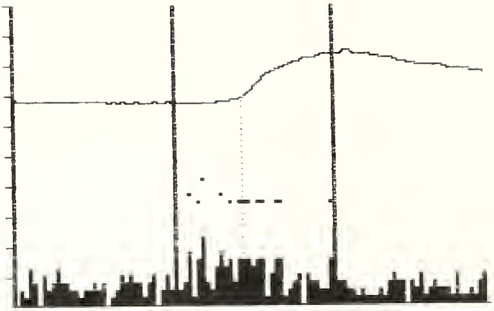

SUB: 46C TRIALS=52 CS=350 MS
BIN=10 MS V.CAL.=4 CNTS, 8 VOLTS

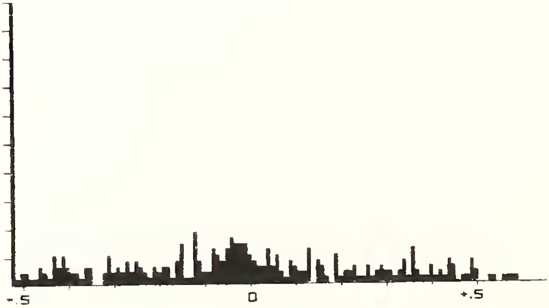

CR ONSET HISTOGRAM FOR CELL 46C
TRIALS=52 BIN=10 MS V.CAL=5 CNTS

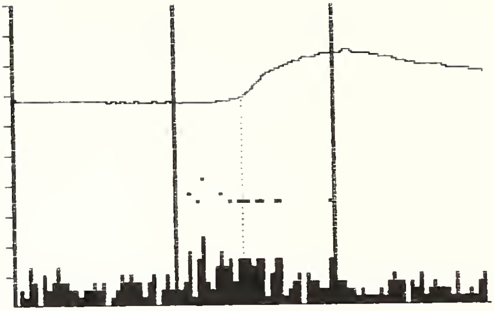

SUB: 46C TRIALS=52 CS=350 MS
BIN=10 MS V.CAL.=4 CNTS, 8 VOLTS

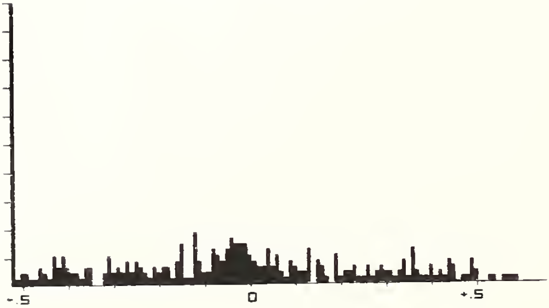

CR ONSET HISTOGRAM FOR CELL 46C
TRIALS=52 BIN=10 MS V.CAL=5 CNTS

relationships between the unit activity and the CR at the trial level.

For all correlational analyses, spike and CR data were sampled exclusively from the 350 ms CS Period. The US Period was not analyzed because it was desirable to pool reinforced and nonreinforced trials, and the presence of US-related responses on some trials but not others could increase error variance. Behavioral variables (treated as dependent variables in regression analyses) of interest were CR onset latency (LA) and CR magnitude. Two measures of CR magnitude were used. CR area (AR) was defined as the sum of the amplitudes of the CR trace relative to baseline over all 10 ms bins in the CS Period, and maximum CR amplitude (MA) was defined as the maximum CR deflection from baseline during the CS Period. Preliminary analyses indicated that spike activity for some cells was more closely correlated with CR area than with maximum CR amplitude, whereas for other cells the converse was true. For still other cells, activity was correlated with both measures of magnitude, each in a qualitatively different manner.

Three spike variables (which were treated as independent variables in regression analyses) were analyzed. The first was the number of spikes (ns) occurring in the CS Period. The second variable was the mean spike time (mt), obtained by summing the time bin numbers for each spike in the CS Period and dividing by the total number of spikes in the period. This variable was included to examine possible correlations between temporal shifts in the distribution of the spikes and the CR. However, because it is possible to observe considerable differences in the temporal distribution of the spikes while the mean remains practically unchanged, a third variable, standard deviation of spike time (ds), was analyzed. This variable provided a measure of temporal dispersion of the spikes, and was obtained by simply computing the standard deviation of the bin times for the spikes in the CS Period. (Note that for convenience, CR variables are abbreviated in uppercase letters and spike variables are in lowercase.)

Thus, for each cell, CR magnitude and CR latency were separately regressed on all three spike variables. Backward elimination (F to remove = 2.0) was used to determine the best set of predictors (Pedhazur, 1982). Scatterplots, such as those in Figures 6 and 7, were generated by computer. The bottom panel of Figure 6 displays AR as a function of ns for Cell 02A (refer to Figure 3 for PSTHs). Figure 7 illustrates a scatterplot of AR as a function of mt for an inhibitory cell (Cell 17A). For all cells analyzed, inspection of scatterplots suggested that linear, rather than polynomial, regression was sufficient for describing spike/CR relationships.

Figure 6

Cross-correlations and scatterplot for Cell 02A. Top: Correlogram obtained when the averaged CR is cross-correlated with CR-associated spike counts. Abcissa depicts the number of 10 ms bins the CR was shifted backward (negative) or forward (positive) in time. Each hash mark represents 2 bins. Ordinate depicts the value of the Pearson r, ranging from +1 to -1. A peak value of r to the left of zero (negative side) indicates that spike activity leads the CR; a peak to the right of zero indicates that the CR leads the spike activity. Maximum absolute value of r obtained at -120 ms ($r = .808$, $Z = 7.7$, $N = 92$, $p < .05$). Middle: Correlogram obtained when averaged CR is cross-correlated with non-CR spike counts. Bottom: Scatterplot and least squares regression line of CR area as a function of the number of spikes in the CS Period.

Figure 6

Cross-correlations and scatterplot for Cell 02A. Top: Correlogram obtained when the averaged CR is cross-correlated with CR-associated spike counts. Abcissa depicts the number of 10 ms bins the CR was shifted backward (negative) or forward (positive) in time. Each hash mark represents 2 bins. Ordinate depicts the value of the Pearson *r*, ranging from +1 to -1. A peak value of *r* to the left of zero (negative side) indicates that spike activity leads the CR; a peak to the right of zero indicates that the CR leads the spike activity. Maximum absolute value of *r* obtained at -120 ms ($r = .808$, $Z = 7.7$, $N = 92$, $p < .05$). Middle: Correlogram obtained when averaged CR is cross-correlated with non-CR spike counts. Bottom: Scatterplot and least squares regression line of CR area as a function of the number of spikes in the CS Period.

Figure 7

CR PSTH, non-CR PSTH, and scatterplot for Cell 17A. Top: CR PSTH. Dotted line indicates CR onset at 5% maximum deflection. Middle: Non-CR PSTH. Bottom: Scatterplot and least squares regression line of CR area as a function of the mean spike time in the CS Period.

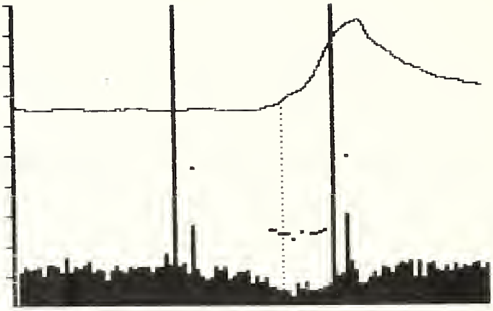

SUB: 17A TRIALS=34 CS=350 MS
BIN=10 MS V.CAL.=16 CNTS, 8 VOLTS

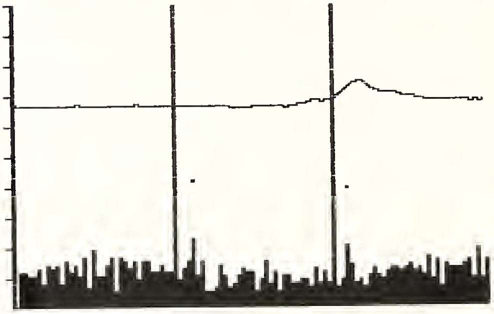

SUB: 17A TRIALS=16 CS=350 MS
BIN=10 MS V.CAL.=8 CNTS, 8 VOLTS

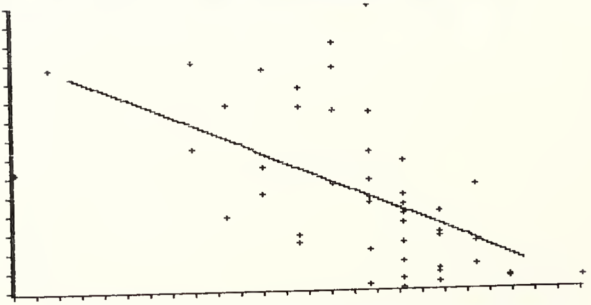

SCATTERPLOT: X=MN SPK TIME, Y=CR AREA
CELL: 17A TRIALS: 49
MIN, MAX VALUES: X=4,20 Y=0,537
HASH MARK CAL.: X=.6, Y=35.8

To increase statistical power, CS+ and CS- trials were pooled whenever possible. Scatterplots were important for determining whether such pooling was appropriate. For example, if CS+ produced a tone-related increase in unit activity and CS- did not, and if CS+ resulted in larger magnitude CRs than CS-, then the correlation of ns and CR magnitude might be spuriously high when CS+ and CS- trials were pooled. However, the scatterplot would reveal separate clusters of points rather than a continuous distribution. PSTHs for CS+ and CS- trial types were also individually inspected prior to pooling. Figure 8 reveals dramatically different unit responses to CS+ and CS- for Cell 61B. A profound inhibitory tone response occurs for a 1200 Hz CS+ (bottom right), but not for a 600 Hz CS- (top left), so pooling was not appropriate. However, analysis of CR and non-CR trials generated in response to CS- was still possible. The binomial histogram comparison for CS- is illustrated in the top right panel of Figure 8.

In this study, the presence or absence of significant correlations was used to distinguish cells which were CR-related from those which were not. Further distinctions were made among CR-related cells based upon the types of correlations that were observed, and these distinctions are discussed in the Results.

Figure 8

PSTHs and binomial histogram comparison for Cell 61B. Top left: CR PSTH for nonreinforced 600 Hz tone (CS-) trials. Dotted line indicates CR onset at 5% maximum deflection. Bottom left: Non-CR PSTH for nonreinforced 600 Hz tone trials. Top right: Binomial comparison for PSTH's depicted in left column. Bottom right: CR PSTH for reinforced 1200 Hz tone (CS+) trials. Note the tone-related depression of neural firing in the CS Period, and how the tone response differs from the 600 Hz CS (graphs in left column). This illustrates a case where CS+ and CS- trials cannot be pooled for correlational analyses.

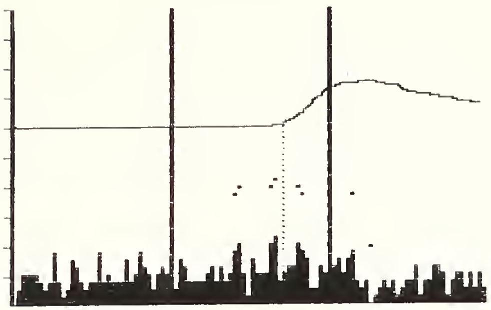

SUB: 61B.6- CR TRIALS=6 CS=350 MS
BIN=10 MS V.CAL.=4 CNTS, 16 VOLTS

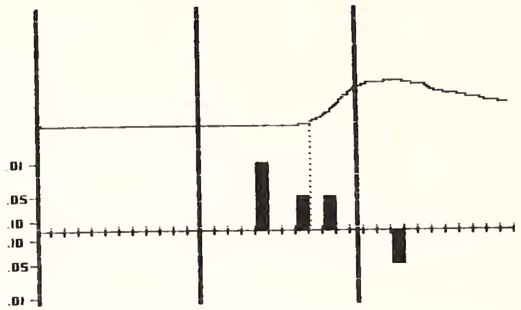

CELL: 61B BIN: 30 MS CS: 350 MS
BINOMIAL HISTOGRAM COMPARISON
CR ONSET AT 5% MAX AMP

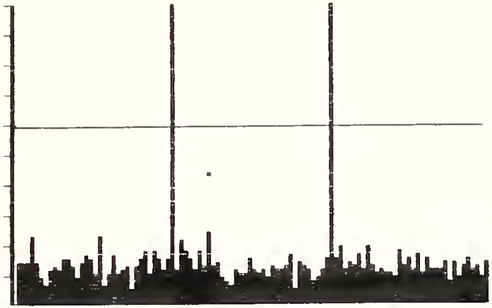

SUB: 61B.6- NO CR TRIALS=16 CS=350 MS
BIN=10 MS V.CAL.=8 CNTS, 16 VOLTS

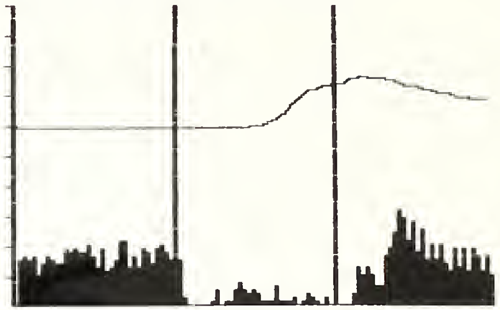

SUB: 61B.12+ CR TRIALS=19 CS=350 MS
BIN=10 MS V.CAL.=8 CNTS, 16 VOLTS

Cross-correlations

Although the multiple correlation/regression analyses discussed above are very useful for determining if a spike/CR relationship exists, these analyses do not address the temporal relationship of the unit activity and the behavior. The cross-correlation of unit activity and the CR is a sensitive technique for assessing lead or lag time, and this technique has been used to investigate spike and CR temporal relationships in the hippocampus (Berger, Laham, and Thompson, 1980).

Consider a neuron which increases its rate of firing prior to the CR onset, and assume that the rate of firing is linearly related to the amplitude of the CR. If a large number of trials are collected, the "waveforms" of the averaged CR and the cumulative spike counts will be nearly identical, but will be out of phase because the unit activity precedes the CR. The two waveforms can be positioned so that they are in phase by shifting the averaged CR waveform backwards along the X axis (the axis which represents time in the PSTH). The amount of time shifted is the lead time of the spike activity over the CR.

The phase relationship between the spike and CR waveforms was assessed by performing cross-correlations. These were calculated as follows. First, the Pearson correlation between the spike counts and the corresponding amplitude of the averaged CR in each 10 ms bin of the PSTH for CR trials was computed over all bins. The resulting correlation was the "real time" correlation of the unit activity and the CR. The correlation was then recomputed with the NM response shifted backward in time 10 ms so that each spike count at bin t was paired with the NM response at bin t+1. A total of 20 backward shifts, and then, 20 forward time shifts were performed. The resulting set of correlations were represented in a "correlogram," which depicts the Pearson r as a function of time shifts.

As a control procedure, the averaged CR was cross-correlated with the spikes on the non-CR trials. The resulting correlogram (subsequently referred to as the non-CR correlogram) was compared with the correlogram obtained when the CR was cross-correlated with the CR-related spikes (subsequently referred to as the CR correlogram). If a neuron was truly displaying CR-related activity, then the firing patterns on CR and non-CR trials, and hence, the associated correlograms, should differ substantially. Similarity between the CR and non-CR correlograms would suggest a pattern of neuronal firing that is independent of the CR.

Two types of cross-correlations were computed, unrestricted and restricted. In computing unrestricted cross-correlations, the spike and CR data were obtained from the Pre-CS, CS, and US Periods. In computing restricted cross-correlations, these data were obtained solely from the CS Period (however, portions of the NM response during the US Period and the Pre-CS Period were paired with CS Period spikes because of time shifting). In general, the procedure that yielded the greater maximum value of |*r*| was used in determining lead/lag times. Under some circumstances, however, considerations other than the value of |*r*| dictated the procedure to use. The restricted procedure was employed whenever one of the following situations occurred: (1) Unusual US-related neuronal firing patterns, evident on inspection of the CR PSTH, introduced nonlinearities in the spike/CR relationship. (2) Excitatory neuronal responses to the US on non-CR trials produced large cross-correlations in the non-CR correlogram.

The top and middle panels of Figure 6 illustrate the cross-correlation results for Cell 02A, whose PSTHs were illustrated in Figure 3. The top panel of Figure 6 depicts the CR correlogram, and the middle panel of Figure 6 illustrates the non-CR correlogram. The numbers along the abcissa of the correlogram depict the number of bins the NM response was shifted backward (negative numbers) or forward (positive numbers) in time. A maximum correlation to the left of zero indicates spike activity leading the CR, while a shift to the right indicates a lag. The ordinate represents values of the Pearson r, ranging from +1 to -1.

Cross-correlations were also computed using the rate of change (first derivative) of the NM response, defined as the difference between the CR amplitude at time t and the amplitude at time t-1. In many cases, cross-correlations using the rate of change of the CR resulted in stronger correlations than what was obtained using normal cross-correlation procedures. An example of first derivative correlograms for Cell 52B is illustrated in Figure 9.

Figure 9

CR and non-CR PSTHs and Cross-correlations for Cell 52B. Top left: CR PSTH. Bottom left: Non-CR PSTH. Top right: Correlogram obtained when the first derivative of the averaged CR is cross-correlated with CR-associated spike counts. Abcissa depicts the number of 10 ms bins the CR was shifted backward (negative) or forward (positive) in time. Each hash mark represents 2 bins. Ordinate depicts the value of the Pearson _r_, ranging from +1 to -1. A peak value of _r_ to the left of zero (negative side) indicates that spike activity leads the CR; a peak to the right of zero indicates that the CR leads the spike activity. Maximum absolute value of _r_ obtained at -60 ms ($r = -.462$, $Z = -2.65$, $N = 34$, $p < .05$). Bottom right: Correlogram obtained when first derivative of averaged CR is cross-correlated with non-CR spike counts.

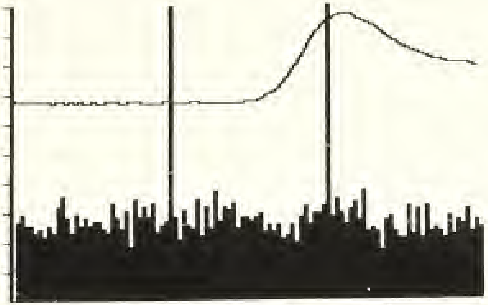

CELL: 52B TRIALS=25 CS=350 MS
BIN=10 MS V.CAL.=8 CNTS, 8 VOLTS

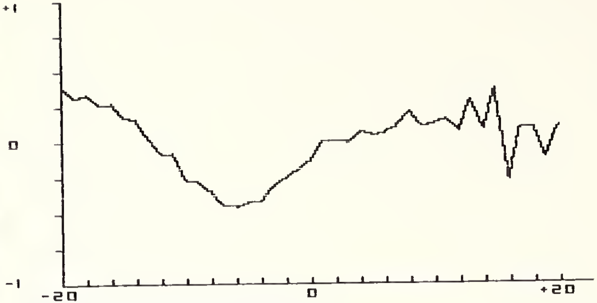

SUB: 52B CORRELOGRAM
RESTRICTED TO CS PERIOD
CR 1ST DER WITH CR SPIKES

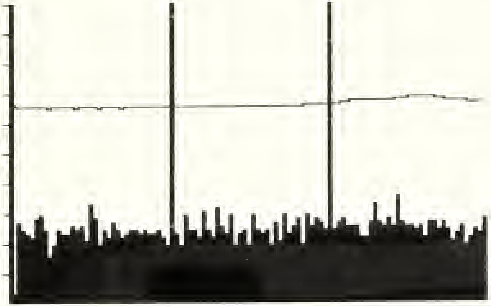

CELL: 52B TRIALS=23 CS=350 MS
BIN=10 MS V.CAL.=8 CNTS, 8 VOLTS

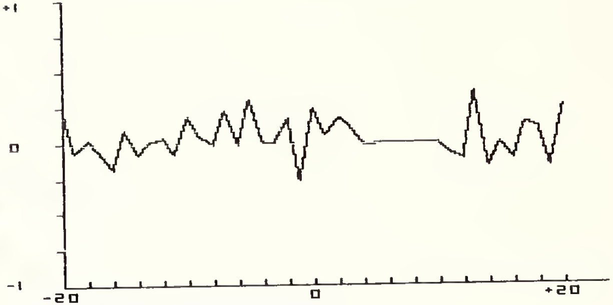

SUB: 52B CORRELOGRAM
RESTRICTED TO CS PERIOD
CR 1ST DER WITH NO CR SPIKES

CHAPTER III

RESULTS

Cell Classifications

Ninety-one cells were analyzed for CR-related activity, and 46 of these had significant spike/CR correlations. The following types of correlations were found. (1) In 27 cases, spikes were correlated with AR or MA, but not with LA. In other words, cell firing in these cases was correlated with CR magnitude only. (2) In 5 cases, spikes were correlated with LA only. That is, neuronal activity was correlated with latency but not magnitude in these cases. (3) In 14 cases, spikes were correlated with LA, and with either AR or MA. Thus, firing of these cells was correlated with both CR magnitude and latency.

Although both measures of CR magnitude, AR and MA, were used in the correlational analyses, a given cell tended to have the same patterns of spike correlations with both of these measures. Differences were observed, however, in the degree to which AR and MA correlated with the spike variables for a given cell. Thus, only the measure of magnitude yielding the greatest proportion of accountable variance was reported for each cell. AR was the measure of magnitude in 24 cases, and MA in 13 cases.

In 4 cases, however, spike correlations with both AR and MA were reported because the patterns of correlation were qualitatively different. Tables 1-3 summarize the results of regressing AR, MA, and LA, respectively, on all 7 combinations of the 3 spike variables. In order to simplify the notation for the multiple correlations, only the first letter of the abbreviations for CR and spike variables appear in Tables 1-3. For example, in Table 1, the numbers appearing under the column A.nd are multiple correlation coefficients obtained by regressing AR on ns and ds.

For each cell, one correlation among the row of correlations appears in brackets. The column containing the bracketed correlation indicates the best set of predictors for the dependent variable. For example, the first row of Table 1 contains the correlation coefficients for Cell 02A. The bracketed multiple correlation coefficient appears under the column A.nd, and the value of the correlation is .62. Thus, using the backward elimination procedure, the spike variable set consisting of ns and ds is the best set of predictors for AR.

Tables 1-3 also contain the number of trials used to compute the correlations, along with the adjusted correlation coefficient (R′) for the bracketed value. The R′ value was used to assess any overestimation of R due to a large ratio of number of independent variables to sample

TABLE 1

REGRESSION OF CR AREA ON SPIKE VARIABLES

CELL	NT	A.n	A.t	A.d	A.nt	A.nd	A.td	A.ntd	R'
02A	50	.49*	.05	.20	.61*	[.62*]	.22	.62*	.60
07	59	[.44*]	.29*	-.03	.46*	.44*	.29	.46*	.42
09	44	.19	.38*	.26	.42	.27	[.46*]	.46	.39
17	33	-.58*	[-.73*]	-.52*	.72*	.59*	.73*	.73*	-.72
17A	49	-.38*	-.59*	-.33*	.61*	.53*	.61*	[.65*]	.62
26	40	.46*	-.09	-.41*	.53*	[.55*]	.41*	.59*	.51
29.12+	62	-.03	-.22	[-.27*]	.24	.29	.28	.30	-.24
32A	25	[.50*]	.14	.06	.54*	.51*	.15	.56*	.47
32D1.N	19	.02	-.46	[-.67*]	.47	.67*	.70*	.70*	-.65
32.N+	20	[-.65*]	-.37	-.24	.72	.72	.39	.73	-.62
35.12+	30	.26	[.65*]	.06	.68*	.29	.65*	.68*	.63
40.12	58	[.32*]	.11	-.03	.35*	.33*	.12	.36	.29
42C	78	.45*	.28*	-.16	[.50*]	.48*	.29*	.51*	.48
42	18	.33	[.53*]	-.08	.54	.26	.60	.60	.49
43A	106	-.14	-.36*	-.18	.35*	.19	[.39*]	.39*	.37
43E	22	.10	.45*	-.14	.46	.29	[.65*]	.68*	.60
46B	38	-.21	-.41*	-.34	[.46*]	.38	.44*	.48	.41
46C	55	-.03	[-.41*]	-.08	.41*	.09	.41*	.41	-.38
46E	94	[.60*]	.00	.17	.57*	.57*	.17	.57*	.59
53	138	[.78*]	.15	.07	.72*	.75*	.17	.76*	.78
53B	30	[.57*]	.06	.35	.57*	.59*	.36	.61*	.55
53C	87	.20	[.41*]	.33*	.41*	.38*	.42*	.43*	.40
54C.12	27	[.61*]	-.24	.49*	.58*	.61*	.55*	.63*	.59
58C.6	149	.19*	.10	.08	[.23*]	.18	.16	.26*	.20
60A2	35	-.07	-.21	[-.43*]	.21	.49*	.44	.49	-.40
60B.12	19	-.28	-.23	-.55*	.33	[.64*]	.55	.64*	.58
61B.6-	22	[.42*]	.30	-.24	.51	.46	.38	.54	.37
64	24	.57*	.55*	-.44*	[.67*]	.64*	.59*	.69*	.63

Abbreviations: NT = Number of trials; A = CR area; n = Number of spikes; t = Mean spike time; d = Standard deviation of spike time; R' = adjusted correlation; correlations with * are statistically significant ($p < .05$)

TABLE 2

REGRESSION OF MAXIMUM CR AMPLITUDE ON SPIKE VARIABLES

CELL	NT	M.n	M.t	M.d	M.nt	M.nd	M.td	M.ntd	R′
17	33	-.77*	-.77*	-.76*	.81*	[.82*]	.81*	.83*	.81
18	17	-.34	-.55*	.12	.61*	.35	[.76*]	.79*	.72
21A	48	.51*	.26	.11	[.55*]	.52*	.30	.55*	.52
35A	77	-.53*	-.69*	-.48*	[.73*]	.55*	.71*	.73*	.72
35.12+	30	.37*	.52*	.25	.61*	.51*	.55*	[.68*]	.63
42	18	[.56*]	.50	.13	.59	.53	.50	.60	.52
46B	38	-.04	[-.52*]	-.31	.51*	.31	.52*	.52*	-.50
46F	141	.46*	.19*	.11	[.49*]	.47*	.24*	.49*	.48
50A	56	[.29*]	.14	.18	.28	.24	.23	.28	.26
50B	80	[.39*]	-.13	.25	.37*	.34	.29	.37	.38
52C	61	-.43*	.29*	.18	[.49*]	.45*	.31	.50*	.46
56	43	[.34*]	.27	.29	.43	.31	.40	.43	.31
60C	71	-.23*	-.28*	-.12	[.35*]	.19	.31*	.35*	.31
61	111	.48*	.58*	-.15	[.70*]	.54*	.60*	.70*	.69
61C	18	.45	.68*	-.55*	[.77*]	.62*	.75*	.80*	.73
64B	41	.33*	.57*	-.06	[.63*]	.28	.59*	.63*	.60
64C	21	[.48*]	.35	.06	.55	.5	.35	.56	.44

Abbreviations: NT = Number of trials; M = Maximum CR amplitude; n = Number of spikes; t = Mean spike time; d = Standard deviation of spike time; R′ = adjusted correlation; correlations with * are statistically significant ($p < .05$)

TABLE 3

REGRESSION OF CR ONSET LATENCY ON SPIKE VARIABLES

CELL	NT	L.n	L.t	L.d	L.nt	L.nd	L.td	L.ntd	R'
26	26	.15	.43*	.39	.43	.44	[.56*]	.56*	.50
29.12+	56	[.27*]	.00	.01	.28	.28	.01	.28	.24
32A	14	-.48	-.39	-.48	[.66*]	.63	.56	.73*	.58
32D1.N	18	-.22	.34	[.59*]	.46	.63*	.64*	.65*	.55
32.N+	20	[.54*]	.29	.31	.67	.67	.37	.67	.50
40.12	22	[-.60*]	.17	.52*	.60*	.63*	.53*	.63*	-.57
42C	47	[-.32*]	-.27	.12	.37*	.35	.27	.38	-.29
43E	17	.44	.31	[.63*]	.50	.63*	.63*	.63	.60
43F	24	-.20	[.56*]	.02	.58*	.24	.57*	.59	.53
46E	60	.01	[.36*]	.00	.37*	.10	.36*	.38*	.34
50	25	.36	[-.57*]	-.17	.56	.39	.62*	.63	-.53
52	16	.14	.54*	-.50	.55	.64	.69*	[.76*]	.69
52B	25	.00	-.39	-.29	.39	.36	[.50*]	.53	.43
53	48	-.16	.52*	-.22	.52*	.27	[.57*]	.57*	.54
53C	62	-.05	-.31*	[-.36*]	.32*	.36*	.38*	.38*	-.34
54A	19	.01	[.76*]	-.42	.76*	.42	.76*	.76*	.74
60A2	27	.32	.21	[.44*]	.33	.45	.44	.45	.40
608.12	15	[.52*]	.27	.30	.59	.62	.33	.63	.46
64	15	-.26	.03	.49	.26	.52	[.65*]	.65	.57

Abbreviations: NT = Number of trials; L = CR onset latency; n = Number of spikes; t = Mean spike time; d = Standard deviation of spike time; R' = adjusted correlation; correlations with * are statistically significant ($p < .05$)

size. The formula used to adjust R (Pedhazur, 1982) was:

$$R' = \left\{1 - \left[(1 - R^2)(N - 1)\right] / (N - k - 1)\right\}^{\frac{1}{2}}$$

where R = obtained correlation, N = sample size, and k = number of predictors. For Cell 02A, N = 50, k = 2, R = .62, and R′ = .60. Note that with sample size and number of predictors held constant, the larger the obtained squared correlation the smaller the shrinkage observed in R′.

Cells were classified as excitatory, inhibitory, or temporal, based upon the types of correlations observed. At least one of the following criteria had to be true for a cell to be classified as either excitatory or inhibitory: (1) The zero-order correlation between ns and CR magnitude was significant, or the best set of predictors of CR magnitude contained ns. The cell was excitatory if the ns/CR magnitude correlation was positive, inhibitory if it was negative. (2) The zero-order correlation between ns and LA was significant, or the best set of predictors of LA contained ns. In this case, the cell was excitatory if the ns/LA correlation was negative, and inhibitory if it was positive.

Cells which did not fit into either the excitatory or inhibitory categories were classified as temporal cells. These neurons displayed CR-related temporal shifts in the distribution of unit activity, but did not have CR-related net increases or decreases in the number of spikes in the CS Period.

The reconstruction of all recording electrode positions is presented in Figure 10. Excitatory cells are depicted as stars, inhibitory cells as diamonds, and temporal cells as triangles. Cells without any significant spike/CR correlations are indicated by circles. The section level (in mm) rostral to the midpoint of AAN (at 0 mm, not depicted in this figure) appears at the bottom of each section. Cells which display an increase or decrease in firing prior to the CR are listed in the figure caption, along with lead times.

Stimulating electrode positions are illustrated in Figure 11. In general, stimulating electrodes were consistently placed near AAN. It will be convenient to refer back to Figures 10 and 11 during the following discussion of the different cell types.

Excitatory Cells

Table 4 summarizes the results of the regression analyses for the 24 cells classified as excitatory. The variance partitioning for both CR latency and CR magnitude is depicted. The measure of CR magnitude for each cell appears to the right of the cell number. For example, Cell 26 has an "AR" under the Magnitude column of Table 4 to

Figure 10

Reconstruction of recording electrode positions. Selected transverse sections are depicted, and numbers at the base of each section represent the distance (mm) rostral to the midpoint of the accessory abducens nucleus (the 0.0 mm section, not depicted). Other numbers refer to individual cells. Stars indicate excitatory cells, diamonds are inhibitory cells, triangles are temporally correlated cells, and circles indicate cells with no significant correlations. Below are the numbers of cells displaying CR-related unit activity which precedes the CR, along with estimated lead times (in ms):

Excitatory		Inhibitory		Temporal	
Cell	Lead	Cell	Lead	Cell	Lead
02A	110-120	17	100-130	43F	80-100
07	30	17A	110-150	46C	40-60
26	80	35A	60-80	50	90-100
32A	40-80	46B	20	52B	60
46E	10			54A	130
53	80-90			60A2	10-50
61	70-90				
61B.6	90-120				
64	20				

Abbreviations: bc = brachium conjunctivum, LC = locus coeruleus, M5 = motor trigeminal nucleus, N7 = facial nerve, PAG = periaqueductal gray, RN = red nucleus.

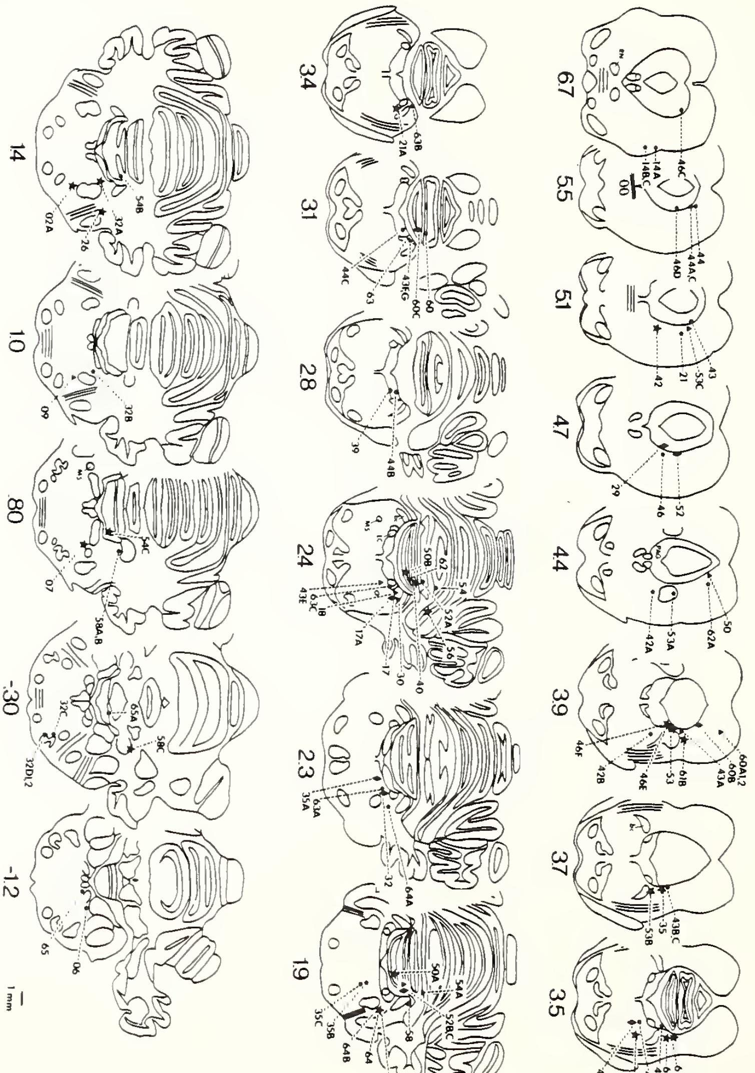
6.7
5.5
5.1
4.7
4.4
3.9
3.7
3.5
3.4
3.1
2.8
2.4
2.3
1.9
1.4
1.0
.80
-.30
-1.2
1 mm
46C
14A
14B,C
44
44A,C
46D
43
53C
21
42
52
46
29
50
62A
53A
42A
60A1,2
60B
43A
61B
53
46E
42B
46F
43B,C
35
53B
61A
61C
43D
46A
42C
46B
63B
21A
60
60C
43F,G
63
44C
44B
39
54
62
50B
52A
56
40
30
17
17A
1B
63C
43E
63A
35A
32
64A
54A
50A
52B,C
58
64C
64
64B
35B
35C
54B
32A
26
02A
32B
09
54C
58A,B
07
65A
58C
32C
32D1,2
06
65

Figure 11

Reconstruction of stimulating electrode positions. Selected transverse sections are depicted, and numbers at the base of each section represent the distance (mm) rostral to the midpoint of the accessory abducens nucleus (the 0.0 mm section). Other numbers refer to individual rabbits, and diamonds indicate tip positions. Abbreviations: AA = accessory abducens nucleus, AB = abducens nucleus, FN = Facial nucleus, M5 = motor trigeminal nucleus, N7 = facial nerve, SO = superior olive.

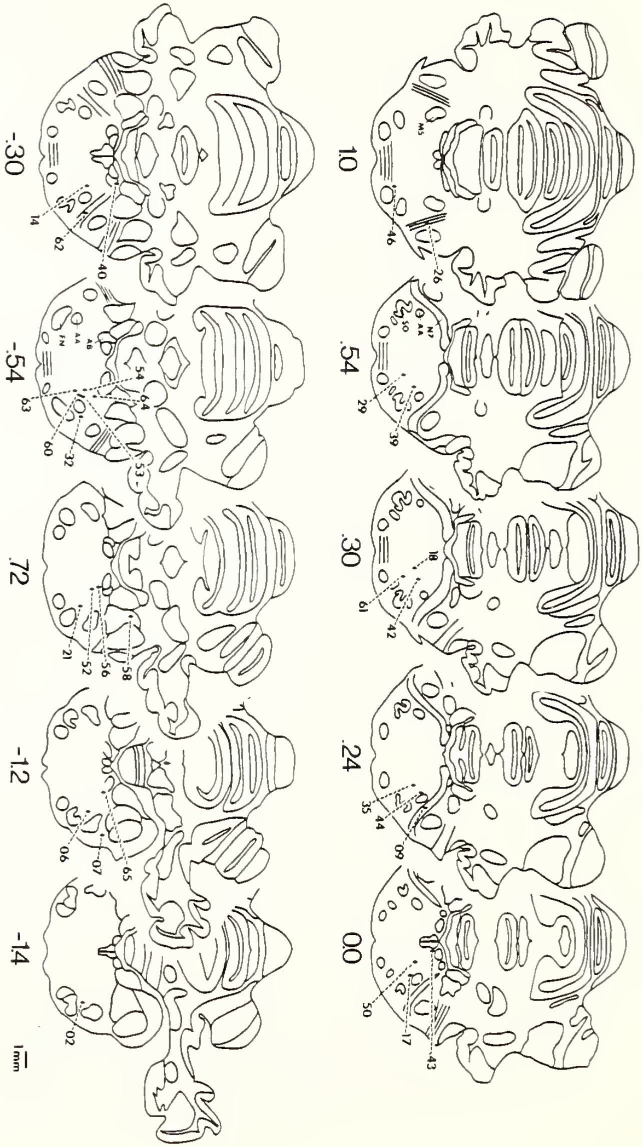
1.0
.54
.30
.24
0.0
-.30
-.54
.72
-1.2
-1.4
1mm
MS
N7
AA
SO
FN
AA
A6
46
26
29
39
18
61
42
35
44
09
50
17
43
14
62
40
54
63
64
60
32
53
21
52
56
58
06
07
65
02

TABLE 4

VARIANCE PARTITIONING FOR EXCITATORY CELLS

		CR Magnitude			CR Latency		
CELL	MAG	ns	mt	ds	ns	mt	ds
02A	AR	++		-			
07	AR	++					
21A	MA	++	+				
26	AR	++		-		++	+
32A	AR	+++			--	--	
35.12+	AR		++++				
35.12+	MA	+	+++	+			
40.12	AR	+			----		
42	AR		+++				
42	MA	+++					
42C	AR	++	+		-		
46E	AR	++++				+	
46F	MA	++	+				
50A	MA	+					
50B	MA	++					
53	AR	++++++				+++	-
53B	AR	+++					
54C.12	AR	++++					
56	MA	+					
58C.6	AR	+					
61	MA	++	+++				
61B.6-	AR	++					
61C	MA	+	+++++				
64	AR	+++	+			++	++
64B	MA	+	+++				
64C	MA	++					

Abbreviations: MAG = Magnitude; ns = Number of spikes; mt = Mean spike time; ds = Standard deviation of spike time; AR = CR Area; MA = Maximum CR amplitude; +,- described in text

indicate that the CR magnitude measure was area. Each "+" and "-" represents approximately 10 percent of accountable variance, the polarity indicating whether the spike variable was positively or negatively correlated with the CR variable.

The order in which variance was partitioned for the spike variables was determined by the magnitude of the _F_ ratio's associated with the partial regression coefficients in the best predictor equation. For example, under the CR Magnitude heading of Table 4, Cell 26 has two pluses under number of spikes, and one minus under standard deviation of spike time. Adding the pluses and minuses indicates that approximately 30 percent of the CR magnitude variance is accountable by virtue of the linear relationships with the two spike variables. The 30 percent figure is obtained by referring to Table 1 for Cell 26. The best set of predictors for CR area is ns and ds. The multiple R under A.nd is .55, and the square of this is .3025, or approximately 30 percent. The further partitioning of this variance, depicted in Table 4, is performed as follows: The proportion of variance for ns is assessed first because the partial regression coefficient for this variable has a greater _F_ ratio than that of ds (partial regression coefficients not depicted in tables). The proportion of variance for ns is obtained by squaring the A.n correlation (.46), which is .2116, or approximately 20 percent. AR and ns are positively correlated, so two pluses appear in Table 4. The variance contribution for ds is obtained by subtracting .2116 from .3025, which is .0909, or approximately 10 percent. Because ds is negatively correlated with AR, one minus appears in Table 4. The breakdown of variance for LA is obtained in a similar manner.

Thus, the information contained in Table 4 is somewhat redundant with that in Tables 1-3. However, the presentation is convenient for comparing the proportion and distribution of accountable variance among the cells. Note that the variance partitioning in Table 4 is not intended to reflect relative importance of the spike variables in generating the CR. The purpose of the partitioning is to indicate for each cell which spike variables have greatest predictive power over the CR variables.

Excitatory cells were concentrated in two regions of the brain stem. One of these regions was dorsal and dorsomedial to the brachium conjunctivum at caudal levels of the inferior colliculus. In Figure 10, this area is located on the sections 3.5-3.9 mm rostral to AAN. Figures 12 and 13 illustrate sample unit activity for one of these neurons, Cell 53, along with PSTHs and scatterplots computed for this cell. Note in Figure 12 that a number of CS Period bins are significant for non-CR as well as CR trials, probably due to tone-related excitation. Thus,

Figure 12

CR and non-CR PSTHs and unit activity for Cell 53. Top left: CR PSTH. Dotted line indicates CR onset at 1% maximum deflection. Bottom left: Non-CR PSTH. Top right: Representative unit activity and CR on a single CS+ (1200 Hz) trial. In top and bottom right panels, triangles below unit activity depict CS onset and offset. US onset (top right only) is contiguous with CS offset. Calibration: 100 ms. Bottom right: A single CS+ trial with no CR. A UR is observed along with post-US spike activity.

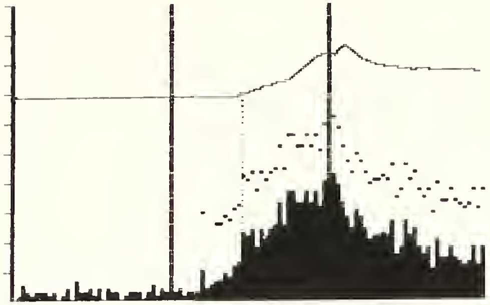

SUB: 53 TRIALS=51 CS=350 MS
BIN=10 MS V.CAL.=8 CNTS, 8 VOLTS

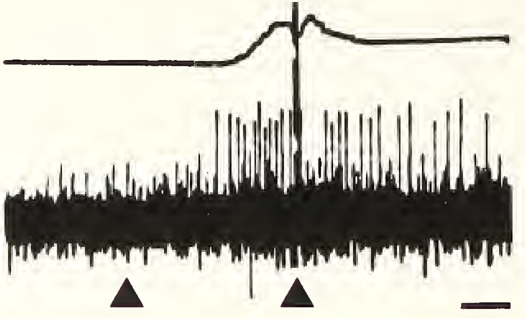

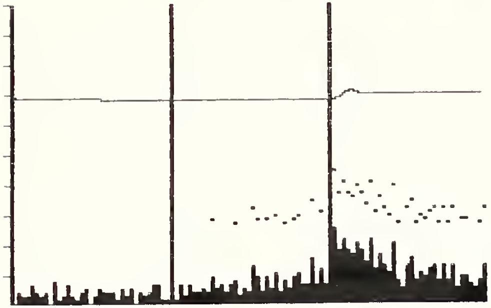

SUB: 53 TRIALS=87 CS=350 MS
BIN=10 MS V.CAL.=8 CNTS, 8 VOLTS

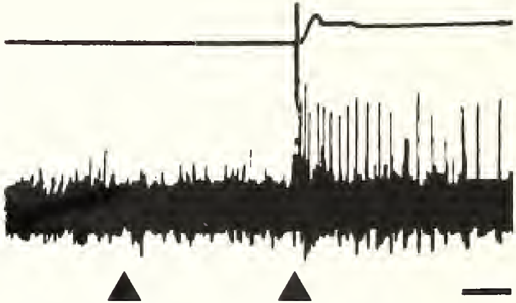

Figure 13

Scatterplots and unit activity for Cell 53. Top left: Scatterplot and least squares regression line of CR area as a function of the number of spikes in the CS Period. Bottom left: Scatterplot and least squares regression line of CR latency as a function of the mean spike time in the CS Period. Top right: Representative unit activity and CR for a nonreinforced 600 Hz tone (CS-) trial. Triangles below unit activity depict CS onset and offset. Calibration: 100 ms. Bottom right: Same as top right except that CR is very small and spike activity similarly decreases.

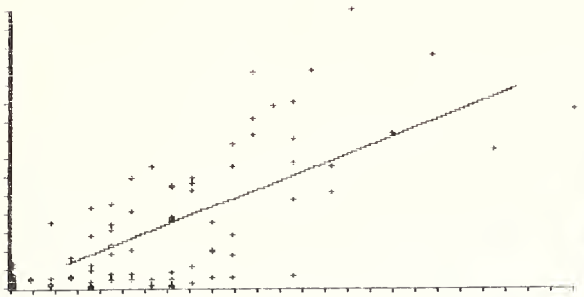

SCATTERPLOT: X=# SPIKES, Y=CR AREA
CELL: 53 TRIALS: 138
MIN, MAX VALUES: X=0,28 Y=0,881
HASH MARK CAL.: X=1.1, Y=58.7

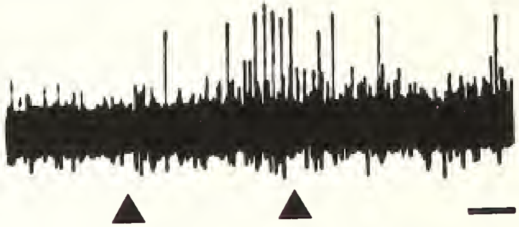

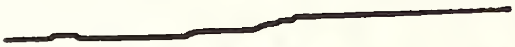

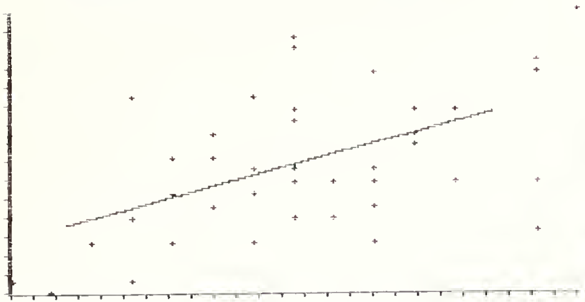

SCATTERPLOT: X=MN. SPIKE TIME, Y=CR LAT
CELL: 53 TRIALS: 48
MIN, MAX VALUES: X=17,31 Y=45,68
HASH MARK CAL.: X=.5, Y=1.5

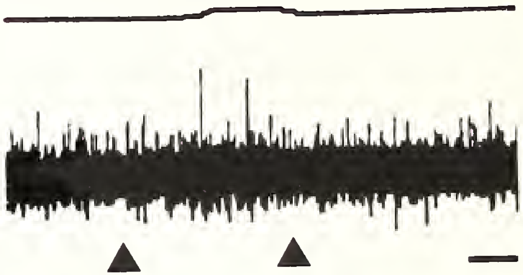

Cell 53 is similar to Cell 02A (see Figure 3) in that the significant bin method of assessing spike activity does not adequately reflect the magnitude of the CR-related firing. The scatterplots in Figure 13 show strong linear AR/ns and LA/mt relationships. Figure 14 illustrates other analytical tools introduced in the Method section: the binomial histogram comparison, the CR onset histogram, and the cross-correlations. The increase in firing for this cell appears to lead the behavior by 80-90 ms.

The unit activity of other cells in this region, including Cell 61 (Figures 15 and 16), Cell 61B (Figure 8), and Cell 46E (Figure 17), also preceded the CR. In the CR onset histogram for Cell 61 in Figure 16, note the gradual increase in unit activity before the CR onset, followed by a sharp increase 20 ms after onset. In Figure 17, the CR onset histogram for Cell 46E reveals an increase in activity at 80-140 ms before CR onset. However, inspection of binomial histogram comparisons (not depicted in figure) indicates that this very early activity is common to both CR and non-CR trials, and only the second increase in activity beginning 10 ms before CR onset is actually CR-related. The nonlinear spike/CR relationship for Cell 46E precluded cross-correlational analyses.

Unit activity of other cells in the dorsomedial parabrachial region, Cells 61C, 35, 46F, and 53B did not lead the CR. A sample of unit activity from one of these

Figure 14

Binomial histogram comparison, CR onset histogram, and cross-correlations for Cell 53. Top left: Binomial comparison of PSTHs depicted in the left column of Figure 12. Bottom left: CR onset histogram. CR onset latency: Mean = 195.30 ms from CS onset; standard deviation = 57.03 ms. Top right: Correlogram obtained when the averaged CR is cross-correlated with CR-associated spike counts. Abcissa depicts the number of 10 ms bins the CR was shifted backward (negative) or forward (positive) in time. Each hash mark represents 2 bins. Ordinate depicts the value of the Pearson $\underline{r}$, ranging from +1 to −1. A peak value of $\underline{r}$ to the left of zero (negative side) indicates that spike activity leads the CR; a peak to the right of zero indicates that the CR leads the spike activity. Maximum absolute value of $\underline{r}$ obtained at −70 ms ($\underline{r}$ = .952, Z = 5.47, N = 34, $p < .05$). Bottom right: Correlogram obtained when averaged CR is cross-correlated with non-CR spike counts.

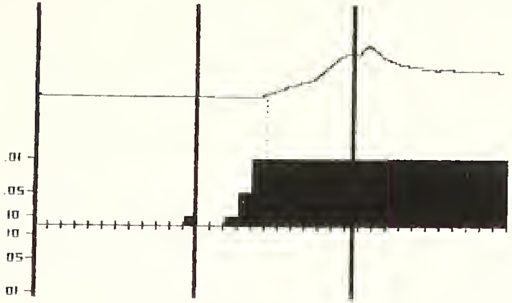

CELL: 53 BIN: 30 MS CS: 350 MS
BINOMIAL HISTOGRAM COMPARISON
CR ONSET AT 1% MAX AMP

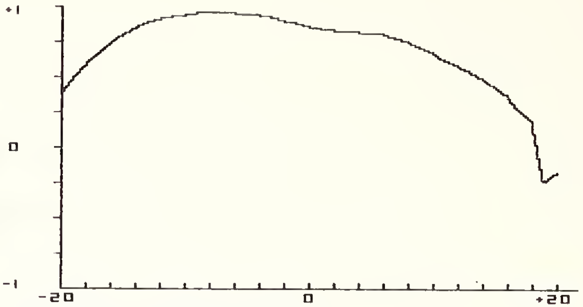

SUB: 53 CORRELOGRAM
RESTRICTED TO CS PERIOD
CR WITH CR SPIKES

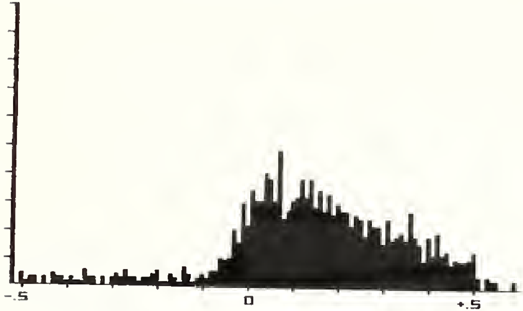

CR ONSET HISTOGRAM FOR CELL 53
TRIALS=49 BIN=10 MS V.CAL=8 CNTS

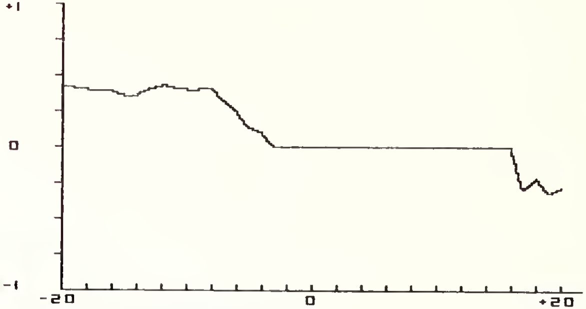

SUB: 53 CORRELOGRAM
RESTRICTED TO CS PERIOD
CR WITH NO CR SPIKES

Figure 15

CR PSTH, non-CR PSTH, and binomial histogram comparison for Cell 61. Top: CR PSTH. Dotted line indicates CR onset at 5% maximum deflection. Middle: Non-CR PSTH. Bottom: Binomial PSTH comparison.

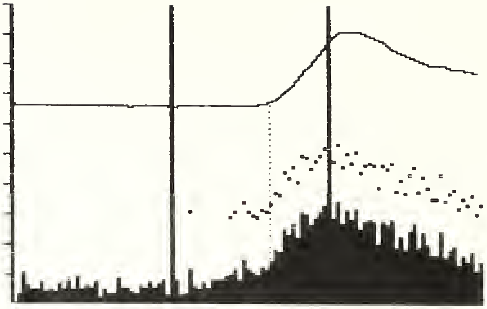

SUB: 61 CR TRIALS=47 CS=350 MS
BIN=10 MS V.CAL.=16 CNTS, 8 VOLTS

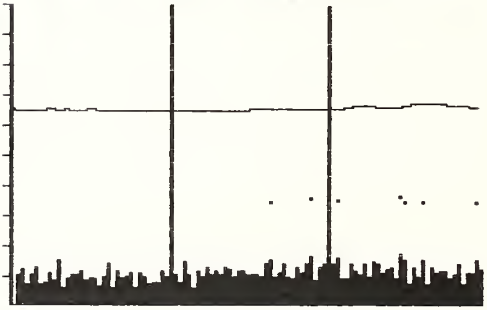

SUB: 61 NO CR TRIALS=64 CS=350 MS
BIN=10 MS V.CAL.=16 CNTS, 8 VOLTS

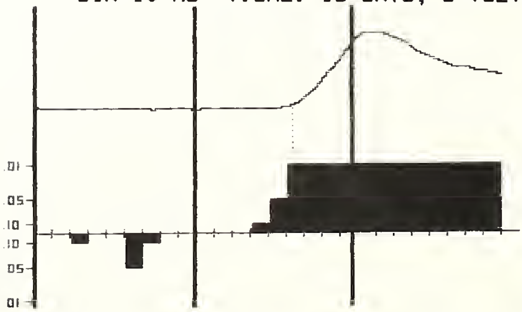

CELL: 61 BIN: 40 MS CS: 350 MS
BINOMIAL HISTOGRAM COMPARISON
CR ONSET AT 5% MAX AMP

Figure 16

CR onset histogram and cross correlations for Cell 61. Top: CR onset histogram. CR onset latency: Mean = 242.17 ms from CS onset; standard deviation = 32.63 ms. Middle: Correlogram obtained when the averaged CR is cross-correlated with CR-associated spike counts. Abcissa depicts the number of 10 ms bins the CR was shifted backward (negative) or forward (positive) in time. Each hash mark represents 2 bins. Ordinate depicts the value of the Pearson *r*, ranging from +1 to -1. A peak value of *r* to the left of zero (negative side) indicates that spike activity leads the CR; a peak to the right of zero indicates that the CR leads the spike activity. Maximum absolute value of *r* obtained at -70 ms (*r* = .957, Z = 9.4, N = 97, $p < .05$). Bottom: Correlogram obtained when averaged CR is cross-correlated with non-CR spike counts.

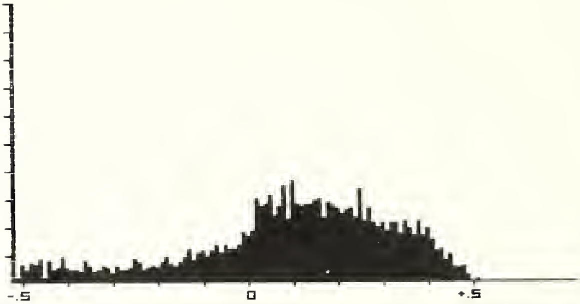

CR ONSET HISTOGRAM FOR CELL 61
TRIALS=46 BIN=10 MS V.CAL=15 CNTS

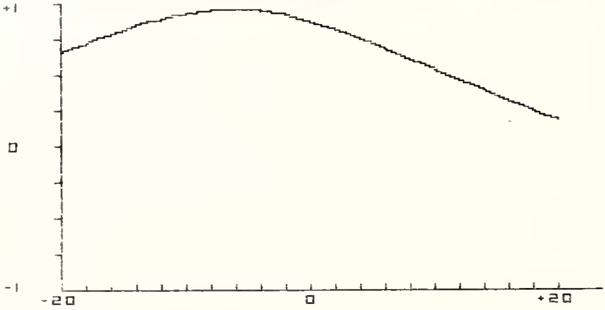

SUB: 61 CORRELOGRAM
CR WITH CR SPIKES

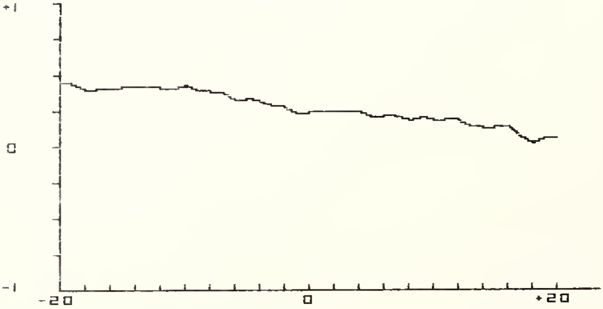

SUB: 61 CORRELOGRAM
CR WITH NO CR SPIKES

Figure 17

CR onset histogram and scatterplot for Cell 46E. Top: CR onset histogram. CR onset latency: Mean = 184.92 ms from CS onset; standard deviation = 28.99 ms. Bottom: Scatterplot and least squares regression line of CR area as a function of the number of spikes in the CS Period.

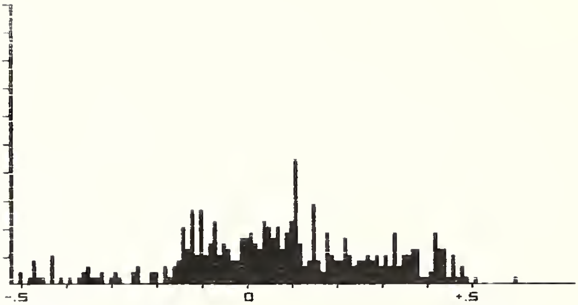

CR ONSET HISTOGRAM FOR CELL 46E
TRIALS=63 BIN=10 MS V.CAL=5 CNTS

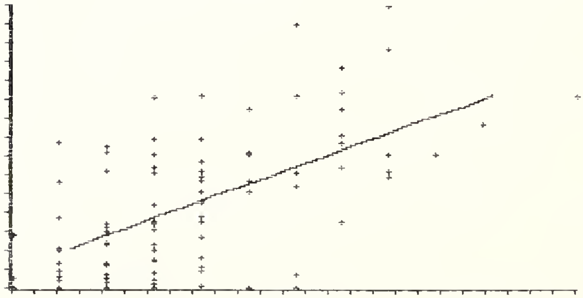

SCATTERPLOT: X=# SPIKES, Y=CR AREA
CELL: 46E TRIALS: 94
MIN, MAX VALUES: X=0,12 Y=0,897
HASH MARK CAL.: X=.4, Y=59.8

cells, Cell 61C, is illustrated in Figure 18. Figure 19 contains the binomial histogram comparison and correlograms for this cell. All statistical measures suggest that the spike activity for Cell 61C increased concurrently with the CR onset; however the failure to detect a lead may be partially due to the small sample size. Results for Cell 35 are presented in Figures 20 and 21. Note in the top panel of Figure 20 the high baseline firing rate of the cell (approximately 50 Hz) and the interesting patterns of excitation and inhibition in the US Period.

Excitatory neurons were also concentrated in a second region, namely, cell group h of Meessen and Olszewski (1949). This is a reticular zone surrounding the motor trigeminal nucleus, and includes most of the SR. Cells 02A (Figures 3 and 6) and 07 (Figure 2) represent ventral and caudal recordings, respectively, within this zone. Cell 32A, obtained in a dorsomedial portion of zone h, is illustrated in Figure 22. Sample unit activity and CR on a CS+ trial appears in the upper right panel of the figure, and the binomial histogram comparison in the lower right panel indicates 3 excitatory regions in the CS Period.

Cell 26 was recorded on the extreme dorsolateral reaches of zone h. Sample unit activity and PSTHs are illustrated in Figure 23. In the right column of the figure, observe how unit activity bursts prior to CR onset on a CR trial, but maintains a steady firing rate on a

Figure 18

CR and non-CR PSTHs and unit activity for Cell 61C. Top left: CR PSTH. Dotted line indicates CR onset at 5% maximum deflection. Bottom left: Non-CR PSTH. Top right: Representative unit activity and CR on a single CS+ (1200 Hz) trial. In top and bottom right panels, triangles below unit activity depict CS onset and offset. US onset (in top right panel) is contiguous with CS offset. Calibration: 100 ms. Bottom right: Unit activity on a single CS- (600 Hz) trial with no CR.

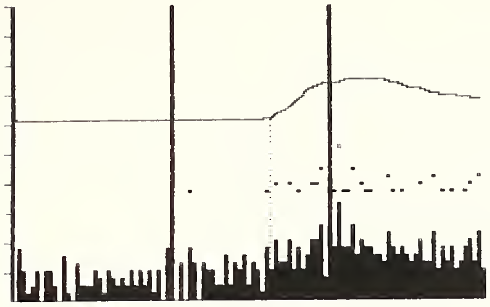

SUB: 61C CR TRIALS=10 CS=350 MS
BIN=10 MS V.CAL.=4 CNTS, 16 VOLTS

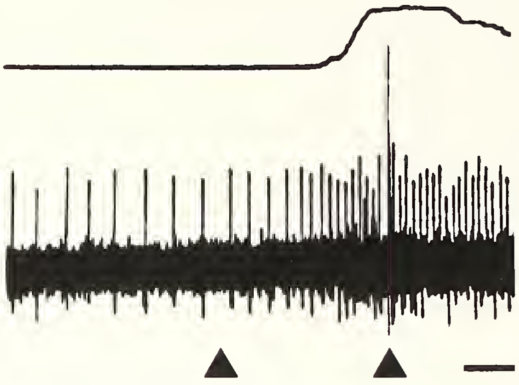

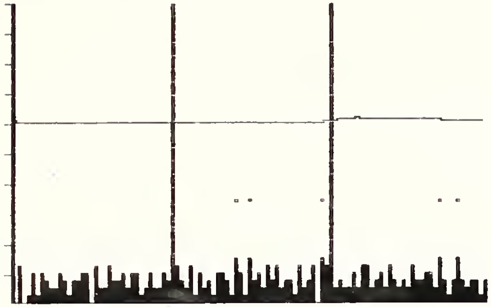

SUB: 61C.6- NO CR TRIALS=8 CS=350 MS
BIN=10 MS V.CAL.=4 CNTS, 16 VOLTS

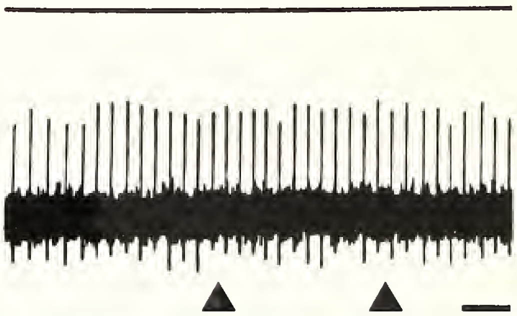

Figure 19

Binomial histogram comparison and cross-correlations for Cell 61C. Top: Binomial comparison of PSTHs depicted in the left column of Figure 18. Middle: Correlogram obtained when the first derivative of the averaged CR is cross-correlated with CR-associated spike counts. Abcissa depicts the number of 10 ms bins the CR was shifted backward (negative) or forward (positive) in time. Each hash mark represents 2 bins. Ordinate depicts the value of the Pearson $\underline{r}$, ranging from +1 to −1. A peak value of $\underline{r}$ to the left of zero (negative side) indicates that spike activity leads the CR; a peak to the right of zero indicates that the CR leads the spike activity. Maximum absolute value of $\underline{r}$ obtained at +10 ms ($\underline{r} = .549$, $Z = 3.16$, $N = 34$, $\underline{p} < .05$). Bottom: Correlogram obtained when the first derivative of the averaged CR is cross-correlated with non-CR spike counts.

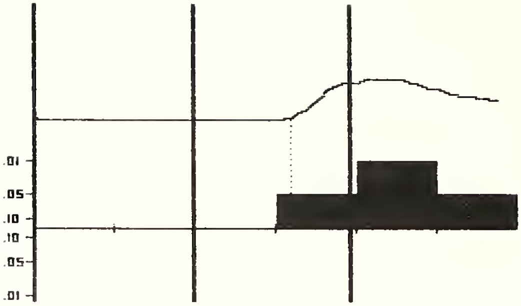

CELL: 61C BIN: 180 MS CS: 350 MS
BINOMIAL HISTOGRAM COMPARISON
CR ONSET AT 5% MAX AMP

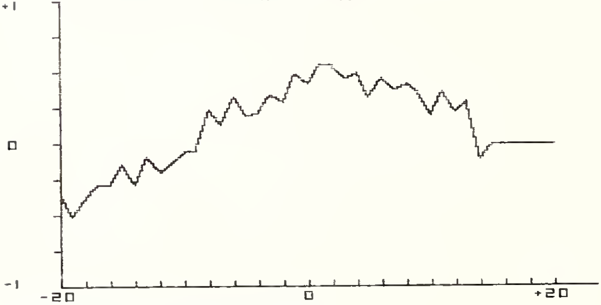

SUB: 61C CORRELOGRAM
RESTRICTED TO CS PERIOD
CR 1ST DER WITH CR SPIKES

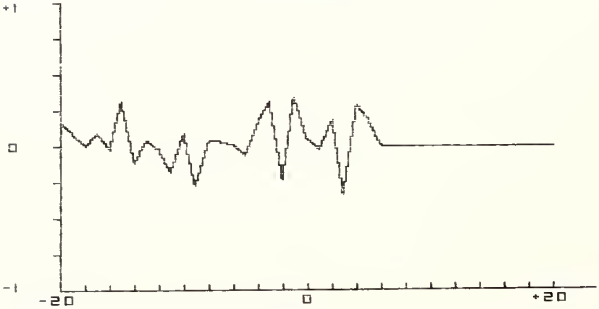

SUB: 61C CORRELOGRAM
RESTRICTED TO CS PERIOD
CR 1ST DER WITH NO CR SPIKES

Figure 20

CR PSTH, non-CR PSTH, and binomial histogram comparison for Cell 35. Top: CR PSTH. Middle: Non-CR PSTH. Bottom: Binomial PSTH comparison.

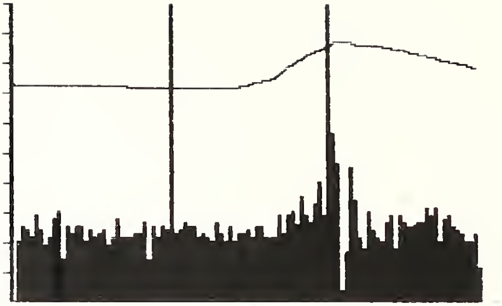

CELL: 35 TRIALS=30 CS=350 MS
BIN=10 MS V.CAL.=8 CNTS, 8 VOLTS

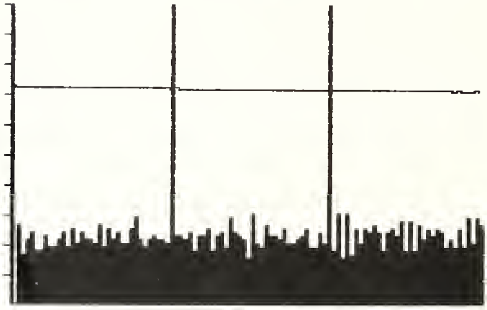

CELL: 35 TRIALS=29 CS=350 MS
BIN=10 MS V.CAL.=8 CNTS, 8 VOLTS

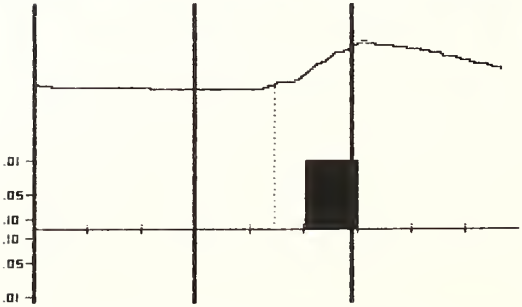

CELL: 35 BIN: 120 MS CS: 350 MS
BINOMIAL HISTOGRAM COMPARISON
CR ONSET AT 5% MAX AMP

Figure 21

Scatterplot and cross-correlations for Cell 35. Top: Scatterplot and least squares regression line of CR area as a function of the mean spike time in the CS Period. Middle: Correlogram obtained when the averaged CR is cross-correlated with CR-associated spike counts. Abcissa depicts the number of 10 ms bins the CR was shifted backward (negative) or forward (positive) in time. Each hash mark represents 2 bins. Ordinate depicts the value of the Pearson _r_, ranging from +1 to −1. A peak value of _r_ to the left of zero (negative side) indicates that spike activity leads the CR; a peak to the right of zero indicates that the CR leads the spike activity. Maximum absolute value of _r_ obtained at +10 ms (r = .758, Z = 4.36, N = 34, $p < .05$). Bottom: Correlogram obtained when averaged CR is cross-correlated with non-CR spike counts.

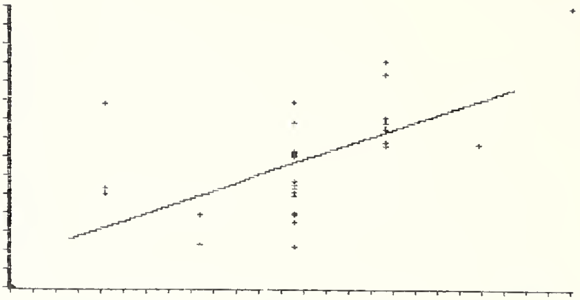

SCATTERPLOT: X=MN SPK TIME, Y=CR AREA
CELL: 35 TRIALS: 30
MIN, MAX VALUES: X=15,21 Y=61,544
HASH MARK CAL.: X=.2, Y=32.2

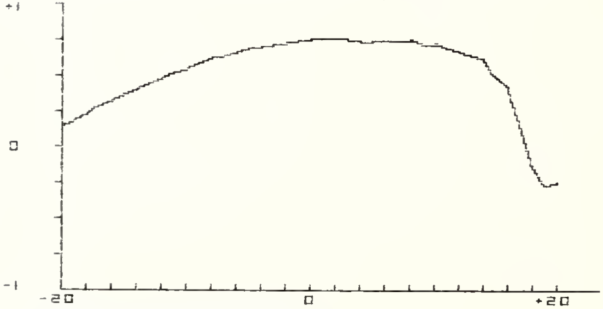

SUB: 35 CORRELOGRAM
RESTRICTED TO CS PERIOD
CR WITH CR SPIKES

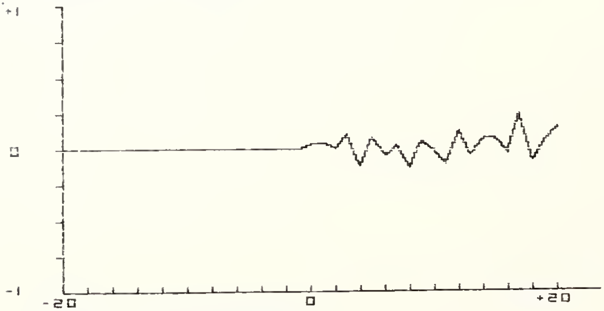

SUB: 35 CORRELOGRAM
RESTRICTED TO CS PERIOD
CR WITH NO CR SPIKES

Figure 22

PSTHs, binomial histogram comparison, and unit activity for Cell 32A. Top left: CR PSTH. Dotted line indicates CR onset at 1% maximum deflection. Bottom left: Non-CR PSTH. Top right: Representative unit activity and CR for a CS+ (white noise) trial. Triangles below unit activity represent CS onset and offset. The US is contiguous with the CS offset. Calibration: 100 ms. Bottom right: Binomial comparison of PSTHs depicted on the top and bottom left panels of the figure.

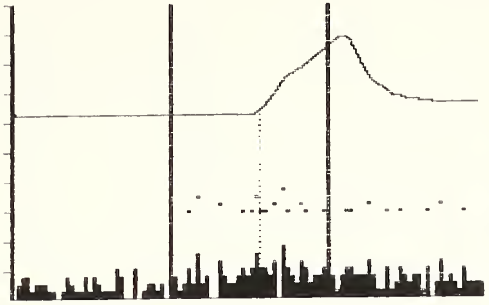

SUB: 32A TRIALS=14 CS=350 MS
BIN=10 MS V.CAL.=4 CNTS, 8 VOLTS

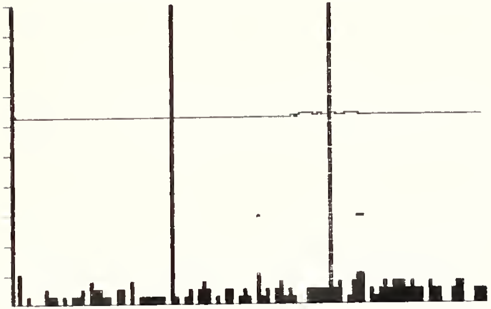

SUB: 32AT- NO CR TRIALS=11 CS=350 MS
BIN=10 MS V.CAL.=4 CNTS, 8 VOLTS

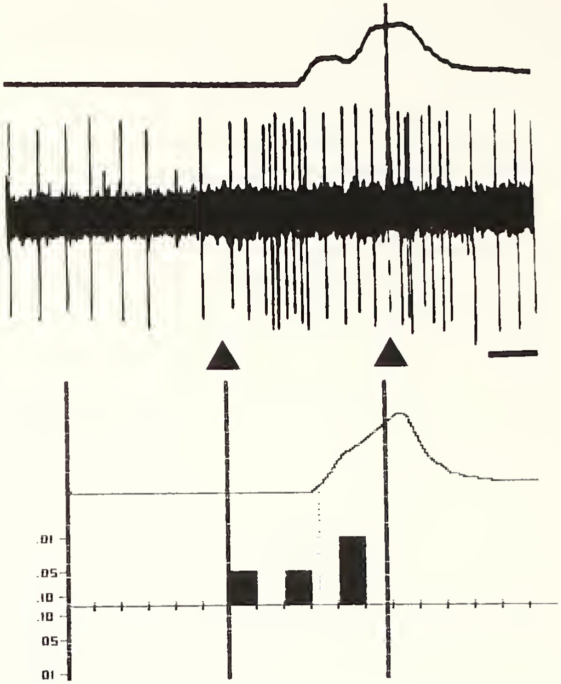

CELL: 32A BIN: 60 MS CS: 350 MS
BINOMIAL HISTOGRAM COMPARISON
CR ONSET AT 1% MAX AMP

Figure 23

CR and non-CR PSTHs and unit activity for Cell 26. Top left: CR PSTH. Dotted line indicates CR onset at 5% maximum deflection. Bottom left: Non-CR PSTH. Top right: Representative unit activity and CR on a single CS+ (1200 Hz) trial. In top and bottom right panels, triangles below unit activity depict CS onset and offset. US onset (in top right panel) is contiguous with CS offset. Calibration: 100 ms. Bottom right: Unit activity on a single CS- (white noise) trial with no CR.

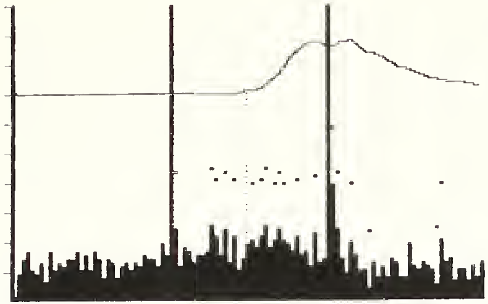

SUB: 26 TRIALS=21 CS=350 MS
BIN=10 MS V.CAL.=8 CNTS, 8 VOLTS

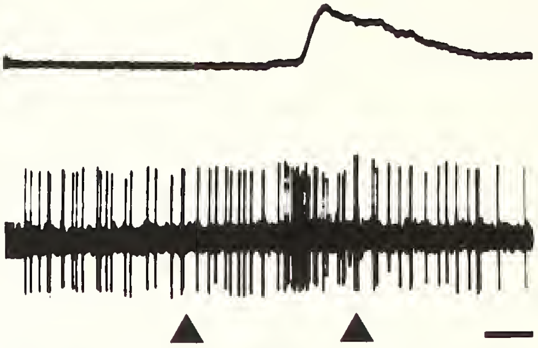

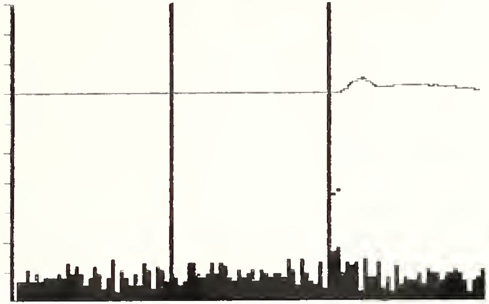

SUB: 26 TRIALS=14 CS=350 MS
BIN=10 MS V.CAL.=8 CNTS, 8 VOLTS

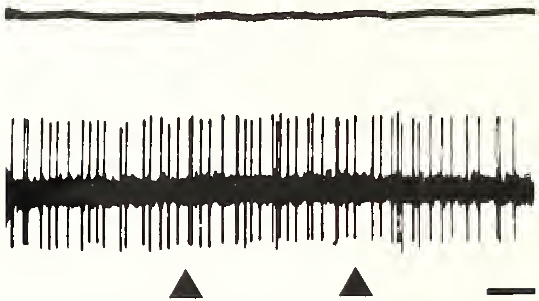

non-CR trial. The CR and non-CR PSTHs are consistent with these single-trial impressions. Note how the unit activity is aggregated toward the center of the CS Period in the CR PSTH but not in the non-CR PSTH. The interpretation of CR-related burst activity for Cell 26 is also consistent with the negative correlation between AR and ds (Tables 1 and 4).

Cells 64, 64B, and 64C were located medial and rostral to Cell 26. Sample unit activity and PSTHs for Cell 64 are depicted in Figure 24. The usefulness of the CR onset histogram is evident in Figure 25, as this histogram clearly illustrates how the increase in activity of Cell 64 precedes the CR by 20 ms. Cells 64B and 64C were recorded very close to Cell 64 and were also classified as excitatory. However, the increase in unit activity of these cells occurred concurrent with, rather than prior to, the CR.

Cell 42 was the only excitatory cell located rostral to the 3.9 mm level. This cell was recorded just lateral to ventral portions of the periaqueductal gray at the 5.1 mm level. Figure 26 depicts the CR PSTH along with the scatterplot of MA as a function of ns. Because there were no non-CR trials for this cell, one cannot conclude solely from the increased activity in the CR PSTH that the firing is CR-related. However, the significant spike/CR correlations (see Table 4) suggest that the increased

Figure 24

CR and non-CR PSTHs and unit activity for Cell 64. Top left: CR PSTH. Dotted line indicates CR onset at 5% maximum deflection. Bottom left: Non-CR PSTH. Top right: Representative unit activity and CR on a single CS+ (600 Hz) trial. In top and bottom right panels, triangles below unit activity depict CS onset and offset. US onset (in top right panel) is contiguous with CS offset. Calibration: 100 ms. Bottom right: Unit activity on a single CS- (1200 Hz) trial with no CR.

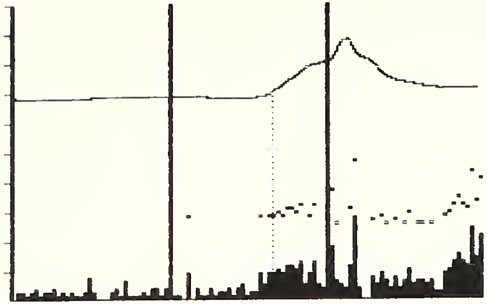

SUB: 64 TRIALS=15 CS=350 MS
BIN=10 MS V.CAL.=8 CNTS, 10.66 VOLTS

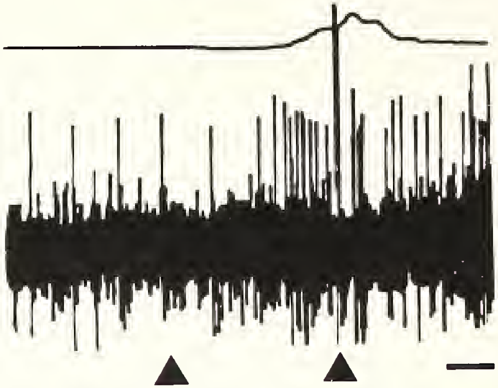

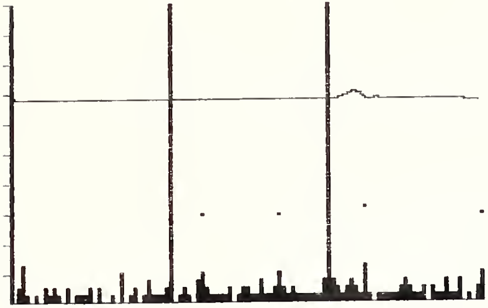

SUB: 64 TRIALS=9 CS=350 MS
BIN=10 MS V.CAL.=4 CNTS, 10.66 VOLTS

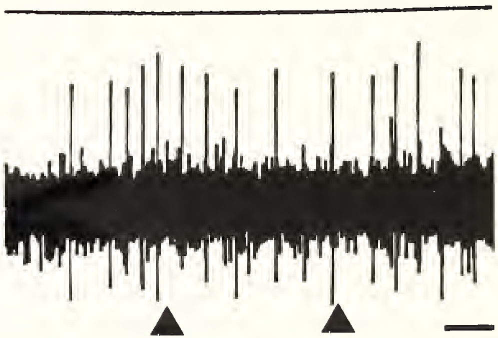

Figure 25

Binomial histogram comparison, CR onset histogram, and cross-correlations for Cell 64. Top left: Binomial comparison of PSTHs depicted in the left column of Figure 24. Bottom left: CR onset histogram. CR onset latency: Mean = 232.66 ms from CS onset; standard deviation = 25.94 ms. Top right: Correlogram obtained when the first derivative of the averaged CR is cross-correlated with CR-associated spike counts. Abcissa depicts the number of 10 ms bins the CR was shifted backward (negative) or forward (positive) in time. Each hash mark represents 2 bins. Ordinate depicts the value of the Pearson *r*, ranging from +1 to -1. A peak value of *r* to the left of zero (negative side) indicates that spike activity leads the CR; a peak to the right of zero indicates that the CR leads the spike activity. Maximum absolute value of *r* obtained at 0 ms ($r = .811$, $Z = 4.66$, $N = 34$, $p < .05$). Bottom right: Correlogram obtained when the first derivative of the averaged CR is cross-correlated with non-CR spike counts.

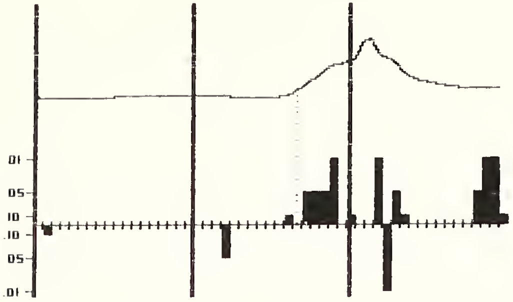

CELL: 64 BIN: 20 MS CS: 350 MS
BINOMIAL HISTOGRAM COMPARISON
CR ONSET AT 5% MAX AMP

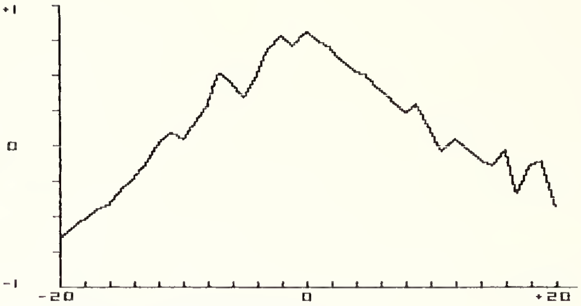

SUB: 64 CORRELOGRAM
RESTRICTED TO CS PERIOD
CR 1ST DER WITH CR SPIKES

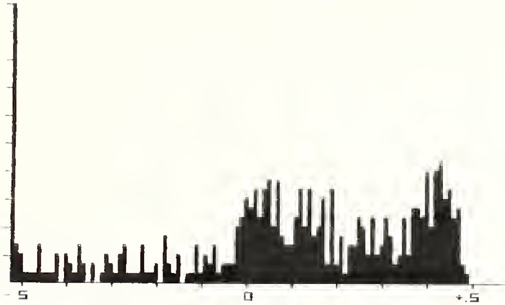

CR ONSET HISTOGRAM FOR CELL 64
TRIALS=15 BIN=10 MS V.CAL=3 CNTS

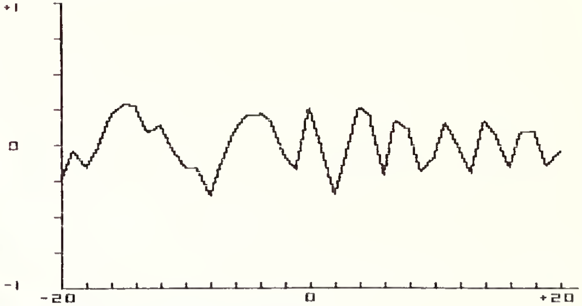

SUB: 64 CORRELOGRAM
RESTRICTED TO CS PERIOD
CR 1ST DER WITH NO CR SPIKES

Figure 26

CR PSTH and scatterplot for Cell 42. Top: CR PSTH. Dotted line indicates CR onset at 1% maximum deflection. Bottom: Scatterplot and least squares regression line of maximum CR amplitude as a function of the number of spikes in the CS Period.

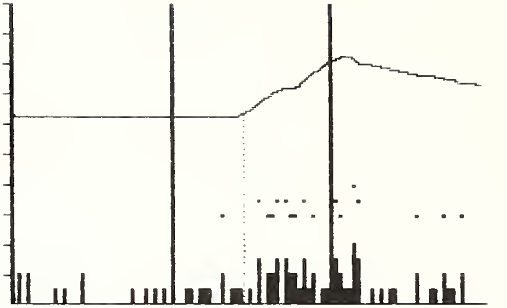

SUB: 42 TRIALS=17 CS=350 MS
BIN=10 MS V.CAL.=2 CNTS, 8 VOLTS

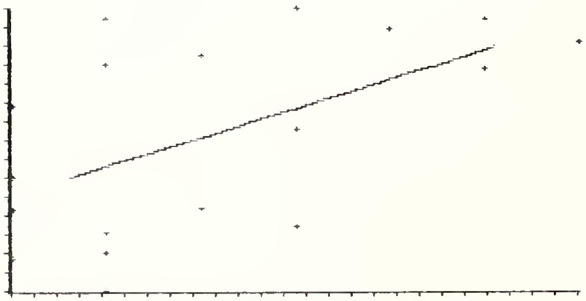

SCATTERPLOT: X=# SPIKES, Y=MAX CR AMP
CELL: 42 TRIALS: 18
MIN, MAX VALUES: X=0,6 Y=1,88
HASH MARK CAL.: X=.2, Y=5.8

firing is indeed related to the CR. Note in Tables 1, 2, and 4 that mt was the best predictor when AR was regressed on ns, mt, and ds, but ns was the best predictor when MA was regressed on the spike variables. This was the most extreme case of differences in regression results using the two measures of CR magnitude. Although the unit activity for this cell was CR-related, the increase in firing did not appear to lead the behavior.

Six excitatory cells were found in the cerebellum: Cell 54C in lobule I of the vermis, Cells 40, 50A, 50B, in lobule II of the vermis, Cell 56 in lobule III of the vermis, and Cell 58C near nucleus interpositus. None of these cells increased firing before the CR. Two other excitatory cells were found in dorsolateral nucleus reticularis pontis oralis. The unit activity for these cells, 21A and 42C, occurred concurrently with the CR.

Cell 42C was the only neuron in this study to be antidromically activated by AAN stimulation. Representative unit activity and PSTHs for Cell 42C are illustrated in Figure 27. The PSTHs, along with the correlograms in Figure 28, and the CR onset histogram in Figure 29 illustrate how the rate of firing of unit activity tends to increase at CR onset, but not before. The upper right panel of Figure 29 illustrates 5 superimposed tracings of a stimulus pulse (onset indicated by the triangle) and the consistent short latency (0.4 ms)

Figure 27

CR and non-CR PSTHs and unit activity for Cell 42C. Top left: CR PSTH. Dotted line indicates CR onset at 1% maximum deflection. Bottom left: Non-CR PSTH. Top right: Representative unit activity and CR on a single CS- (600 Hz) trial. In top and bottom right panels, triangles below unit activity depict CS onset and offset. Calibration: 100 ms. Bottom right: Unit activity on a single CS- trial with no CR.

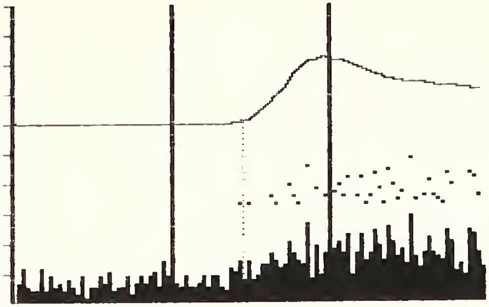

SUB: 42C TRIALS=47 CS=350 MS
BIN=10 MS V.CAL.=8 CNTS, 8 VOLTS

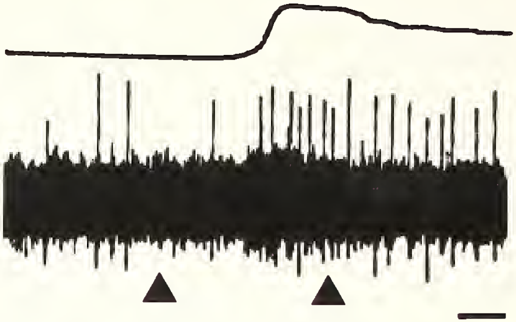

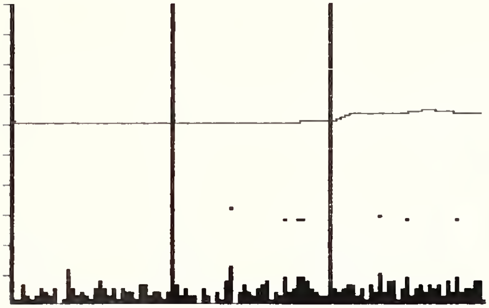

SUB: 42C TRIALS=30 CS=350 MS
BIN=10 MS V.CAL.=8 CNTS, 8 VOLTS

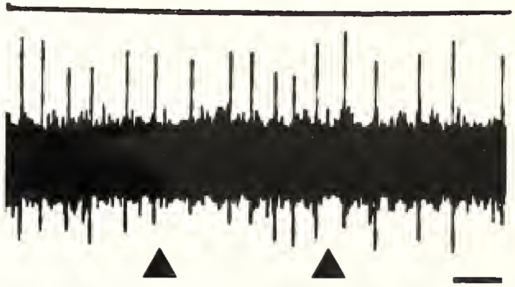

Figure 28

Cross-correlations and scatterplot for Cell 42C. Top: Correlogram obtained when the averaged CR is cross-correlated with CR-associated spike counts. Abcissa depicts the number of 10 ms bins the CR was shifted backward (negative) or forward (positive) in time. Each hash mark represents 2 bins. Ordinate depicts the value of the Pearson r, ranging from +1 to −1. A peak value of r to the left of zero (negative side) indicates that spike activity leads the CR; a peak to the right of zero indicates that the CR leads the spike activity. Maximum absolute value of r obtained at +10 ms ($r = .735$, $Z = 7.4$, $N = 101$, $p < .05$). Middle: Correlogram obtained when averaged CR is cross-correlated with non-CR spike counts. Bottom: Scatterplot and least squares regression line of CR area as a function of the number of spikes in the CS Period.

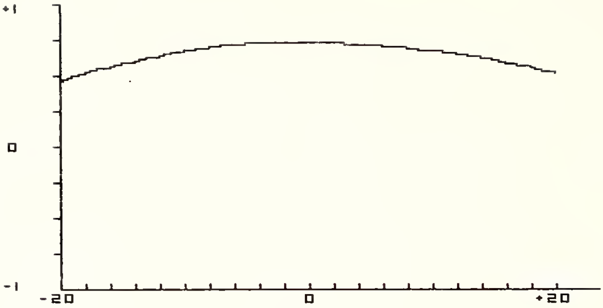

SUB: 42C CORRELOGRAM
CR WITH CR SPIKES

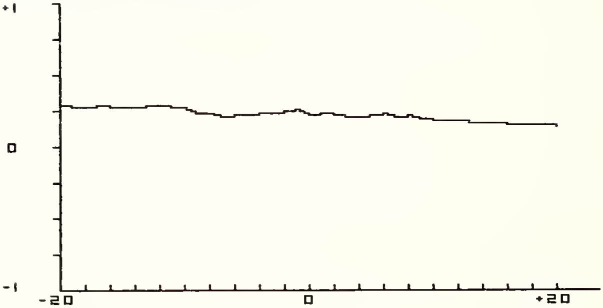

SUB: 42C CORRELOGRAM
CR WITH NO CR SPIKES

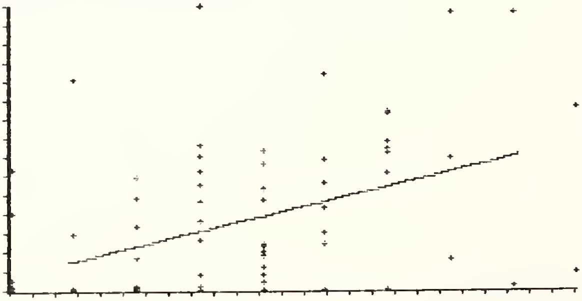

SCATTERPLOT: X=# SPIKES, Y=CR AREA
CELL: 42C TRIALS: 77
MIN, MAX VALUES: X=2,11 Y=0,1412
HASH MARK CAL.: X=.3, Y=94.1

Figure 29

Binomial histogram comparison, CR onset histogram, and antidromically elicited responses for Cell 42C. Top left: Binomial comparison of PSTHs depicted in left column of Figure 27. Bottom left: CR onset histogram. CR onset latency: Mean = 202.55 ms from CS onset; standard deviation = 43.48 ms. Top right: 5 superimposed oscilloscope tracings illustrating short latency (0.4 ms) unit responses to single-pulse AAN stimulation. For this panel and the bottom right panel, the triangles depict stimulus onset, and arrows indicates unit responses. Stimulus parameters: .095 ms duration, 130 uA. Calibration: 0.2 ms. Bottom right: 5 superimposed tracings of twin-pulse stimulation, illustrating maximum frequency following of the unit. Interpulse interval is 3.56 ms. Stimulus parameters same as above. Calibration: 0.5 ms.

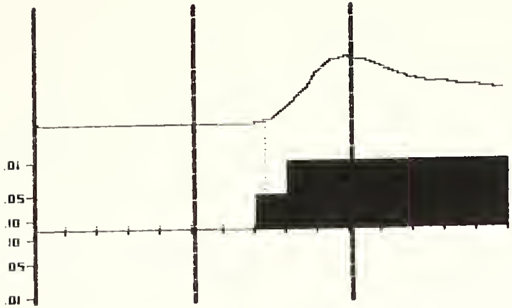

CELL: 42C BIN: 70 MS CS: 350 MS
BINOMIAL HISTOGRAM COMPARISON
CR ONSET AT 1% MAX AMP

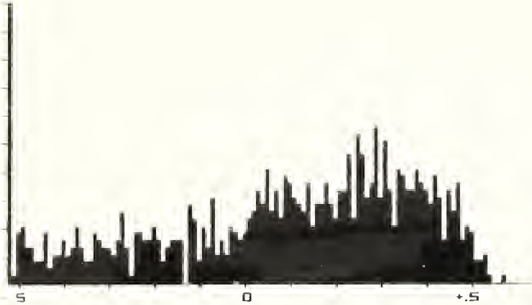

CR ONSET HISTOGRAM FOR CELL 42C
TRIALS=47 BIN=10 MS V.CAL=4 CNTS

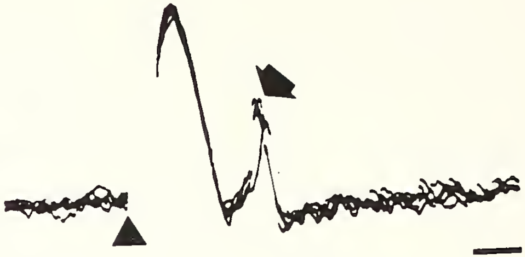

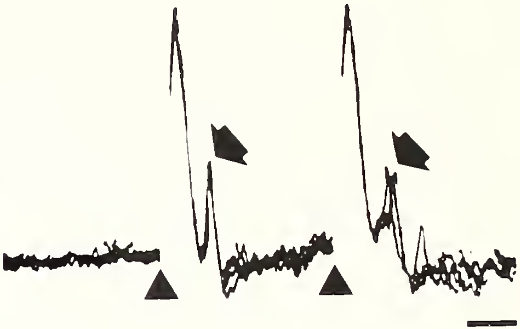

unit response (indicated by arrow). The conduction velocity was estimated at 8 m/sec. The response was elicited by a .095 ms pulse of 130 µA amplitude. The response exhibited a sharp threshold of activation slightly below 130 µA. The lower panel of Figure 29 depicts twin pulse stimulation at 280 Hz (3.56 ms interpulse interval). This was the maximum frequency following obtained, and the stimulation parameters were identical to those used for single pulses.

Inhibitory Cells

The variance partitioning for inhibitory cells is represented in Table 5. The method of interpretating this table is identical to that presented for Table 4. Only 10 cells were classified as inhibitory, and in 4 of these cases the decrease in firing preceded the CR.

The neurons displaying CR-leading activity were located in dorsal and dorsomedial aspects of nucleus reticularis pontis caudalis and oralis. Cells 17 and 17A were sufficiently dorsal to border on the medial parabrachial nucleus and locus subcoeruleus. Figure 30 shows representative unit activity and PSTHs for Cell 17. In contrast to Cell 43 in Figure 1, the CR and non-CR PSTHs for Cell 17 clearly demonstrate CR-related inhibition of firing. Scatterplots in Figure 31 illustrate negative

TABLE 5

VARIANCE PARTITIONING FOR INHIBITORY CELLS

		CR Magnitude			CR Latency		
CELL	MAG	ns	mt	ds	ns	mt	ds
17	AR		-----				
17	MA	--	--	--			
17A	AR	-	---	-			
29.12+	AR			-	+		
32.N+	AR	----			+++		
35A	MA	-	-----				
46B	AR	-	--				
46B	MA		---				
52					+	+++	--
52C	MA	--	+				
60B.12	AR	-		---	+++		
60C	MA	-	-				

Abbreviations: MAG = Magnitude; ns = Number of spikes; mt = Mean spike time; ds = Standard deviation of spike time; AR = CR Area; MA = Maximum CR amplitude; +,- described in text

Figure 30

CR and non-CR PSTHs and unit activity for Cell 17. Top left: CR PSTH. Dotted line indicates CR onset at 1% maximum deflection. Bottom left: Non-CR PSTH. Top right: Representative unit activity and CR on a single reinforced CS (1200 Hz) trial. In top and bottom right panels, triangles below unit activity depict CS onset and offset. US onset (in top right panel) is contiguous with CS offset. Calibration: 100 ms. Bottom right: Unit activity on a single nonreinforced CS trial (also 1200 Hz) with no CR.

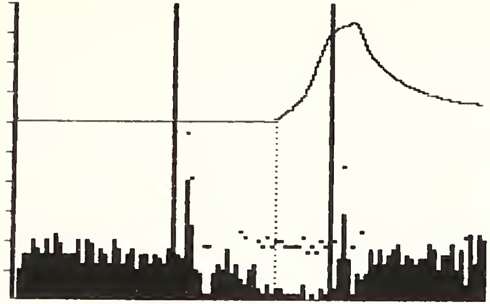

SUB: 17 TRIALS=16 CS=350 MS
BIN=10 MS V.CAL.=6 CNTS, 10.66 VOLTS

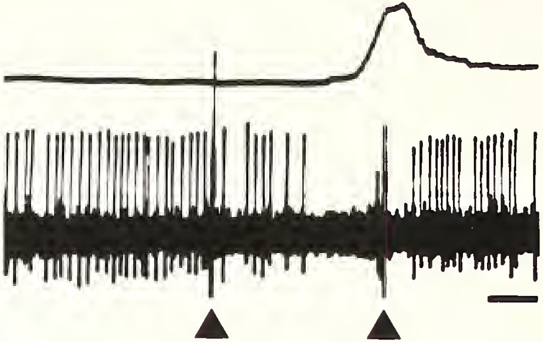

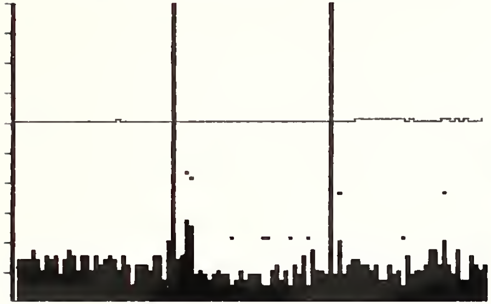

SUB: 17** TRIALS=10 CS=350 MS
BIN=10 MS V.CAL.=6 CNTS, 10.66 VOLTS

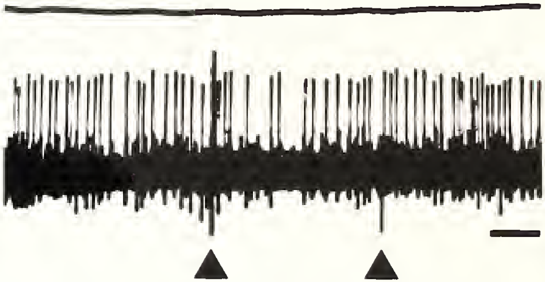

MA/ns and AR/mt relationships. The binomial histogram comparison, CR onset histogram, and correlograms for this cell are depicted in Figure 32. The CR onset histogram illustrates that firing was maximally inhibited at CR onset, but the tendency to decrease started considerably before onset.

Cells 46B and 35A were located more ventrally and medially than Cells 17 and 17A. Figure 4 contains the PSTHs and binomial histogram comparison for Cell 35A. The CR onset histogram and correlograms for Cell 35A are illustrated in Figure 33. The CR correlogram suggests that decrease of neuronal activity leads the CR by 170 ms. Inspection of the averaged CR trace in the top panel of Figure 4 indicates that the CR onset occurs approximately midway through the 350 ms CS Period. Thus, a neuronal lead of 170 ms would correspond to the beginning of the CS Period. However, the binomial histogram comparison in Figure 4 indicates that early CS Period activity does not differ for CR and non-CR PSTHs. The binomial histogram comparison and the CR onset histogram for this cell both suggest that the lead time is more on the order of 60-80 ms.

The decrease in firing of other inhibitory cells did not precede the CR, and these cells were located in a number of different brain regions. These regions include medial to the motor trigeminal nucleus (Cell 32), lateral

Figure 31

Scatterplots for Cell 17. Top: Scatterplot and least squares regression line of maximum CR amplitude as a function of the number of spikes in the CS Period. Bottom: Scatterplot and least squares regression line of CR area as a function of the mean spike time in the CS Period.

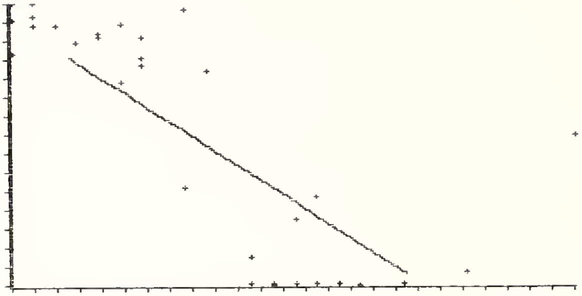

SCATTERPLOT: X=# SPIKES, Y=MAX CR AMP
CELL: 17 TRIALS: 33
MIN, MAX VALUES: X=6,32 Y=1,120
HASH MARK CAL.: X=1, Y=7.9

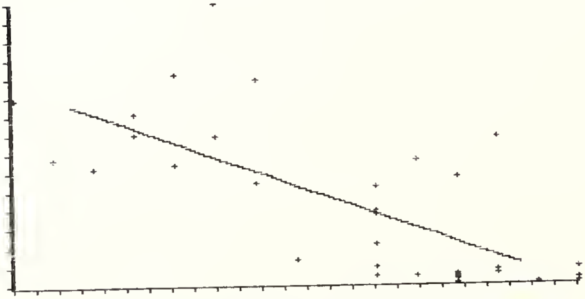

SCATTERPLOT: X=MN SPK TIME, Y=CR AREA
CELL: 17 TRIALS: 33
MIN, MAX VALUES: X=4,18 Y=0,765
HASH MARK CAL.: X=.5, Y=51

Figure 32

Binomial histogram comparison, CR onset histogram, and cross-correlations for Cell 17. Top left: Binomial comparison of PSTHs depicted in the left column of Figure 30. Bottom left: CR onset histogram. CR onset latency: Mean = 245.00 ms from CS onset; standard deviation = 34.27 ms. Top right: Correlogram obtained when the averaged CR is cross-correlated with CR-associated spike counts. Abcissa depicts the number of 10 ms bins the CR was shifted backward (negative) or forward (positive) in time. Each hash mark represents 2 bins. Ordinate depicts the value of the Pearson *r*, ranging from +1 to −1. A peak value of *r* to the left of zero (negative side) indicates that spike activity leads the CR; a peak to the right of zero indicates that the CR leads the spike activity. Maximum absolute value of *r* obtained at −130 ms ($r = -.675$, $Z = -6.25$, $N = 87$, $p < .05$). A total of 5 bins were omitted in the computation of the correlations (2 in CS Period, 3 in US Period). Bottom right: Correlogram obtained when averaged CR is cross-correlated with non-CR spike counts.

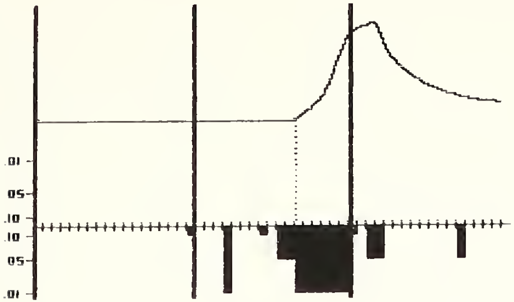

CELL: 17 BIN: 20 MS CS: 350 MS
BINOMIAL HISTOGRAM COMPARISON
CR ONSET AT 1% MAX AMP

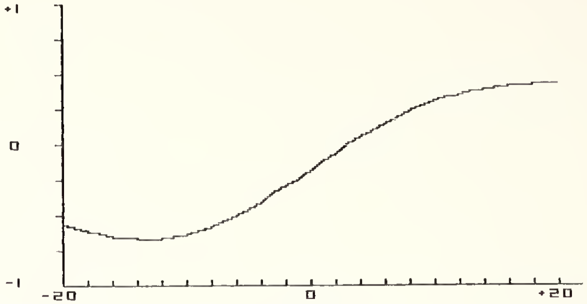

SUB: 17 CORRELOGRAM
CR WITH CR SPIKES

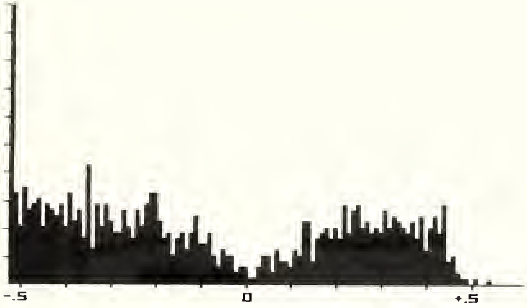

CR ONSET HISTOGRAM FOR CELL 17
TRIALS=20 BIN=10 MS V.CAL=5 CNTS

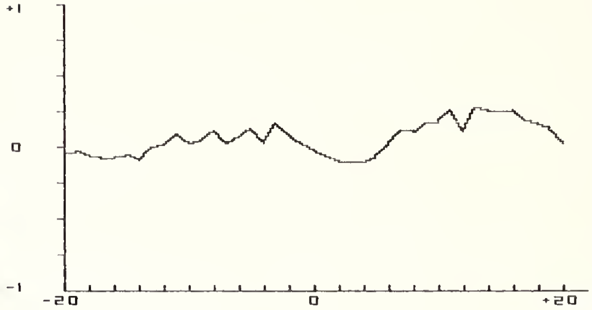

SUB: 17 CORRELOGRAM
CR WITH NO CR SPIKES

Figure 33

CR onset histogram and cross-correlations for Cell 35A. Top: CR onset histogram. CR onset latency: Mean = 223.54 ms from CS onset; standard deviation = 37.97 ms. Middle: Correlogram obtained when the averaged CR is cross-correlated with CR-associated spike counts. Abcissa depicts the number of 10 ms bins the CR was shifted backward (negative) or forward (positive) in time. Each hash mark represents 2 bins. Ordinate depicts the value of the Pearson *r*, ranging from +1 to -1. A peak value of *r* to the left of zero (negative side) indicates that spike activity leads the CR; a peak to the right of zero indicates that the CR leads the spike activity. Maximum absolute value of *r* obtained at -170 ms ($r = -.692$, $Z = -3.97$, $N = 34$, $p < .05$). Bottom: Correlogram obtained when averaged CR is cross-correlated with non-CR spike counts.

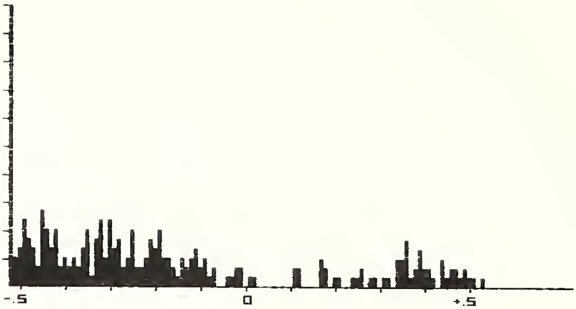

CR ONSET HISTOGRAM FOR CELL 35A
TRIALS=31 BIN=10 MS V.CAL=3 CNTS

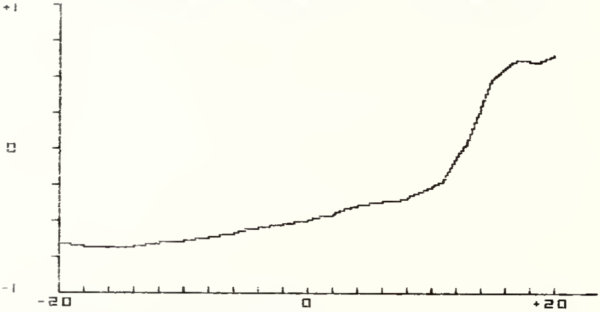

SUB: 35A CORRELOGRAM
RESTRICTED TO CS PERIOD
CR WITH CR SPIKES

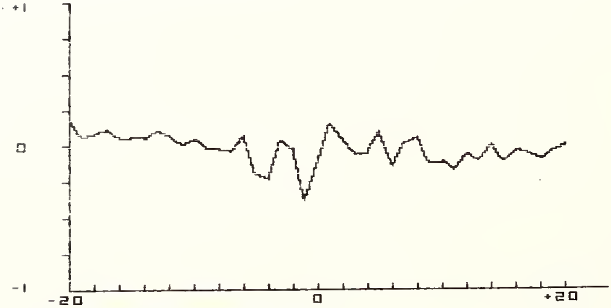

SUB: 35A CORRELOGRAM
RESTRICTED TO CS PERIOD
CR WITH NO CR SPIKES

(Cell 52) or ventral (Cell 29) periaqueductal gray, medial inferior colliculus (Cell 60B), and lobule II of the cerebellar vermis (Cells 52C, 60C). Cell 52 was somewhat unusual because the spike activity depicted in the CR PSTH in Figure 34 does not appear to be inhibitory. Table 5 indicates a weak positive ns/LA correlation in the best set of predictors for CR latency, and this correlation resulted in the inhibitory classification. However, the majority of accountable variance was found in the LA/mt relationship, and the scatterplot of these variables is illustrated at the bottom of Figure 34. The CR onset histogram (middle panel) reveals two bursts of activity occurring 20 and 80 ms after CR onset. Unfortunately, there were practically no non-CR trials, so it was impossible to perform a binomial histogram comparison and analyze further for CR-related inhibition.

Temporal Cells

Table 6 illustrates the variance partitioning for the temporal cells. The unit activity of these cells displayed CR-related shifts in the mean time of spike occurrence during the CS Period, and/or shifts in the dispersion of the spikes around the mean. Note in Table 6 the lack of accountable variance associated with the number of spikes.

Regardless of CR magnitude or latency, the number of

Figure 34

CR PSTH, CR onset histogram, and scatterplot for Cell 52. Top: CR PSTH. Middle: CR onset histogram. CR onset latency: Mean = 253.12 ms from CS onset; standard deviation = 30.35 ms. Bottom: Scatterplot and least squares regression line of CR latency as a function of the mean spike time in the CS Period.

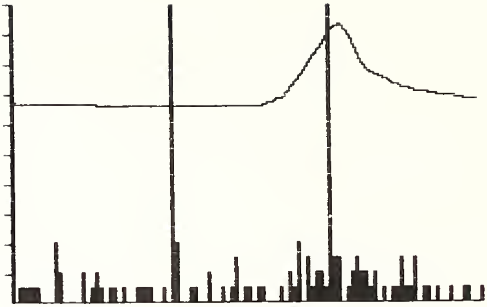

CELL: 52 TRIALS=16 CS=350 MS
BIN=10 MS V.CAL.=2 CNTS, 8 VOLTS

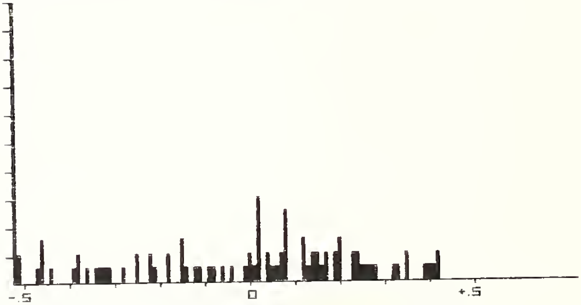

CR ONSET HISTOGRAM FOR CELL 52
TRIALS=16 BIN=10 MS V.CAL=2 CNTS

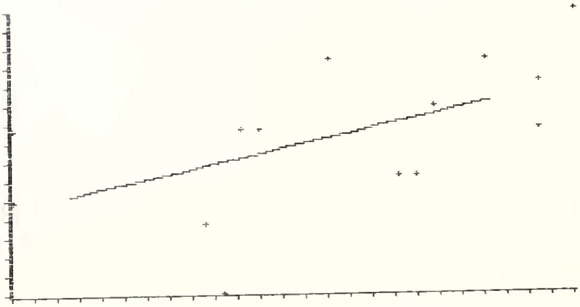

SCATTERPLOT: X=MN. SPIKE TIME, Y=CR LAT
CELL: 52 TRIALS: 14
MIN, MAX VALUES: X=1,33 Y=55,67
HASH MARK CAL.: X=1.2, Y=.8

TABLE 6

VARIANCE PARTITIONING FOR TEMPORAL CELLS

		CR Magnitude			CR Latency		
CELL	MAG	ns	mt	ds	ns	mt	ds
09	AR		+	+			
18	MA		---	+++			
32D1.N	AR			----			+++
43A	AR		-	-			
43E	AR		++	--			++++
43F						+++	
46C	AR		--				
50						---	
52B						--	-
53C	AR		++				-
54A						++++++	
60A2	AR			--			++

Abbreviations: MAG = Magnitude; ns = Number of spikes; mt = Mean spike time; ds = Standard deviation of spike time; AR = CR Area; MA = Maximum CR amplitude; +,- described in text

spikes in the CS Period remains relatively constant for temporal cells. Consequently, a CR-related shifting which produces an excess of spikes in one region of the CS Period also produces a paucity of spikes in one or more other regions of this period. Thus, in a binomial histogram comparison, CR trials can exhibit temporal regions of excitation or inhibition or both, relative to non-CR trials.

For example, Cell 43F was one of 6 temporal cells which increased or decreased firing prior to the CR. This cell displayed a decrease in activity prior to the CR onset followed by an increase in activity after onset. These firing patterns are illustrated in the binomial histogram comparison in Figure 35, and the CR onset histogram in Figure 36. The scatterplot at the bottom of Figure 36 also illustrates the high positive correlation between LA and mt. This cell was located medial to the brachium conjunctivum at the 3.1 mm section level.

Cell 46C was located in the dorsolateral periaqueductal gray at the 6.7 mm section level. The CR PSTH and CR onset histogram for Cell 46C have been presented in Figure 5. Note in the CR onset histogram how the cell increased firing prior to the CR onset. The regression analyses revealed a significant negative correlation between AR and mt, a result typically observed for inhibitory cells. A possible explanation for this

Figure 35

CR PSTH, non-CR PSTH, and binomial histogram comparison for Cell 43F. Top: CR PSTH. Middle: Non-CR PSTH. Bottom: Binomial PSTH comparison.

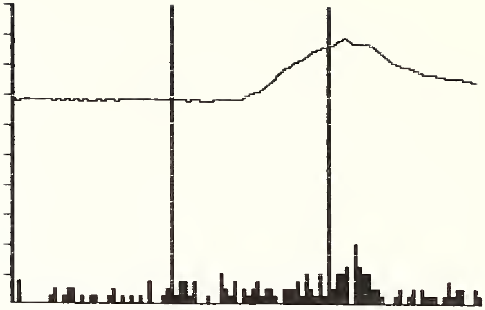

CELL: 43F TRIALS=24 CS=350 MS
BIN=10 MS V.CAL.=4 CNTS, 8 VOLTS

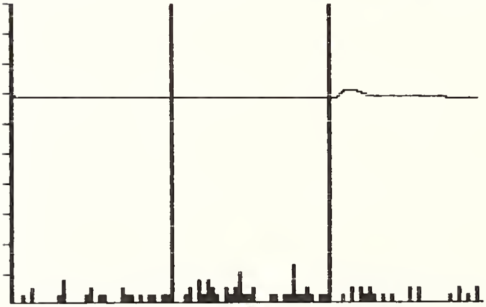

CELL: 43F TRIALS=16 CS=350 MS
BIN=10 MS V.CAL.=4 CNTS, 8 VOLTS

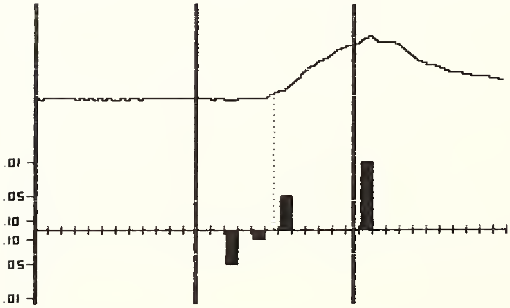

CELL: 43F BIN: 30 MS CS: 350 MS
BINOMIAL HISTOGRAM COMPARISON
CR ONSET AT 5% MAX AMP

Figure 36

CR onset histogram and scatterplot for Cell 43F. Top: CR onset histogram. CR onset latency: Mean = 193.75 ms from CS onset; standard deviation = 41.61 ms. Bottom: Scatterplot and least squares regression line of CR latency as a function of the mean spike time in the CS Period.

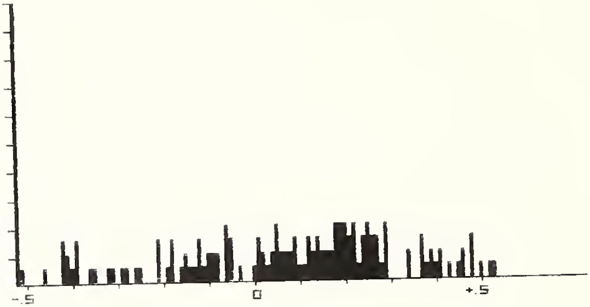

CR ONSET HISTOGRAM FOR CELL 43F
TRIALS=24 BIN=10 MS V.CAL=2 CNTS

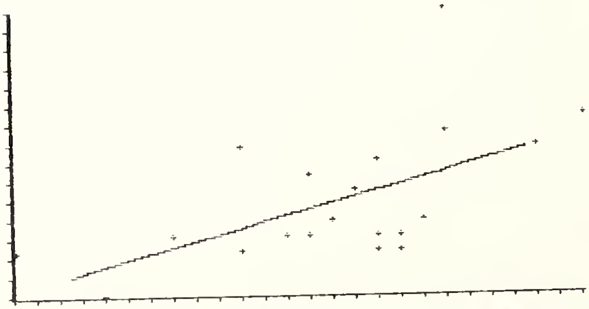

SCATTERPLOT: X=MN. SPIKE TIME, Y=CR LAT
CELL: 43F TRIALS: 21
MIN, MAX VALUES: X=5,30 Y=49,68
HASH MARK CAL.: X=1, Y=1.2

result is postponed for the Discussion.

Cell 50 was also located near the dorsolateral periaqueductal gray, at the 4.4 mm section level. The PSTHs and binomial histogram comparison are illustrated in Figure 37. The binomial histogram comparison reveals only CR-related inhibition, but the CR onset histogram in Figure 38 demonstrates a short burst of activity occurring 100 ms before CR onset. An unusual feature of Cell 50 was the negative correlation between LA and mt, illustrated by the scatterplot in Figure 38. Cell 52B (see Figure 9) similarly had a negative LA/mt correlation; this cell was located in the cerebellum (lobule II) at the 1.9 mm section level.

Cell 54A, located in lobule II of the cerebellar vermis, had a very strong positive LA/mt correlation, as illustrated in the bottom panel of Figure 39. The CR onset histogram (middle panel) reveals 3 distinct bursts of activity at 130 ms and 50 ms before CR onset, and another burst 60 ms after onset. These CR-locked responses are not as distinguishable in the CR PSTH (top panel).

Cell 60A2 demonstrated CR-related changes in standard deviation of spike time. This variable was negatively correlated with AR and positively correlated with LA. The CR and non-CR PSTHs are illustrated in the top and middle panels, respectively, of Figure 40. The binomial histogram comparison at the bottom of the figure reveals a decrease

Figure 37

CR PSTH, non-CR PSTH, and binomial histogram comparison for Cell 50. Top: CR PSTH. Middle: Non-CR PSTH. Bottom: Binomial PSTH comparison.

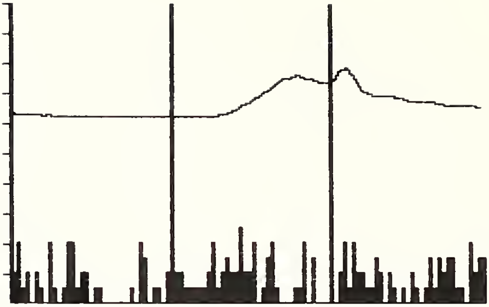

CELL: 50 TRIALS=25 CS=350 MS
BIN=10 MS V.CAL.=2 CNTS, 8 VOLTS

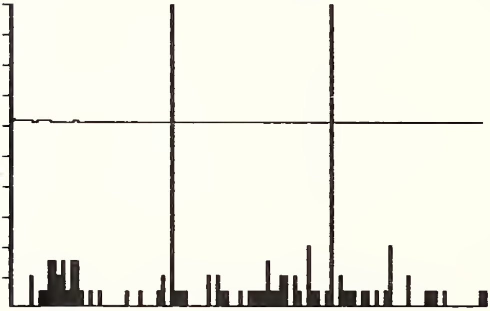

CELL: 50 TRIALS=8 CS=350 MS
BIN=10 MS V.CAL.=2 CNTS, 8 VOLTS

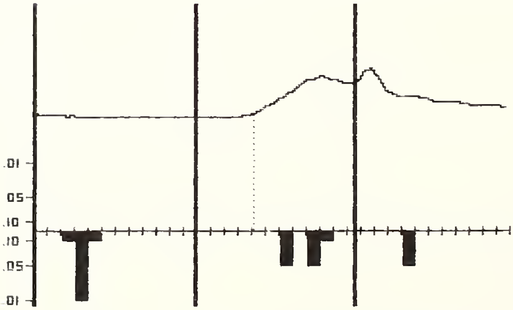

CELL: 50 BIN: 30 MS CS: 350 MS
BINOMIAL HISTOGRAM COMPARISON
CR ONSET AT 5% MAX AMP

Figure 38

Scatterplot and CR onset histogram for Cell 50. Top: Scatterplot and least squares regression line of CR latency as a function of the mean spike time in the CS Period. Bottom: CR onset histogram. CR onset latency: Mean = 169.59 ms from CS onset; standard deviation = 44.94 ms.

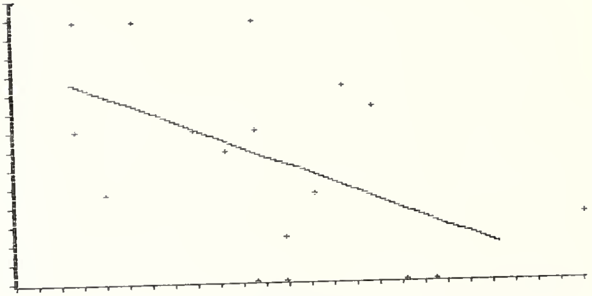

SCATTERPLOT: X=MN. SPIKE TIME, Y=CR LAT
CELL: 50 TRIALS: 18
MIN, MAX VALUES: X=9,28 Y=48,61
HASH MARK CAL.: X=.7, Y=.8

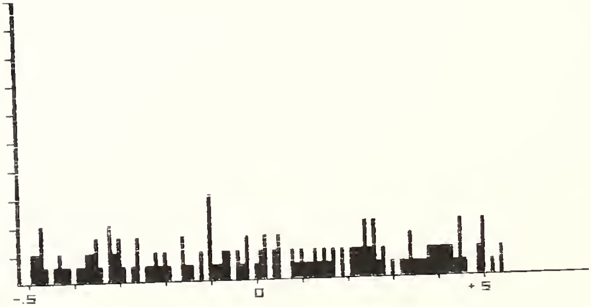

CR ONSET HISTOGRAM FOR CELL 50
TRIALS=25 BIN=10 MS V.CAL=2 CNTS

Figure 39

CR PSTH, CR onset histogram, and scatterplot for Cell 54A. Top: CR PSTH. Dotted line indicates CR onset at 5% maximum deflection. Middle: CR onset histogram. CR onset latency: Mean = 200.00 ms from CS onset; standard deviation = 27.33 ms. Bottom: Scatterplot and least squares regression line of CR latency as a function of the mean spike time in the CS Period.

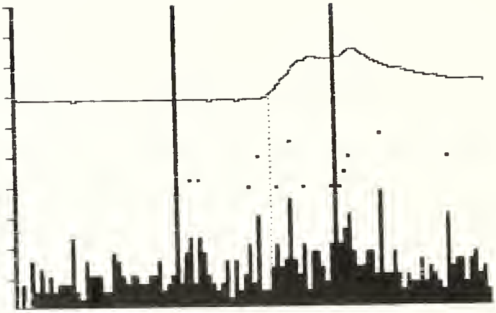

SUB: 54A TRIALS=19 CS=350 MS
BIN=10 MS V.CAL.=4 CNTS, 8 VOLTS

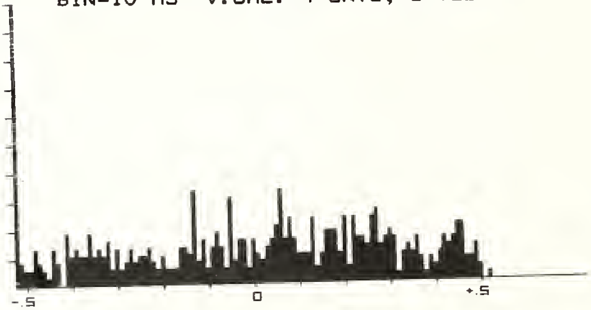

CR ONSET HISTOGRAM FOR CELL 54A
TRIALS=19 BIN=10 MS V.CAL=4 CNTS

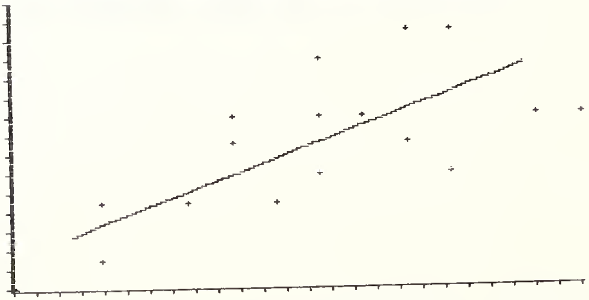

SCATTERPLOT: X=MN. SPIKE TIME, Y=CR LAT
CELL: 54A TRIALS: 19
MIN, MAX VALUES: X=11,24 Y=51,61
HASH MARK CAL.: X=.5, Y=.6

in unit activity prior to CR onset, an increase at onset, and another decrease prior to the US. This cell was located in dorsal inferior colliculus at the 3.9 mm section level.

The unit activity for the remaining temporal cells did not precede the CR. These cells include Cell 09, located in the ventral portion of zone h. Figure 41 illustrates differences in the CR and non-CR spike distributions. The binomial histogram comparison indicates that, relative to non-CR spikes, CR spikes were more concentrated toward the end of the CS Period. That the increase in spikes occurred after CR onset is evident in the CR onset histogram in Figure 42 as well as the binomial histogram comparison of Figure 41.

Cell 43A, located dorsal and medial to brachium conjunctivum, displayed mild excitation at CR onset, followed by inhibition. Cell 43E, located in the subcoeruleus region, was similar to Cell 09 in that spikes were concentrated toward the end of the CS Period on CR trials.

Cell 18 was located medial to the brachium conjunctivum and lateral to the mesencephalic trigeminal nucleus; its location was just medial to that of Cell 17, which was classified as inhibitory. The activity of Cell 18 also displayed inhibitory patterns. However, unlike Cell 17, the inhibition occurred briefly and only at the

Figure 40

CR PSTH, non-CR PSTH, and binomial histogram comparison for Cell 60A2. Top: CR PSTH. Middle: Non-CR PSTH. Bottom: Binomial PSTH comparison.

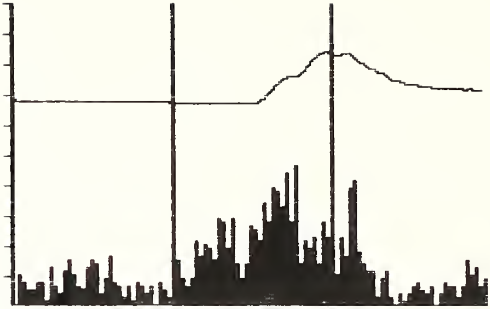

CELL: 60A TRIALS=27 CS=350 MS
BIN=10 MS V.CAL.=8 CNTS, 8 VOLTS

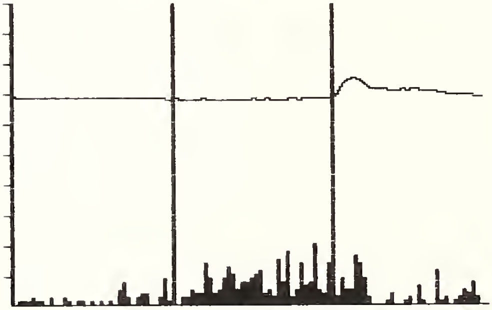

CELL: 60A TRIALS=8 CS=350 MS
BIN=10 MS V.CAL.=8 CNTS, 8 VOLTS

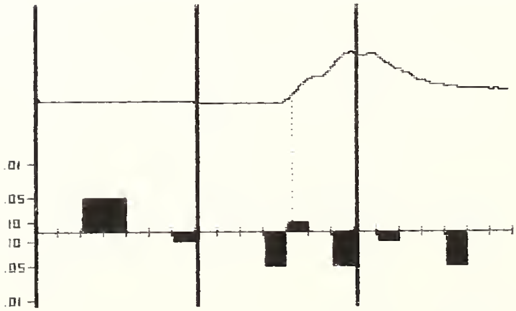

CELL: 60A BIN: 50 MS CS: 350 MS
BINOMIAL HISTOGRAM COMPARISON
CR ONSET AT 5% MAX AMP

Figure 41

CR PSTH, non-CR PSTH, and binomial histogram comparison for Cell 09. Top: CR PSTH. Middle: Non-CR PSTH. Bottom: Binomial PSTH comparison.

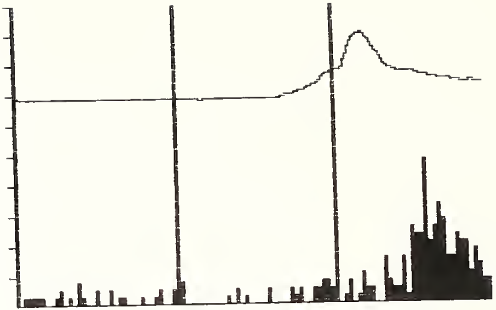

CELL: 09 TRIALS=17 CS=350 MS
BIN=10 MS V.CAL.=4 CNTS, 10.66 VOLTS

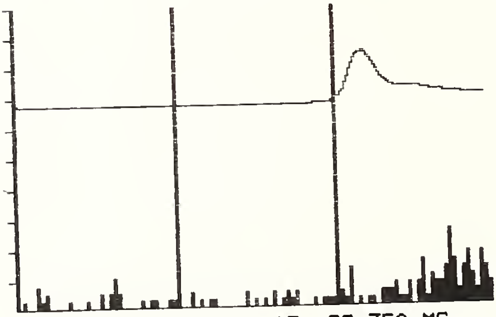

CELL: 09 TRIALS=17 CS=350 MS
BIN=10 MS V.CAL.=4 CNTS, 10.66 VOLTS

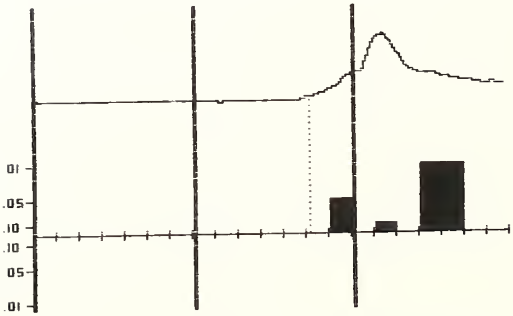

CELL: 09 BIN: 50 MS CS: 350 MS
BINOMIAL HISTOGRAM COMPARISON
CR ONSET AT 5% MAX AMP

Figure 42

CR onset histogram and cross-correlations for Cell 09. Top: CR onset histogram. CR onset latency: Mean = 226.00 ms from CS onset; standard deviation = 81.63 ms. Middle: Correlogram obtained when the first derivative of the averaged CR is cross-correlated with CR-associated spike counts. Abcissa depicts the number of 10 ms bins the CR was shifted backward (negative) or forward (positive) in time. Each hash mark represents 2 bins. Ordinate depicts the value of the Pearson *r*, ranging from +1 to -1. A peak value of *r* to the left of zero (negative side) indicates that spike activity leads the CR; a peak to the right of zero indicates that the CR leads the spike activity. Maximum absolute value of *r* obtained at +20 ms (r = .667, Z = 3.8, N = 34, $p < .05$). Bottom: Correlogram obtained when the first derivative of the averaged CR is cross-correlated with non-CR spike counts.

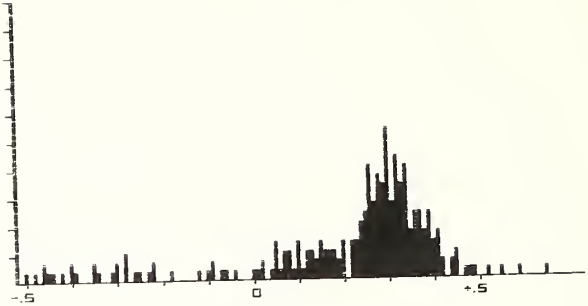

CR ONSET HISTOGRAM FOR CELL 09
TRIALS=20 BIN=10 MS V.CAL=3 CNTS

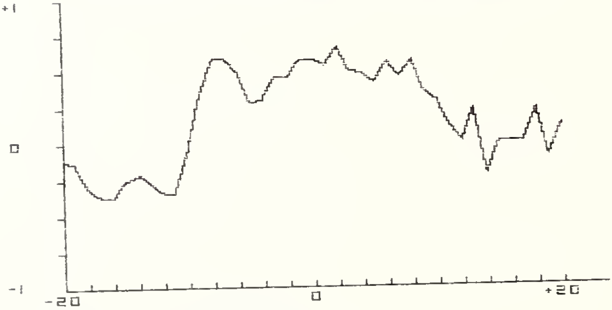

SUB: 09 CORRELOGRAM
RESTRICTED TO CS PERIOD
CR 1ST DER WITH CR SPIKES

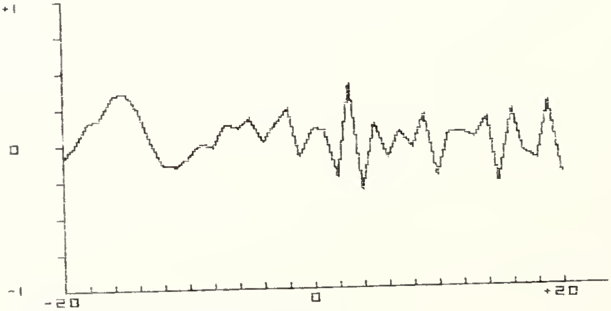

SUB: 09 CORRELOGRAM
RESTRICTED TO CS PERIOD
CR 1ST DER WITH NO CR SPIKES

initiation of the CR. Figure 43 illustrates the CR PSTH, CR onset histogram, and sample unit activity for Cell 18.

Figure 43

CR PSTH, CR onset histogram, and unit activity for Cell 18. Top left: CR PSTH. Dotted line indicates CR onset at 5% maximum deflection. Bottom left: CR onset histogram. CR onset latency: Mean = 203.57 ms from CS onset; standard deviation = 23.48 ms. Top right: Representative unit activity and CR on a single CS+ (1200 Hz) trial. In top and bottom right panels, triangles below unit activity depict CS onset and offset. US onset (in both panels) is contiguous with CS offset. Calibration: 100 ms. Bottom right: Unit activity on a single CS+ trial with no CR.

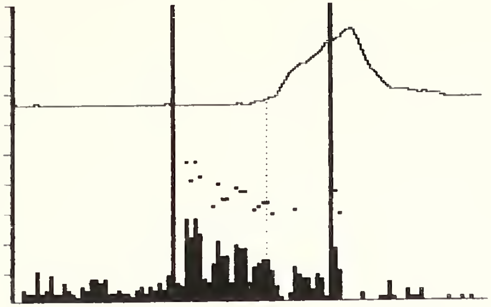

SUB: 18 TRIALS=14 CS=350 MS
BIN=10 MS V.CAL.=8 CNTS, 8 VOLTS

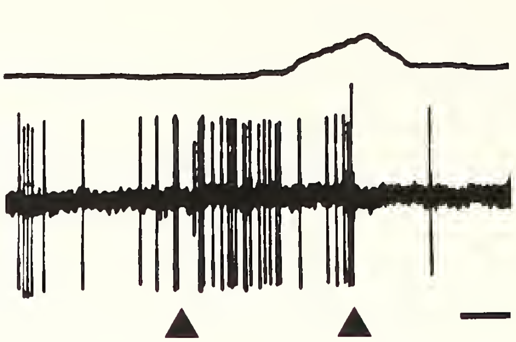

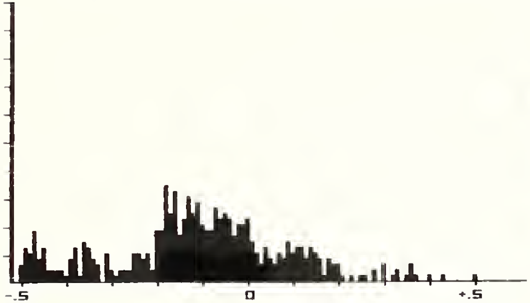

CR ONSET HISTOGRAM FOR CELL 18
TRIALS=14 BIN=10 MS V.CAL=5 CNTS

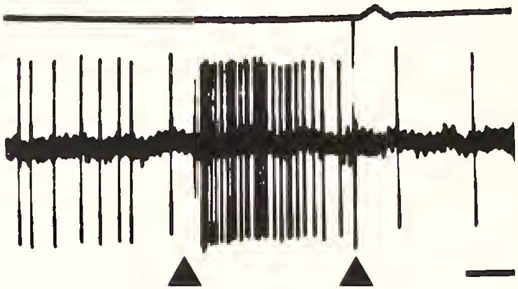

CHAPTER IV

DISCUSSION

Analysis of CR-related Unit Activity

In this experiment, discriminative CSs were presented during single-unit recording in order to obtain both CR and non-CR neuronal activity. Differential conditioning offers a number of advantages over other methods of obtaining these two trial types, and these advantages are as follows: (1) CR and non-CR trials are obtained more reliably with this procedure than with other methods. For example, simple nonreinforcement of a previously conditioned stimulus does not always rapidly extinguish the behavior, and consequently, many cells are lost before non-CR trials can be collected. (2) CR and non-CR trials are alternately, rather than serially, obtained. Thus, any changes in baseline firing over time tend to be evenly distributed to both trial types. (3) Because CR and non-CR trials are acquired non-serially, CR-related activity can be quickly identified during a recording session. Although rapid identification is not always possible, the experimenter can often detect within several trials whether differential CR and non-CR activity is present. (4) CR and non-CR activity can be obtained from a number of cells in succession during a single recording session. Other conditioning protocols severely limit the number of cells that can be obtained. Consider, for example, a procedure in which unit activity is recorded from a naive animal while the animal is undergoing acquisition training. The trials collected before development of the CR provide the non-CR unit activity, whereas the trials obtained after development of the CR provide the CR unit activity. However, only one cell per animal can be analyzed with this method, because an animal is naive only once (Kraus and Disterhoft, 1982). Such a procedure is appropriate if the specific focus of the experiment is to observe the changes in neuronal activity produced by behavioral acquisition. If, however, the focus is to assess CR-related firing, then differential conditioning is a more efficient method of obtaining CR and non-CR firing.

The firing patterns on CR and non-CR trials were compared by visually inspecting CR and non-CR PSTHs, and by using a variety of statistical procedures. In one of these procedures, the binomial histogram comparison, CR and non-CR trials were divided into time bins of 10 ms or greater, and for every time bin, a nonparametric binomial test was used to compare CR and non-CR cumulative spike counts. The results indicated whether the firing rate in any CR-trial bin was significantly greater or less than the rate in the corresponding non-CR bin. Comparisons of Pre-CS bins were used to assess baseline activity; in this study, baseline firing for CR and non-CR trials generally showed few or no differences. In comparing CS Period bins, both bins in each pair were equivalent with respect to the amount of time elapsed since CS onset. Thus, stimulus- and time-dependent firing was matched, and rate differences that were observed were presumably related to the CR. One might predict, therefore, that the same patterns of conditioned activity would have been observed to a CS of a different sensory modality, such as a light. Although the present experiment used only auditory CSs, other experiments, which employed multiple-unit recordings (Desmond and Moore, 1983) from the brain stem, have indicated that CR-related activity is not specific to one CS modality.

CR onset histograms were also used to assess CR-related firing. The purpose of these histograms was to illustrate the temporal distribution of spikes relative to the point in time in which the CR onset occurs. Such a representation is often useful in determining the lead time of the spike activity relative to the CR, or in detecting a firing pattern that occurs at a specific time before or after CR onset. However, this method has two disadvantages. (1) Non-CR trials cannot be used in the construction of the CR onset histogram. Thus, there is neither a comparison histogram nor a test of significance available. (2) A neuron may respond to a phase of the CR other than the onset. If this phase varies in time with respect to this onset, then the CR onset histogram can not adequately depict the spike/CR coupling.

Multiple correlation techniques quantified the trial-by-trial relationships of spike and CR variables, and scatterplots verified the linearity of these relationships. These analyses offer considerable sensitivity in detecting spike/CR relationships. For example, some rabbits which could not discriminate CS+ and CS- made CRs on nearly every trial, yet the covariance of the spikes and the CR on the CR trials alone was sufficient for the spike/CR relationship to be detected.

Excitatory, inhibitory, and temporal cells were classified on the basis of whether the CR was significantly correlated with the number of spikes occurring in the CS Period. However, the neuronal coding necessary for generating the CR probably requires more than simply increasing or decreasing the number of spikes in the CS Period. The increase or decrease in firing probably occurs at a specific time in relation to the CR. In an attempt to examine the more complex temporal aspects of neuronal coding, the mean and standard deviation of the time of spike occurrence were included in the analyses. Inspection of Tables 1-3 reveals the advantages, in terms of accounting for a greater proportion of variance, of including spike variables other than ns. Overall, 42% of the bracketed (best predictor) correlations involved more than one spike variable. Of the remaining 58% that had only one spike variable as the best predictor, ns was the spike variable in 51% of these correlations, mt in 30%, and ds in 19%.

The collection of spike and NM data in 10 ms time bins placed limitations on the types of analyses that could be performed. The mt and ds spike variables were somewhat crude measures of the temporal distribution of spikes. More sophisticated temporal analyses would be possible if the precise time of spike occurrence is recorded. For example, instantaneous spike frequency can be calculated from the interspike intervals, and changes in spike frequency can be compared with the changes in the NM response.

Although the multiple correlation approach is very sensitive in detecting significant spike/CR relationships, statistical significance does not in itself indicate that a relationship is meaningful. A spike variable may account for a minute proportion of variance in predicting a CR variable, but, if sample size is large enough, the correlation of these variables will be significant (for example, Cell 58C in Table 1). On the other hand, if a large number of cells possessing overtly weak spike/CR relationships influence the AAN all at once, their combined effect on AAN could be profound. Thus, such cells should not be dismissed as unimportant. Tables 4-6 were constructed so that the reader can quickly assess both the source and the magnitude of accountable spike/CR variance.

Cross-correlations were used primarily to examine the lead or lag of the spike activity relative to the CR. The results of a cross-correlation were graphically depicted in a correlogram. Although powerful in detecting latency relationships, correlograms have limitations. First, the relationship between the unit activity and the CR (or the CR first derivative) must be linear. In addition, the strength of the correlation depends on the amount of noise in the unit activity, which in turn is largely dependent upon three factors: the number of trials, the firing rate of the spikes, and the change in firing rate due to the CR. The number of trials collected is the only factor which the experimenter can influence. If this number is small, even a strong spike/CR relationship will usually not yield an impressive correlogram.

In many cross-correlations, the maximum positive or negative correlation obtained using the CR first derivative was greater than that obtained using CR amplitude. Those cells with greater first derivative cross-correlations (referred to as first derivative types; cells with greater cross-correlations using CR amplitude are referred to as ordinary types) tended to increase or decrease firing around CR onset, but did not sustain the increase or decrease throughout the entire time-course of the CR (examples: Cell 46C in Figure 5, Cell 52B in Figure 9, Cell 32A in Figure 22, Cell 26 in Figure 23, Cell 64 in Figure 24, Cell 50 in Figure 37, Cell 60A2 in Figure 40). In addition, first-derivative types were three times more likely than ordinary types to have either (1) a significant LA/mt correlation or (2) MA as the preferred measure of CR magnitude. One could speculate that the activity of some of these cells provides rapid recruitment of the motoneurons that participate in the NM/eyeblink response. Such rapid recruitment might be necessary to generate the onset of the CR, and might also determine the maximum CR amplitude. In contrast, the activity of ordinary type cells might be more associated with shaping and sustaining the NM extension over time, and thus, would be more correlated with the total area of the CR.

The temporal relationship between the spike activity and the NM response was assessed by considering the correlograms in conjunction with the CR onset histogram, the t-tests of significant bins, and the binomial histogram comparison. Not all of these measures were appropriate in every case. For example, cross-correlational analyses might be inappropriate due to nonlinearity in the spike/CR relationship. In such a case, the other measures would be relied upon to determine the lead/lag time. Consistency among the measurements was one factor that was considered in choosing a lead or lag value. In cases where measurements were not consistent, judgement dictated whether to include a range of values or to choose one measurement in preference over the others.

Locations of CR-related Recordings

The anatomical distribution of CR-related recording sites in this experiment is consistent with the previously reported distribution of multiple-unit recordings in the SR (Desmond and Moore, 1983). One group of excitatory cells was found in a reticular zone, referred to as cell zone h, circumscribing the motor trigeminal nucleus (see Figure 10). The dorsal portion of this zone corresponds to the SR. Many of the cells in zone h increased firing prior to the CR. However, cells near the intertrigeminal region (Cells 64, 64B, 64C) demonstrated only a small lead time (20 ms for Cell 64), or fired concurrently with the CR onset (Cells 64B, 64C).

A second group of excitatory cells was found dorsal and medial to the brachium conjunctivum. The activity of some of the units in this region was among the most highly CR-correlated, and preceded the CR by substantial intervals (e.g., Cells 53 and 61). Other units in this region, although CR-related, fired concurrently with or after the CR. Interestingly, Mis (1977) found that administering brain stimulation during a CR to regions medial and dorsal to the brachium conjunctivum produced a diminution or alteration of the CR topography.

In addition to CR-related excitation, CR-related inhibition of neuronal activity was also discovered using single-unit recording methods. Cells which decreased firing prior to the CR were located in dorsal and dorsomedial aspects of nucleus reticularis pontis caudalis and oralis (Figure 10). Inspection of Table 5 reveals that mt was a better predictor of CR magnitude than ns for the inhibitory cells. In contrast, ns was typically the better predictor of CR magnitude for the excitatory cells.

Cells which did not demonstrate significant CR-related increases or decreases in the number of spikes occurring in the CS Period, but did demonstrate CR-related shifts in the temporal distribution of the spikes, were classified as temporal cells. Although these cells displayed no CR-related net changes in the number of CS Period spikes, they did demonstrate CR-related increases or decreases within portions of this period, as revealed by binomial histogram comparisons. Thus, many of the temporal cells might have been classified differently had the classification criteria involved the number of spikes occurring within a specific region of the CS Period (e.g., 50 ms before and after CR onset) rather than the total number of spikes in this period.

Some of the temporal cells displayed unusual patterns of correlations. The activity of these cells may have contributed in a complex manner to the production of the CR. For example, Cell 46C displayed an increase in firing prior to the CR (see Figure 5), but the negative AR/mt relationship (Table 6) indicates that spikes were distributed earlier in the CS Period for larger CRs and later in the period for smaller CRs. Although there are probably a number of possible explanations for this effect, one could speculate that such activity served to dampen or shape the CR; firing during later parts of the CS Period, which would be closer in time to the CR, would have a greater dampening effect. Other examples of unusual correlations were observed for Cells 50 and 52B. These cells displayed negative LA/mt correlations (Table 6), and thus, earlier firing in the CS Period was associated with greater CR onset latencies. Such firing patterns could conceivably be involved in delaying the onset of the CR. Cells 46C and 50 were located in dorsal periaqueductal gray, and Cell 52B was found in lobule II of the cerebellar vermis.

The behavioral and statistical methods used in this study were designed to maximize the likelihood of detecting CR-related neuronal activity. Although the present study is not an exhaustive investigation of brain stem structures, it is nevertheless appropriate to mention the regions in which CR-related unit activity was not detected.

Many of the recording sites where significant spike/CR correlations were not observed overlapped with sites where excitatory, inhibitory, or temporal cells were found. However, recordings from the more rostral regions (greater than 3.9 mm in Figure 10), mostly in the inferior and superior colliculi, were less likely to be correlated with the CR. The latter result is somewhat inconsistent with the results of a multiple-unit investigation of the brain stem (McCormick, Lavond, and Thompson, 1983) in which CR-related activity was detected in the superior colliculus. However, the portion of the superior colliculus sampled by these investigators was somewhat more lateral than the regions sampled in the present study. Another region that consistently failed to yield CR-related unit activity was the lateral periventricular gray at the 2.8-3.5 mm levels. However, this structure was not thoroughly investigated, and it is possible that CR-related activity could be obtained from medial, caudal, or rostral aspects of this region.

CR-related Activity and Concomitant Responses

In the process of conditioning the NM response, it is likely that a number of concomitant muscular responses are also conditioned. Thus, cells exhibiting CR-related firing do not necessarily influence the AAN motoneurons, but may instead be related to other conditioned responses. For example, a conditioned neck muscle response might serve to withdraw the head or to prevent the head from moving toward the reinforced eye. Neurons in ventrocaudal nucleus gigantocellularis and rostral nucleus ventralis excite neck and back motoneurons in cats, whereas neurons in caudal nucleus ventralis inhibit neck motoneurons (Peterson, 1977; 1984). These regions are in medial reticular formation caudal to the level of abducens nucleus (caudal to the 0 mm section level in Figure 11), and thus, do not correspond to the locations of the CR-related recording sites of the present study. However, HRP injections into the spinal cord did label cells in regions relevant to the present study. Injections in the ventral horn at C3 levels of the spinal cord (Peterson, 1977) labeled neurons in the medial principal sensory trigeminal nucleus, in a position bordering the intertrigeminal region (close to Cells 64, 64B, and 64C). It is not known whether these neurons influence neck muscles. Cells in SR were labeled only after HRP was injected into the ventral horn at L7 levels of the spinal cord (Peterson, 1977).

Conditioned extension of the NM might require concurrent suppression of saccadic eye movements. A number of studies suggest that the reticular formation is involved in the generation of horizontal and vertical saccadic movements. However, the cells responsible for horizontal saccades are mostly located in the paramedian pontine reticular formation (Buttner-Ennever, 1977; Cohen and Komatsuzaki, 1972; Keller, 1980; Luschei and Fuchs, 1972), a narrow medial region of the reticular formation at the level of the abducens nucleus and ventral to this nucleus. The central mesencephalic reticular formation, which is located dorsolateral to the oculomotor nucleus, has also been implicated in horizontal eye movements (Cohen, Matsuo, Fradin, and Raphan, 1985). Cells of the reticular formation participating in vertical eye movements are in the mesencephalon, just rostral to the oculomotor nucleus (Buttner-Ennever, 1977; Keller, 1980). Thus, the CR-related recording sites of the present study appear to lie in reticular regions that are separate from those known to be involved in saccadic movements. However, bilateral labeling of cells lateral to locus coeruleus and medial to the brachium conjunctivum (close to the position of Cell 32A and Cell 18) were observed after injections of HRP into the flocculus of cats (Graybiel, 1977). These cells may send information concerning eye position and velocity to the cerebellum, and could affect pursuit movements of the eyes.

The eyeblink response is almost perfectly correlated with the NM response with regard to rate of conditioning and shifts in CR onset latency (McCormick, Lavond, and Thompson, 1982). The eyeblink response is generated by the orbicularis oculi muscle, and this muscle is innervated by the intermediate cell group of the facial nucleus. Dendrites of AAN motoneurons extend into the intermediate group of the facial nucleus (Gray et al., 1981; Harvey et al., 1984). Thus, if a CR circuit ultimately sent information to the intermediate facial nucleus, such dendritic arborizations of AAN neurons would provide a means for concurrent contraction of retractor bulbi and orbicularis oculi muscles, and hence, a closely-coupled NM and eyeblink response. In the present study, the CR-related cells found in the subcoeruleus and medial parabrachial regions would be the most likely candidates for such facial projections. In cats, HRP injections into the facial nucleus labeled cells in ipsilateral subcoeruleus and medial parabrachial regions (Takeuchi, Nakano, Uemura, Matsuda, Matsushima, and Mizuno, 1979). In monkeys, anterograde tracing with autoradiographic procedures revealed subcoeruleus and medial parabrachial projections to the ipsilateral intermediate facial nucleus (Westlund and Coulter, 1980). In rabbits, stimulation (30 µA) to medial parabrachial and subcoeruleus regions elicited ipsilateral NM and eyeblink responses (Desmond and Moore, 1983).

If the CR-related units in the present study did in fact project to the facial nucleus, a nucleus which is caudal to AAN, then the trajectory of these projections might have been such that stimulation to the AAN would fail to elicit a response. Such a scenario might explain the paucity of antidromically activated units in this study. On the other hand, alternative explanations for the lack of antidromic activation are tenable. For example, the labeled SR cells that were observed after HRP injection to the AAN (Desmond et al., 1983) were small-diameter cells. It is therefore possible that the bias for large cells in single-unit recording precluded isolation of these smaller cells. Another possibility is that HRP administration to AAN interrupted SR projections to spinal regions such as L7 (Peterson, 1977), and that the SR neurons projecting to the spinal cord are not the same cells that exhibit CR-related activity. Further experimentation with WGA-HRP and autoradiography is needed to clarify the SR/AAN relationship.

The Relationship of Brain Stem and Cerebellar Circuits

Of critical importance for understanding the neural substrates of NM conditioning is determining whether or not the lesion, recording, and stimulation results obtained from the DLP/SR can be explained in terms of the cerebellar circuit. One possible explanation for the CR-disrupting effects of DLP lesions is that interpositus efferents in the brachium conjunctivum were interrupted (Desmond and Moore, 1982; Lavond et al., 1981; McCormick, Guyer, and

Thompson, 1982). Although all of the disruptive DLP lesions did produce some damage to the brachium conjunctivum, the damage to this structure was only minute in some cases. In addition, Rosenfield, Dovydaitis, and Moore (1985) report a CR-disrupting DLP lesion that did not affect the brachium conjunctivum. Furthermore, the multiple-unit activity recorded from the SR (Desmond and Moore, 1983) was, in all probability, not derived from the brachium conjunctivum, because low impedance electrodes record multiple-unit activity only within a radius of 350 micrometers or less (Buchwald, Holstein, and Weber, 1973), and the electrodes in this study were well beyond this distance from the brachium conjunctivum. Many of the single-unit recordings of the present study were in close proximity to the brachium conjunctivum, but were clearly located in reticular regions outside the boundaries of this structure. Thus, it is extremely unlikely that the CR-related unit activity in the DLP is of brachium conjunctivum origin. The possibility still remains, however, that DLP lesions produce CR disruption by damaging the brachium conjunctivum. Fiber-sparing lesions that destroy cell bodies of the DLP, but spare the interpositus axons, are needed to resolve this issue.

Given that the red nucleus is probably involved in relaying conditioning information from the cerebellum to the brain stem (Rosenfield and Moore, 1983), a second possible explanation for the disruptive effects of DLP lesions is that these lesions interrupted projections from the contralateral red nucleus. However, this account is unlikely in light of the anterograde rubrobulbar projections observed by Rosenfield, Dovydaitis and Moore (1985) after administering HRP to the red nucleus. These projections course ventral to the motor trigeminal nucleus and do not send collaterals to the DLP.

To date, there are few studies addressing possible anatomical interconnections of DLP/SR with the cerebellum or cerebellum-related structures. Red nucleus or nucleus interpositus projections to the DLP/SR were not supported by the results of HRP administration to the DLP (Desmond et al., 1983). HRP administration to HVI (Yeo et al., 1985c) or red nucleus (Rosenfield, Dovydaitis, and Moore, 1985) failed to reveal any labeling in SR or the DLP. Thus, present evidence suggests that the DLP is not directly connected with nucleus interpositus, red nucleus, or HVI. However, multisynaptic connections between any of these structures and the DLP are possible. In addition, there are other brain stem structures, such as inferior olive, nucleus reticularis tegmenti pontis, pontine nuclei, and the lateral reticular nucleus, that have connections with the cerebellum; the SR may be interconnected with some of these structures.

On the basis of lesioning and electrophysiological evidence, some investigators have postulated that a cerebellar circuit is essential for NM conditioning. However, the results of Norman, Buchwald, and Villablanca (1977) are inconsistent with the notion of a key role for the cerebellum. In that study, pontine and mesencephalic transections of the the brain stem of cats did not prevent the acquisition of eyelid CRs to an auditory CS. At least 5 of these animals were transected at the level of the inferior colliculus. These transections were clearly caudal to the red nucleus, and thus, interrupted nucleus interpositus efferents in the brachium conjunctivum as well as red nucleus projections to the motoneurons controlling the eyeblink response in the facial nucleus. Given the close correlation of the NM response and the eyeblink in rabbit, these results imply that alternative circuits, perhaps involving the reticular formation, are capable of independently supporting conditioning. However, under normal circumstances, the reticular formation may function in coordination with the cerebellum to generate conditioned responding.

Theories of cerebellar cortex (Marr, 1969; Albus, 1971) provide insights as to how the reticular formation might participate in conditioning. These theories assume that (1) the activity of Purkinje cells is capable of eliciting the elemental movements involved in a motor pattern, and (2) concurrent activation of parallel and climbing fibers, both of which form axo-dendritic synapses on Purkinje cells, produces changes in the parallel fiber synapses. The climbing fibers originate exclusively from the inferior olivary nuclei, and these fibers produce a powerful depolarization response in Purkinje cells. Parallel fibers are the axons of granule cells, and these cells are activated via mossy fibers. Mossy fibers are derived from a number of sources, including pontine nuclei, nucleus reticularis tegmenti pontis, and the lateral reticular nucleus. In learning movements, the mossy fibers are assumed to convey information regarding the current state of the muscles (context information) to the Purkinje cells via parallel fibers. The activity of the parallel fibers is initially incapable of eliciting the desired Purkinje cell output. The desired Purkinje cell output is determined by the activity of the inferior olivary nuclei. These nuclei are hypothesized to relay instruction signals from the cerebral cortex to the Purkinje cells via the climbing fibers. The concurrent activity of the parallel and climbing fibers modifies the parallel fiber synapses; eventually, the activitv of the parallel fibers alone, which codes the muscle context, becomes capable of producing the desired Purkinje response and elicits an elemental movement. This movement creates a new context, which then elicits a second elemental movement. Such a process continues until the entire motor pattern has been executed.

Recent physiological investigations suggest that inferior olivary activity may also signal discrepancies between expected and actual events encountered in a motor sequence (Gellman, Hand, and Houk, 1985). The expected events are the motor instructions generated by a command center. Although it is often assumed that the cerebral cortex is the source of motor instructions, this structure is not essential for the development of conditioning in the rabbit NM response, as previously discussed in the Introduction. Thus, an alternative structure, such as the DLP/SR, may generate the necessary motor commands. The results of the present study indicated that both excitatory and inhibitory unit activity in DLP/SR anticipates the CR by approximately 100 ms, an amount of time sufficient for an expectation to reach the olivary nuclei. One could speculate that the inferior olive compares the DLP/SR commands to the reinforcement signal, the US. A discrepancy would exist whenever the DLP/SR units fail to fire prior to the US, or whenever the DLP/SR units fire and the US does not occur. The inferior olive would then send any mismatch signals to HVI, the region of cerebellar cortex essential for the conditioned NM response (Yeo et al., 1985b). Such mismatch signals would alter the strength of parallel fibers carrying CS information. The CS input is probably derived from mossy fibers originating in bilateral pontine nuclei or nucleus reticularis tegmenti pontis (Yeo et al., 1985c).

Such a scenario is built upon the assumption that the inferior olivary nuclei receive an input from the US as well as from the DLP/SR. It is likely that the rostromedial dorsal accessory olivary nucleus receives US input via the spinal trigeminal nucleus (Berkley and Hand, 1978; Gellman, Houk, and Gibson, 1983). Thus, either the rostromedial dorsal accessory olivary nucleus or the spinal trigeminal nucleus are the most likely structures involved in detecting discrepancies between the US and the DLP/SR input. Although some medial portions of the pontine reticular formation have been shown to project to caudal regions of the inferior olive in the opossum (Martin, Beattie, Hughes, Linauts, and Panneton, 1977), it is not known whether the DLP/SR innervates either the olivary nuclei or the spinal trigeminal nucleus. Future experiments will be conducted to determine if such connections exist.

BIBLIOGRAPHY

Albus, J. S. A theory of cerebellar function. Mathematical Biosciences, 1971, 10, 25-61.

Bach-y-Rita, P. Neurophysiology of eye movements. In: P. Bach-y-Rita and C. Collins (Eds.), Symposium on the control of Eye Movements. New York: Academic Press, 1971.

Baker, R., McCrea, R. A., and Spencer, R. F. Synaptic organizations of the cat accessory abducens nucleus. Journal of Neurophysiology, 1980, 43, 771-791.

Baldissera, F. and Broggi, G. Analysis of a trigemino-abducens reflex in the cat. Brain Research, 1968, 7, 313-316.

Berger, T. W. Long-term potentiation of hippocampal synaptic transmission affects rate of behavioral learning. Science, 1984, 224, 627-630.

Berger, T. W. and Orr, W. B. Hippocampectomy selectively disrupts discrimination reversal conditioning of the rabbit nictitating membrane response. Behavioural Brain Research, 1983, 8, 49-68.

Berger, T. W. and Thompson, R. F. Limbic system interrelations: Functional division among hippocampal-septal connections. Science, 1977, 197, 587-589.

Berger, T. W. and Thompson, R. F. Neuronal plasticity in the limbic system during classical conditioning of the rabbit nictitating membrane response. II. Septum and mammillary bodies. Brain Research, 1978, 156, 293-314.

Berger, T. W., Alger, B. and Thompson, R. F. Neuronal substrates of classical conditioning in the hippocampus. Science, 1976, 192, 483-485.

Berger, T. W., Laham, R. I., and Thompson, R. F. Hippocampal unit-behavior correlations during classical conditioning. Brain Research, 1980, 193, 229-248.

Berkley, K. J. and Hand, P. J. Projections to the inferior olive of the cat. II. Comparisons of input from the gracile, cuneate and spineal trigeminal nuclei. Journal of Comparative Neurology, 1978, 180, 253-264.

Berry, S. D. and Thompson, R. F. Medial septal lesions retard classical conditioning of the nictitating membrane response of rabbits. Science, 1979, 205, 2009-2010.

Berthier, N. E. The role of the extraocular muscles in the rabbit nictitating membrane response: a re-examination. Behavioural Brain Research, 1984, 14, 81-84.

Berthier, N. E. and Moore, J. W. Role of extraocular muscles in the rabbit (Oryctolagus cuniculus) nictitating membrane response. Physiology and Behavior, 1980, 24, 931-937.

Berthier, N. E. and Moore, J. W. The nictitating membrane response: An electrophysiological study of the abducens nerve and nucleus and the accessory abducens nucleus in rabbit. Brain Research, 1983, 258, 201-210.

Berthier, N. E., Desmond, J. E., and Moore, J. W. Brain stem control of the nictitating membrane response. In: I. Gormezano, W. F. Prokasy, and R. F. Thompson (Eds.), Classical Conditioning III. Hillsdale, N.J.: Lawrence Erlbaum Associates, in press.

Blazis, D. E. J. Effects of bilateral posterior hypothalamic and mesencephalic lesions upon conditioned inhibition of the nictitating membrane response in the rabbit. Honor's Thesis, 1984.

Buchwald, J. S., Holstein, S. B., and Weber, D. S. Multiple unit recording: Technique, interpretation, and experimental applications. In: R. F. Thompson and M. M. Patterson (Eds.), Bioelectric Recording Techniques: Part A. Cellular Processes and Brain Potentials. New York: Academic Press, 1973.

Buttner-Ennever, J. A. Pathways from the pontine reticular formation to structures controlling horizontal and vertical eye movements in the monkey. In: R. Baker and A. Berthoz (Eds.), Control of Gaze by Brain Stem Neurons. Developments in Neuroscience, Vol. 1. Amsterdam: Elsevier/North-Holland Biomedical Press, 1977.

Cegavske, C. F., Thompson, R. F., Patterson, M. M., and Gormezano, I. Mechanisms of efferent control of the nictitating membrane response in rabbit (Oryctolagus cuniculus). Journal of Comparative and Physiological Psychology, 1976, 90, 411-423.

Clark, G. A., McCormick, D. A., Lavond, D. G., and Thompson, R. F. Effects of lesions of cerebellar nuclei on conditioned behavioral and hippocampal responses. Brain Research, 1984, 291, 125-136.

Cohen, B. and Komatsuzaki, A. Eye movements induced by stimulation of the pontine reticular formation: Evidence for integration in oculomotor pathways. Experimental Neurology, 1972, 36, 101-117.

Cohen, B., Matsuo, V., Fradin, J., and Raphan, T. Horizontal saccades induced by stimulation of the central mesencephalic reticular formation. Experimental Brain Research, 1985, 57, 605-616.

Cohen, D., Chambers, W. W., and Sprague, J. M. Experimental study of the efferent projections from the cerebellar nuclei to the brain stem of the cat. _Journal of Comparative Neurology_, 1958, _109_, 233-259.

Davis, K. D. and Dostrovsky, J. O. Red nucleus effects on trigeminal subnucleus oralis neurons. _Society for Neuroscience Abstracts_, 1984, _10_, 482.

Desmond, J. E., Berthier, N. E., and Moore, J. W. Brain stem elements essential for the classically conditioned nictitating membrane response of rabbit. _Society for Neuroscience Abstracts_, 1981a, _7_, 650.

Desmond, J. E., Berthier, N. E., and Moore, J. W. Rabbit nictitating membrane response: Neural elements essential for conditioned but not unconditioned responding. _Eastern Psychological Association. New York, N.Y., April_. 1981b.

Desmond, J. E. and Moore, J. W. A brain stem region essential for the classically conditioned but not unconditioned nictitating membrane response. _Physiology and Behavior_, 1982, _28_, 1092-1033.

Desmond, J. E. and Moore, J. W. A Supratrigeminal region implicated in the classically conditioned nictitating membrane response. _Brain Research Bulletin_, 1983, _10_, 765-773.

Desmond, J. E., Rosenfield, M. E., and Moore, J. W. Red nucleus and supratrigeminal reticular formation: Brain stem components of the conditioned nictitating membrane response. Society for Neuroscience Abstracts, 1983, 9, 331.

Desmond, J. E., Rosenfield, M. E., and Moore, J. W. An HRP study of the brainstem afferents to the accessory abducens region and dorsolateral pons in rabbit: Implications for the conditioned nictitating membrane response. Brain Research Bulletin, 1983, 10, 747-763.

Disterhoft, J. F., Quinn, K. J., Weiss, C., and Shipley, M. T. Accessory abducens nucleus and conditioned eye retraction/nictitating membrane extension in rabbit. Journal of Neuroscience, 1985, 5, 941-950.

Disterhoft, J. R. and Shipley, M. T. Accessory abducens innervation of rabbit retractor bulbi motoneurons localized with HRP retrograde transport. Society for Neuroscience Abstracts, 1980, 6, 478.

Dorrscheidt, G. H. The statistical significance of the peristimulus time histogram (PSTH). Brain Research, 1981, 220, 397-401.

Evinger, C., Shaw, M. D., Peck, C. K., Manning, K. A., and Baker, R. Blinking and associated eye movements in humans, guinea pigs, and rabbits. Journal of Neurophysiology, 1984, 52, 323-339.

Foy, M. R., Steinmetz, J. E., and Thompson, R. F. Single unit analysis of cerebellum during classically conditioned eyelid response. Society for Neuroscience Abstracts, 1984, 10, 122.

Francis, J., Hernandez, L. L., and Powell, D. A. Lateral hypothalamic lesions: Effects on Pavlovian cardiac and eyeblink conditioning in the rabbit. Brain Research Bulletin, 1981, 6, 155-163.

Fuller, J. H. and Schlag, J. D. Determination of antidromic excitation by the collision test: Problems of interpretation. Brain Research, 1976, 112, 283-298.

Gellman, R., Gibson, A. R., and Houk, J. C. Inferior olivary neurons in the awake cat: Detection of contact and passive body displacement. Journal of Neurophysiology, 1985, 54, 40-60.

Gellman, R., Houk, J. C., and Gibson, A. R. Somatosensory properties of inferior olive of the cat. Journal of Comparative Neurology, 1983, 215, 228-243.

Glickstein, M., Hardiman, M. J., and Yeo, C. H. Lesions of cerebellar lobulus and simplex abolish the classically conditioned nictitating membrane response of the rabbit. Journal of Physiology, 1984, 350, 31P.

Gormezano, I. Classical conditioning. In: J. B. Sidowski (Ed.), Experimental Methods and Instrumentation in Psychology. New York: McGraw-Hill, 1966.

Gormezano, I., Kehoe, E. J., and Marshall, B. S. Twenty years of classical conditioning with the rabbit. Progress in Psychobiology & Physiological Psychology, 1983, 10, 197-275.

Grant, K., Gueritaud, J., Horcholle-Bossavit, G., and Tyc-Dumont, S. Anatomical and physiological identification of motoneurons supplying cat retractor bulbi muscle. Experimental Brain Research, 1979, 34, 249-274.

Gray, T., McMaster, S., Harvey, J., and Gormezano, I. Localization of retractor bulbi motoneurons in the rabbit. Brain Research, 1981, 226, 93-106.

Graybiel, A. Organization of oculomotor pathways in the cat and rhesus monkey. In: R. Baker and A. Berthoz (Eds.), Control of Gaze by Brain Stem Neurons. Developments in Neuroscience, Vol. 1. Amsterdam: Elsevier/North-Holland Biomedical Press, 1977.

Guegan, M., Gueritaud, J., and Horcholle-Bossavit, G. Localization of motoneurons of bulbi retractor muscle by retrograde transport of exogene horseradish peroxidase in the cat. Comptes Rendus (D), 1978, 286, 1355-1358.

Haley, D. A., Lavond, D. G., and Thompson, R. F. Effects of contralateral red nucleus lesions on retention of the classically conditioned nictitating membrane/eyelid response. Society for Neuroscience Abstracts, 1983, 9, 643.

Harrison, T. A., and Cegavske, C. F. Role of the levator palpebrae superioris (LPS) muscle in effecting nictitating membrane movement in rabbit. Physiology and Behavior, 1981, 26, 159-162.

Harvey, J. A., Land, T., and McMaster, E. Anatomical study of the rabbit's corneal-VIth nerve reflex: Connections between cornea, trigeminal sensory complex, and the abducens and accessory abducens nuclei. Brain Research, 1984, 301, 307-321.

Harvey, J. W., Marek, G. J., Johannsen, A. M., McMaster, S. E., Land, T., and Gormezano, I. Role of the accessory abducens nucleus in the nictitating membrane response of the rabbit. Society for Neuroscience Abstracts, 1983, 9, 330.

Ito, M. The Cerebellum and Neural Control. New York: Raven Press, 1984.

Kao, K. T. and Powell, D. A. Substantia nigra lesions and Pavlovian conditioning of eyeblink and heart rate responses in the rabbit. Society for Neuroscience Abstracts, 1983, 9, 330.

Keller, E. L. Oculomotor specificity within subdivisions of the brain stem reticular formation. In: J. A. Hobson and M. A. B. Brazier (Eds.), The Reticular Formation Revisited: Specifying Function for a Nonspecific System. New York: Raven Press, 1980.

Kraus, N. and Disterhoft, J. F. Response plasticity of single neurons in rabbit auditory association cortex during tone-signalled learning. Brain Research, 1982, 246, 205-215.

Lavond, D. G., McCormick, D. A., Clark, G. A., Holmes, D. T., and Thompson, R. F. Effects of ipsilateral rostral pontine reticular lesions on retention of classically conditioned nictitating membrane and eyelid responses. Physiological Psychology, 1981, 9, 335-339.

Lincoln, J. S., McCormick, D. A., and Thompson, R. F. Ipsilateral cerebellar lesions prevent learning of the classically conditioned nictitating membrane/eyelid response. Brain Research, 1982, 242, 190-193.

Lockhart, M. and Moore, J. W. Classical differential and operant conditioning in rabbits (Oryctolagus cuniculus) with septal lesions. Journal of Comparative and Physiological Psychology, 1975, 88, 147-154.

Lorente de No, R. The interaction of the corneal reflex and vestibular nystagmus. American Journal of Physiology, 1932, 103, 704-711.

Luschei, E. S. and Fuchs, A. F. Activity of brain stem neurons during eye movements of alert monkeys. Journal of Neurophysiology, 1972, 35, 445-461.

Madden, J., Haley, D. A., Barchas, J. D., and Thompson, R. F. Microinfusion of picrotoxin into the caudal red nucleus selectively abolishes the classically conditioned nictitating membrane/eyelid response in the rabbit. Society for Neuroscience Abstracts, 1983, 9, 830.

Mamounas, L. A., Madden, J.,IV, Barchas, J. D., and Thompson, R. F. Microinfusion of GABA antagonists into the cerebellar deep nuclei selectively abolishes the classically conditioned eyelid response in the rabbit. Society for Neuroscience Abstracts, 1983, 9, 830.

Marr, D. A theory of cerebellar cortex. Journal of Physiology, 1969, 202, 437-470.

Martin, G. F., Beattie, M. S., Hughes, H. C., Linauts, M., and Panneton, M. The organization of reticulo-olivo-cerebellar circuits in the North American opossum. Brain Research, 1977, 137, 253-256.

Maser, J. D., Dienst, F. T., and O'Neal, E. C. The acquisition of a Pavlovian conditioned response in septally damaged rabbits: Role of a competing response. Physiological Psychology, 1974, 2, 133-136.

Mauk, M. D., and Thompson, R. F. Classical conditioning using stimulation of the inferior olive as the unconditioned stimulus. Society for Neuroscience Abstracts, 1984, 10, 122.

McCormick, D. A., Clark, G. A., Lavond, D. G., and Thompson, R. F. Initial localization of the memory trace for a basic form of learning. Proceedings of the National Academy of Science (USA), 1982, 79, 2731-2735.

McCormick, D. A., Guyer, P. E., and Thompson, R. F. Superior cerebellar peduncle lesions selectively abolish the ipsilateral classically conditioned nictitating membrane/eyelid response of the rabbit. Brain Research, 1982, 244, 347-350.

McCormick, D. A., Lavond, D. G., and Thompson, R. F. Concommitant classical conditioning of the rabbit nictitating membrane and eyelid responses: Correlations and implications. Physiology and Behavior, 1982, 28, 769-775.

McCormick, D. A., Lavond, D. G., and Thompson, R. F. Neuronal responses of the rabbit brainstem during performance of the classically conditioned nictitating membrane/eyeblink response in the rabbit. Brain Research, 1983, 271, 73-88.

McCormick, D. A., Lavond, D. G., Clark, G. A., Kettner, R. E., Rising, C. E., and Thompson, R. F. The engram found? Role of the cerebellum in classical conditioning of nictitating membrane and eyelid responses. Bulletin of the Psychonomic Society, 1981, 18, 103-105.

McCormick, D. A. and Thompson, R. F. Cerebellum: Essential involvement in the classically conditioned eyelid response. Science, 1983a, 223, 296-299.

McCormick, D. A. and Thompson, R. F. Possible neuronal substrate of classical conditioning within the mammalian CNS: Dentate and interposed nuclei. Society for Neuroscience Abstracts, 1983b, 9, 643.

Meessen, H. and Olszewsky, J. A Cytoarchetectonic Atlas of the Rhombencephalon of the Rabbit. Basel: S. Karger, 1949.

Mis, F. W. A midbrain-brain stem circuit for conditioned inhibition of the nictitating membrane response in the rabbit (Oryctolagus cuniculus). Journal of Comparative and Physiological Psychology, 1977, 91, 975-988.

Mizuno, N. Projection fibers from the main sensory trigeminal nucleus and the supratrigeminal region. _Journal of Comparative Neurology_, 1970, _139_, 457-472.

Mizuno, N., Mochizuki, K., Akimoto, C., Matsushima, R., and Nakamura, Y. Rubrobulbar projections in the rabbit. A light and electron microscopic study. _Journal of Comparative Neurology_, 1973, _147_, 267-280.

Moore, J. W. Brain processes and conditioning. In: A. Dickinson and R. A. Boakes (Eds.), _Mechanisms of Learning and Motivation: A Memorial Volume to Jerzy Konorski_. Hillsdale, NJ: Erlbaum, 1979.

Moore, J. W. Stimulus control: Studies of auditory generalization in rabbits. In: A. H. Black and W. F. Prokasy (Eds.), _Classical Conditioning II. Current Theory and Research_. New York: Appleton-Century-Crofts, 1972.

Moore, J. W., Berthier, N. E., and Desmond, J. E. Brain stem electrophysiological correlates of the classically conditioned nictitating membrane response in the rabbit. _Society for Neuroscience Abstracts_, 1981, _7_, 358.

Moore, J. W. and Desmond, J. E. Latency of the nictitating membrane response to periocular electrostimulation in unanesthetized rabbits. _Physiology and Behavior_, 1982, _28_, 1041-1046.

Moore, J. W., Desmond, J. E., and Berthier, N. E. The metencephalic basis of the conditioned nictitating membrane response. In: C. H. Woody (Ed.), Conditioning: Representation of involved neural function. New York: Plenum, 1982.

Moore, J. W. and Solomon, P. R. Forebrain-brainstem interaction: Conditioning and the hippocampus. In: N. Butters and L. R. Squire (Eds.), The Neuropsychology of Memory. New York: Guilford, 1984.

Moore, J. W. and Solomon, P. R. (Eds.) Role of the hippocampus in learning and memory. Physiological Psychology (Special Edition), 1980, 8, 145-296.

Moore, J. W., Yeo, C. H., Oakley, D. A. and Russell, I. S. Conditioned inhibition of the nictitating membrane response in neodecorticate rabbits. Behavioural Brain Research, 1980, 1, 397-409.

Nakamura, Y. and Mizuno, N. An electron microscopic study of the interposito-rubral connection in the cat and rabbit. Brain Research, 1971, 35, 283-286.

Norman, R. F., Buchwald, J. S., and Villablanca, J. R. Classical conditioning with auditory discrimination of the eye blink in decerebrate cats. Science, 1977, 196, 551-553.

Oakley, D. A. and Russell, I. S. Neocortical lesions and Pavlovian conditioning. Physiology and Behavior, 1972, 8, 915-926.

Oakley, D. A. and Russell, I. S. Differential and reversal conditions in partially neodecorticate rabbits. Physiology and Behavior, 1974, 13, 221-230.

Oakley, D. A. and Russell, I. S. Role of cortex in Pavlovian discrimination learning. Physiology and Behavior, 1975, 15, 315-321.

Oakley, D. A. and Russell, I. S. Subcortical storage of Pavlovian conditioning in the rabbit. Physiology and Behavior, 1977, 18, 931-937.

Orr, W. B. and Berger, T. W. Hippocampal lesions disrupt discrimination reversal learning of the rabbit nictitating membrane response. Society for Neuroscience Abstracts, 1981, 7, 648.

Pedhazur, E. J. Multiple Regression in Behavioral Research. Second Edition. New York: Holt, Rinehart, and Winston, 1982.

Peterson, B. W. The reticulospinal system and its role in the control of movement. In: C. D. Barnes (Ed.), Brainstem Control of Spinal Cord Function. Orlando, FL: Academic Press, Inc., 1984.

Peterson, B. W. Identification of reticulospinal projections that may participate in gaze control. In: R. Baker and A. Berthoz (Eds.), *Control of Gaze by Brain Stem Neurons. Developments in Neuroscience, Vol. 1.* Amsterdam: Elsevier/North-Holland Biomedical Press, 1977.

Port, R. L. and Patterson, M. M. Fimbrial lesions and sensory preconditioning. *Behavioral Neuroscience*, 1984, *98*, 584-589.

Powell, D. A., Mankowski, D., and Buchanan, S. Concomitant heart rate and corneoretinal potential conditioning in the rabbit (*Oryctolagus cuniculus*): Effects of caudate lesions. *Physiology and Behavior*, 1978, *20*, 143-150.

Quinn, K. J., Kennedy, P., Weiss, C., and Disterhoft, J. Eyeball retraction latency in the conscious rabbit measured with a new photodiode technique. *Journal of Neuroscience Methods*, 1984, *10*, 29-39.

Rosenfield, M. E. and Moore, J. W. Red nucleus lesions impair acquisition of the classically conditioned nictitating membrane response but not eye-to-eye savings or UR amplitude. In press.

Rosenfield, M. E. and Moore, J. W. Red nucleus lesions disrupt the classically conditioned nictitating membrane response in rabbits. *Behavioural Brain Research*, 1983, *10*, 393-398.

Rosenfield, M. E., Dovydaitis, A., and Moore, J. W. Brachium cunjunctivum and rubrobulbar tract: Brain stem projections of red nucleus essential for the conditioned nictitating membrane response. Physiology and Behavior, 1985, 34, 751-759.

Schlag, J. Electrophysiological mapping techniques. In: R. T. Robertson (Ed.), Neuroanatomical Research Techniques. New York: Academic Press, 1978.

Solomon, P. R. Role of the hippocampus in blocking and conditioned inhibition of the rabbit's nictitating membrane response. Journal of Comparative and Physiological Psychology, 1977, 91, 407-417.

Solomon, P. R. and Moore, J. W. Latent inhibition and stimulus generalization of the classically conditioned nictitating membrane response in rabbits (Oryctolagus cuniculus) following dorsal hippocampal ablation. Journal of Comparative and Physiological Psychology, 1975, 89, 1192-1203.

Solomon, P. R., Solomon, S. D., Schaaf, E. V., and Perry, H. E. Altered activity in the hippocampus is more detrimental to classical conditioning than removing the structure. Science, 1983, 220, 329-331.

Solomon, P. R., Vander Schaaf, E. R., Nobre, A. C., Weisz, D. J., and Thompson, R. F. Hippocampus and trace conditioning of the rabbit's nictitating membrane response. Society for Neuroscience Abstracts, 1983, 9, 645.

Solomon, P. R., Weisz, D. J., Clark, G. A., Hall, J., and Babcock, B. A. A microprocessor control system and solid state interface for controlling electrophysiological studies of conditioning. Behavior Research Methods & Instrumentation, 1983, 15, 57-65.

Spencer, R. F., Baker, R., and McCrea, R. H. Localization and morphology of cat retractor bulbi motorneurons. Journal of Neurophysiology, 1980, 43, 754-770.

Steinmetz, J. E., McCormick, D. A., Baier, C. A., and Thompson, R. F. Involvement of the inferior olive in classical conditioning of the rabbit eyelid. Society for Neuroscience Abstracts, 1984, 10, 122.

Takeuchi, Y., Nakano, K, Uemura, M., Matsuda, K., Matsushima, R., and Mizuno, N. Mesencephalic and pontine afferent fiber system to the facial nucleus in the cat. A study using horseradish peroxidase and silver impregnation techniques. Experimental Neurology, 1979, 66, 330-342.

Thompson, R. F., Berger, T. W., Berry, S. D., Hoehler, F. K., Kettner, R. E., and Weisz, D. Hippocampal substrate of classical conditioning. _Journal of Physiological Psychology_, 1980, _8_, 262-279.

Thompson, R. F., Berger, T. W., Cegavske, C. F., Patterson, M. M., Roemer, R. A., Teyler, T. J., and Young, R. A. The search for the engram. _American Psychologist_, 1976, _31_, 209-227.

Torigoe, Y., Wenokor, W., and Cegavske, C. F. Neural substrates of the classically conditioned rabbit nictitating membrane preparation: Trigeminal system afferents. _Society for Neuroscience Abstracts_, 1981, _7_, 753.

Weisz, D. W., Solomon, P. R., and Thompson, R. F. The hippocampus appears necessary for trace conditioning. _Bulletin of the Psychonomic Society_. 1980.

Westlund, K. N. and Coulter, J. D. Descending projections of the locus coeruleus and subcoeruleus/medial parabrachial nuclei in monkey: Axonal transport studies and dopamine-beta-hydroxylase immunocytochemistry. _Brain Research Reviews_, 1980, _2_, 235-264.

Yeo, C. H., Hardiman, M. J., and Glickstein, M. Cerebellar pathways in the conditioned nictitating membrane response. _Society for Neuroscience Abstracts_, 1984a, _10_, 793.

Yeo, C. H., Hardiman, M. J., and Glickstein, M. Discrete lesions of the cerebellar cortex abolish the classically conditioned nictitating membrane response of the rabbit. _Behavioural Brain Research_, 1984b, _13_, 261-266.

Yeo, C. H., Hardiman, M. J., and Glickstein, M. Classical conditioning of the nictitating membrane response of the rabbit: I. Lesions of the cerebellar nuclei. _Experimental Brain Research_. 1985a, in press.

Yeo, C. H., Hardiman, M. J., and Glickstein, M. Classical conditioning of the nictitating membrane response of the rabbit. II. Lesions of the cerebellar cortex. _Experimental Brain Research_. 1985b, in press.

Yeo, C. H., Hardiman, M. J., and Glickstein, M. Classical conditioning of the nictitating membrane response of the rabbit: III. Connections of cerebellar lobule HVI. _Experimental Brain Research_. 1985c, in press.

Yeo, C. H., Hardiman, M. J., Moore, J. W., and Steele-Russell, I. Retention of conditioned inhibition of the nictitating membrane response in decorticate rabbits. _Behavioural Brain Research_, 1983, _10_, 383.